On the Effect of Walking Surface Stiffness on Inter-leg Coordination during Human Walking: a Unique Perspective to Robot-assisted Gait Rehabilitation

by

Jeffrey Alan Skidmore

A Dissertation Presented in Partial Fulfillment
of the Requirements for the Degree
Doctor of Philosophy

Approved April 2017 by the
Graduate Supervisory Committee:

Panagiotis Artemiadis, Chair
Marco Santello
Spring Berman
Hyunglae Lee
Hamidreza Marvi

ARIZONA STATE UNIVERSITY

May 2017

ABSTRACT

Millions of individuals suffer from gait impairments due to stroke or other neurological disorders. A primary goal of patients is to walk independently, but most patients only achieve a poor functional outcome five years after injury. Despite the growing interest in using robotic devices for rehabilitation of sensorimotor function, state-of-the-art robotic interventions in gait therapy have not resulted in improved outcomes when compared to traditional treadmill-based therapy. Because bipedal walking requires neural coupling and dynamic interactions between the legs, a fundamental understanding of the sensorimotor mechanisms of inter-leg coordination during walking is needed to inform robotic interventions in gait therapy. This dissertation presents a systematic exploration of sensorimotor mechanisms of inter-leg coordination by studying the effect of unilateral perturbations of the walking surface stiffness on contralateral muscle activation in healthy populations. An analysis of the contribution of several sensory modalities to the muscle activation of the opposite leg provides new insight into the sensorimotor control mechanisms utilized in human walking, including the role of supra-spinal neural circuits in inter-leg coordination. Based on these insights, a model is created which relates the unilateral deflection of the walking surface to the resulting neuromuscular activation in the opposite leg. Additionally, case studies with hemiplegic walkers indicate the existence of the observed mechanism in neurologically impaired walkers. The results of this dissertation suggest a novel approach to gait therapy for hemiplegic patients in which desired muscle activity is evoked in the impaired leg by only interacting with the healthy leg. One of the most significant advantages of this approach over current rehabilitation protocols is the safety of the patient since there is no direct manipulation of the impaired leg. Therefore, the methods and results presented in this dissertation represent a potential paradigm shift in robot-assisted gait therapy.

DEDICATION

I dedicate this dissertation to my family, especially

Elisa - my wife and my love

Cary - my father and my hero

Wendy - my mother and my strength

Elena - my daughter and my light

Abigail - my daughter and my joy

ACKNOWLEDGMENTS

My entire PhD experience has been an incredible experience, and I am indebted to many people who have helped me along this journey. I am especially thankful to my parents who have always believed in me and gave me confidence that I could obtain a doctoral degree and to my wife and daughters for their unfailing love and support.

I pay tribute to Panos, who accepted me into the HORC lab and mentored me every step of the way through this process. I am permanently indebted to Panos for his guidance, counsel, and support which has shaped my career aspirations. Any accomplishment that I may achieve in my career will be in large part due to how Panos has helped shape me into an independent researcher.

I also gratefully acknowledge the rest of the HORC lab and other colleagues for their feedback, support, and friendship. I thank Andrew Barkan, Adrian Ion, Linda Fou, Sebastian Klype, Jeremy Johnson, and Ryan Frost for working with me on the treadmill project. I am especially thankful to Andrew Barkan for designing and building the VST which allowed me to hit the ground running with my research. I am thankful to Bryan Whitsell, George Karavas, Mark Ison, Justin Hunt, Zahi Kakish, Chuong Nguyen, Keivan Mojtahedi, Patrick McGurrin, and others for their input and friendship.

This dissertation serves as the culmination of all the incredible support and guidance I have received over the past four years, and is by no means a one-man show. Hopefully it can impact the scientific community the way the journey to create it has impacted me.

TABLE OF CONTENTS

CHAPTER Page

LIST OF TABLES

LIST OF FIGURES

Figure Page

Figure Page

PREFACE

The following dissertation is the culmination of four academic years of research in the Human Oriented Robotics and Control Lab at Arizona State University. The research performed during this time has currently resulted in 4 published peer-reviewed journal articles and 5 published peer-reviewed conference proceedings. These contributions are outlined in Appendix A.

Much of the work presented in this dissertation has not been published, and only select portions from previously published articles are included in this dissertation. The following chapters contain portions of these papers which are correspondingly cited within the text. These portions from previously published papers have been included, with permission, because they each contribute to the exploration of the effect of walking surface stiffness on sensorimotor mechanisms of inter-leg coordination, which is the subject of this dissertation. Permission has been granted for using copyrighted material in this dissertation (see Appendix B), and all co-authors have given permission to include material from co-authored papers (see Appendix C).

Chapters 1 and 2 provide an introduction and background to human locomotion, inter-leg coordination, and gait therapy. Select ideas and sentences from several of the aforementioned papers are used in these chapters and are appropriately cited within the text.

Chapter 3 describes the development and characterization of a novel experimental platform for investigating mechanisms of inter-leg coordination. Portions of this chapter come from a journal publication in IEEE Transactions on Mechatronics (Skidmore *et al.*, 2015) and publications in the proceedings of the 2014 IEEE International Conference on Robotics and Automation (Barkan *et al.*, 2014) and the 2014 IEEE/RSJ International Conference on Intelligent Robots and Systems (Skidmore *et al.*, 2014).

Chapter 4 includes a series of experiments that detail the contralateral effect in response to unilateral stiffness perturbations. This chapter comes from portions of journal publications in IEEE Transactions on Neural Systems and Rehabilitation Engineering (Skidmore and Artemiadis, 2015b) and Journal of NeuroEngineering and Rehabilitation (Skidmore and Artemiadis, 2016a).

Chapter 5 provides an investigation into an identified sensorimotor mechanism of inter-leg coordination, including the role of supra-spinal neural pathways. The EEG portion of this chapter comes from part of a publication in the proceedings of the 2016 IEEE International Conference on Robotics and Automation (Skidmore and Artemiadis, 2016c).

Finally, chapter 7 presents three case studies with hemiplegic walkers. The section detailing the third case study largely comes from portions of a publication in the proceedings of the 2016 International Conference of the IEEE Engineering in Medicine and Biology Society (Skidmore and Artemiadis, 2016b).

Chapter 1

INTRODUCTION

Gait impairments due to stroke or other neurological disorders impacts millions of individuals throughout the world and has become an important problem of the 21st century. Stroke is a leading cause of long-term disability with 795,000 new strokes occurring each year in the United States alone (AHA, 2010; Langhorne *et al.*, 2011). Nearly 90% of stroke survivors require therapy but the majority of patients only achieve poor functional outcome five years after the onset of stroke (AHA, 2010; Barker-Collo *et al.*, 2010). Since a primary goal of impaired patients is to walk independently (Ditunno Jr *et al.*, 2005), improved gait therapy will significantly improve the well-being of millions of individuals.

1.1 Traditional Gait Rehabilitation

Neural plasticity, or the brain's ability to learn and adapt, is believed to be the basis for relearning after neurological injury (Kleim and Jones, 2008). Thus the aim of gait therapy after stroke is to provide interventions that facilitate neural plasticity in the brain (Belda-Lois *et al.*, 2011; Pekna *et al.*, 2012). Conventional gait rehabilitation strategies are largely based on physical therapy where patients are guided through walking practice in an effort to acquire the ability to produce gait patterns which were lost after injury (Belda-Lois *et al.*, 2011; Kleim, 2011). However, conventional approaches to gait training do not restore a normal gait pattern in the majority of stroke patients (Belda-Lois *et al.*, 2011; Dohring and Daly, 2008). While the majority of stroke patients achieve an independent gait after therapy, many do not reach a walking level that enable them to perform all of their daily activities (Belda-Lois *et al.*, 2011; Flansbjer *et al.*, 2005).

Moreover, traditional gait rehabilitation therapies are very labor intensive, often requiring three or more therapists working together to manually assist and stabilize the legs and torso of the patient during training (Díaz *et al.*, 2011). This fact severely limits patients from receiving appropriate duration and frequency of training that are critical for functional improvement after stroke (Kleim and Jones, 2008). Moreover, this leads to higher costs and a financial burden for individuals and a country's healthcare system (Gelderblom *et al.*, 2009). With an aging population and expected shortages of health care personnel, there is a need for better solutions for providing gait therapy (Gelderblom *et al.*, 2009).

1.2 Robot-assisted Gait Therapy

Rehabilitation robotics is an emerging field in which gait training is largely automated, replacing the need for several therapists (Chang and Kim, 2013; Díaz *et al.*, 2011). A benefit of robot-assisted gait therapy is that robots can perform many repetitions with high accuracy, thus replacing the physical effort required of a therapist and allowing more intensive, repetitive motions which are important for facilitating neural plasticity (Kleim and Jones, 2008). A variety of robotic rehabilitation devices have been developed in the last several years for gait therapy (Banala *et al.*, 2007; Hesse *et al.*, 2000; Jezernik *et al.*, 2003; Morbi *et al.*, 2012; Peshkin *et al.*, 2005; Veneman *et al.*, 2007). However, there is no clear evidence that robot-assisted gait training training is superior to conventional physiotherapy for either chronic or subacute stoke patients (Chang and Kim, 2013; Hidler *et al.*, 2009; Hornby *et al.*, 2008; Mayr *et al.*, 2007; Pohl *et al.*, 2007).

A limitation of the robotic devices used for gait therapy is that they do not consider mechanisms of inter-leg coordination and how the sensory feedback from one leg affects the motion of the other leg (Skidmore and Artemiadis, 2016a). Rather, the

state-of-the-art devices, ranging from kinematically controlled exoskeletons (Mehrholz *et al.*, 2007) to impedance controlled orthotic devices (Blaya and Herr, 2004; Roy *et al.*, 2009), impose motion on the impaired limb. A recent review suggests that utilizing inter-limb coupling in stroke rehabilitation therapies will lead to improved functional outcome (Arya and Pandian, 2014). Therefore, a fundamental understanding of underlying sensorimotor mechanisms of inter-leg coordination may facilitate improved robotic interventions in gait therapy (Skidmore and Artemiadis, 2016a).

1.3 Sensorimotor Mechanisms

Investigation of the role of afferent feedback to gait control mechanisms of inter-leg coordination usually involve sensory perturbations and the analysis of their effects (Skidmore and Artemiadis, 2016a). Various platforms and protocols have been used to investigate bilateral reflex mechanisms during different phases of the gait cycle (Artemiadis and Krebs, 2011a,b; Dietz *et al.*, 1989; Nakazawa *et al.*, 2004; van der Linden *et al.*, 2007). While the majority of the experimental protocols focus on over-ground walking and dropping of the supportive surfaces at distinct phases of the gait cycle (Artemiadis and Krebs, 2011a,b; Nakazawa *et al.*, 2004; van der Linden *et al.*, 2007), a few studies have utilized compliant surfaces in researching sensorimotor mechanisms in human locomotion (Dixon *et al.*, 2000; Ferris *et al.*, 1999; Hardin *et al.*, 2004; MacLellan and Patla, 2006; Marigold and Patla, 2005; Moritz *et al.*, 2004).

A significant limitation of all of the previously mentioned works is that the previous studies have failed to separate the mechanisms of inter-leg coordination from that of balance support. Most studies do not even consider balance support. As a result, mechanical perturbations and sudden load changes would have likely triggered reflex mechanisms and vestibular responses to maintain balance and stability. However, little is known whether the bilateral activations are exclusively caused by

the mechanisms required for body stabilization and balance maintenance, or if it is also brought about from inter-limb coordination and mechanisms of gait. This lack of knowledge leaves a significant gap in our understanding of sensorimotor control of gait (Skidmore and Artemiadis, 2016a).

1.4 Research objective

The objective of this research is to identify and model mechanisms of inter-leg coordination in human gait by applying unilateral perturbations to the walking surface stiffness, with the end goal of improving gait rehabilitation for hemiplegic patients. Identification and modeling of mechanisms of inter-leg coordination will lead to bilaterally informed robotic gait rehabilitation, which can revolutionize current approaches to gait therapy. As opposed to simply automating existing gait training approaches, providing therapy through sensorimotor mechanisms of inter-leg coordination represents a potential paradigm shift in robot-assisted gait therapy. In this novel approach to gait therapy, specifically designed for hemiplegic patients, desired muscle activity is evoked in the impaired leg by perturbing sensory feedback of the healthy leg. A conceptual illustration of this approach utilizing sensorimotor mechanisms of inter-leg coordination is shown in Figure 1.1. One of the most significant advantages of this approach over current rehabilitation protocols is the safety of the patient since there is no direct manipulation of the impaired leg (Skidmore and Artemiadis (2015a), ©2015 IEEE; Skidmore and Artemiadis (2016c), ©2016 IEEE).

The rest of this dissertation describes the methods and results of the proposed exploration of sensorimotor mechanisms of inter-leg coordination through unilateral perturbations to walking surface stiffness. Chapter 2 provides an overview of human locomotion, current approaches to rehabilitation, and a discussion of inter-leg coordi-

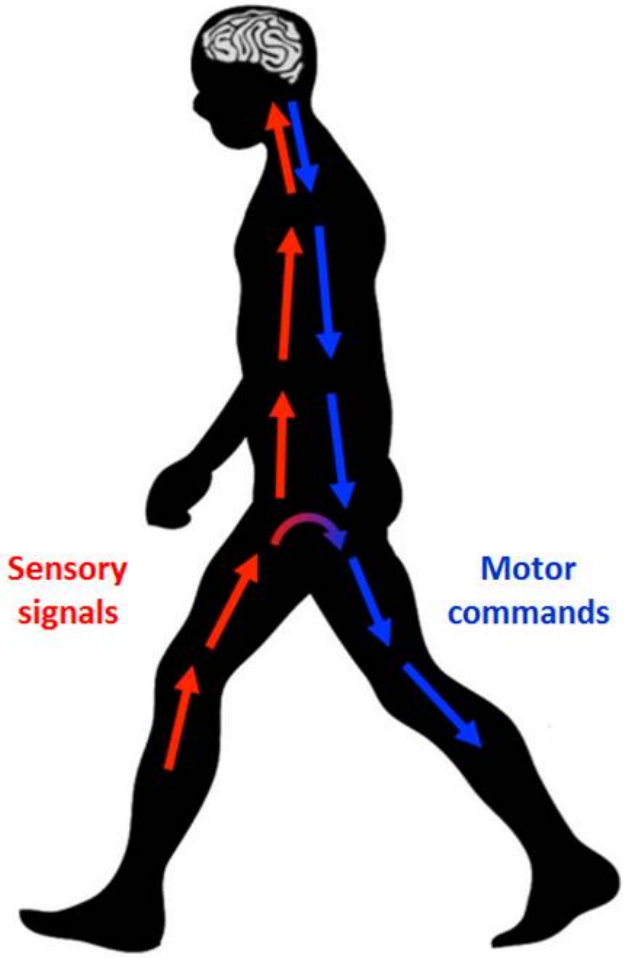

Figure 1.1: Conceptual illustration of sensorimotor mechanisms of inter-leg coordination.

nation in order to establish the significance of this research. Chapter 3 describes the development and characterization of a novel experimental platform for investigating mechanisms of inter-leg coordination. Chapter 4 includes a series of experiments that detail the contralateral effect in response to unilateral stiffness perturbations. Chapters 5 and 6 provide an investigation and subsequent modeling of the sensorimotor mechanism underlying the observed contralateral effect. Chapter 7 presents three case studies with hemiplegic walkers which indicates the existence of the observed mechanism in neurologically impaired walkers. Finally, Chapter 8 summarizes the findings and impact of this research.

Chapter 2

BACKGROUND AND RELATED WORKS

2.1 Human Locomotion

The ability to stand upright and walk is one of the defining characteristics and unique abilities of humans. Locomotion results from intricate dynamic interactions between a central program, the dynamics of the body, and feedback mechanisms (Rossignol *et al.*, 2006). The central program relies on central pattern generators (CPGs) capable of generating the basic locomotor pattern (Dietz, 2003; Grillner, 2003; Guertin, 2009) and on various descending pathways that can trigger, stop, and steer locomotion (Nielsen, 2003; Rossignol *et al.*, 2006). The feedback originates from muscles and skin afferents as well as from supraspinal senses (vision, audition, vestibular) that dynamically adapt the locomotor pattern to the requirements of the environment (Rossignol *et al.*, 2006). Thus, the basic motor pattern for stepping is generated in the spinal cord, while fine control of walking involves various brain regions, including cerebral motor cortex, cerebellum, and brain stem (Dietz, 1996). A simplified diagram of human locomotion is shown in Figure 2.1.

2.1.1 Supra-spinal neural circuitry

Recent work has stressed the importance of descending inputs from motor cortex in shaping the CPG function and particularly in guiding post-lesional plasticity mechanisms (Yang and Gorassini, 2006). In fact it has been shown that for over-ground walking, a spinal pattern generator does not appear to be sufficient. Supraspinal control is needed to provide both the drive for locomotion as well as the coordination to negotiate a complex environment (Choi and Bastian, 2007; Christensen *et al.*, 2000a; Forrester *et al.*, 2008; Grillner *et al.*, 2008; Kuo, 2002; Nielsen, 2003; Norton,

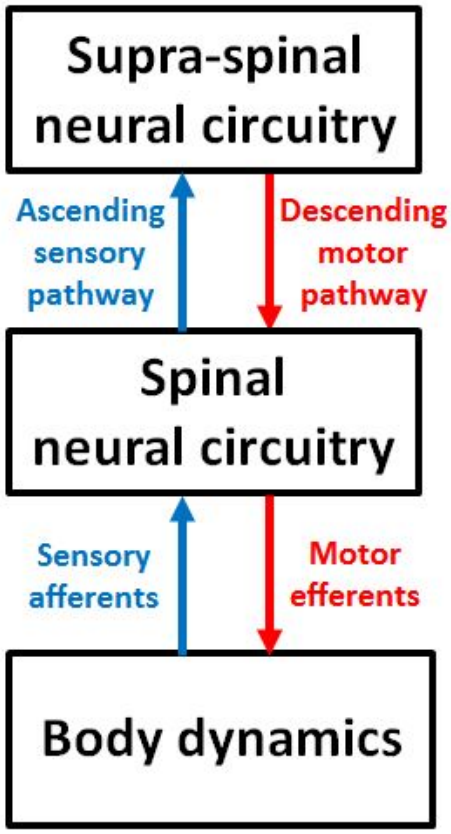

Figure 2.1: Simplified diagram of interactions between the central program and sensory feedback mechanisms with regard to human locomotion.

2010; Petersen *et al.*, 2012; Rossignol *et al.*, 2006). The latter is further supported by neuroimaging studies showing that rhythmic leg movements recruit the primary motor cortex (Dobkin *et al.*, 2004; Luft *et al.*, 2002; Sahyoun *et al.*, 2004; Wieser *et al.*, 2010). Electroencephalography (EEG) has been informative in recording of brain activity during walking by showing that measured brain activity is coupled to the gait cycle phase (Gwin *et al.*, 2011), suggesting distinct neural networks for feed-forward and feedback control (Presacco *et al.*, 2012), and correlation with kinematic parameters of gait (Fitzsimmons *et al.*, 2009).

The role of supraspinal centers on gait parameters has also been studied with transcranial magnetic stimulation (TMS) (Christensen *et al.*, 2001; Petersen *et al.*, 1998, 2001) and by frequency and time-domain analyses of muscle electromyography

(EMG) during gait (Molinari, 2009; Yang and Gorassini, 2006). Results from these two different approaches suggest that improvements in walking are associated with strengthening of descending input from the brain (Dollar and Herr, 2008).

2.1.2 Spinal neural circuitry

Substantial research has indicated that spinal cord contains neural circuitry capable of creating cyclical flexion/extension motor patterns independent of sensory feedback or supraspinal input (Dietz, 2003; Duysens and Van de Crommert, 1998; Grillner, 2003; Guertin, 2009; Yang *et al.*, 2004). In his highly influential work, Grillner (2003) defined these central pattern generators (CPGs) as networks of nerve cells that generate movements and enclose the information necessary to activate different motor neurons in the suitable sequence and intensity to generate motor patterns. The three key principles that characterize CPGs are the following: (a) the capacity to generate intrinsic pattern of rhythmic activity independently of sensory inputs; (b) the presence of a developmentally defined neuronal circuit; (c) the presence of modulatory influences from central and peripheral inputs.

2.1.3 Body Dynamics

In general, the human leg can be thought of as a structure with 7 degrees of freedom (DOF), with three rotational DOFs at the hip, one at the knee, and three at the ankle. Figure 2.2 (from Dollar and Herr (2008)) shows a description of the human anatomical planes (left) as well as a kinematic model of the human leg in the sagittal plane (right), which is the dominant plane of motion during human locomotion. In this dissertation, joint motion is only considered in the sagittal plane and is referred to as flexion (positive direction) and extension (negative direction) for the hip and knee

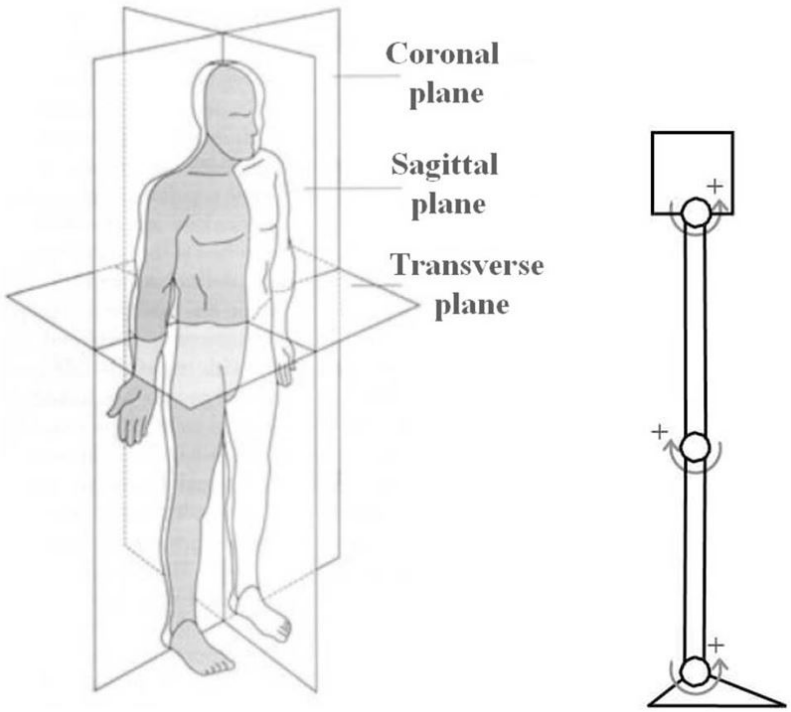

Figure 2.2: Description of the anatomical planes (left) and diagram of the leg shown with all joints at 0 degrees with the positive direction indicated (right), (from Dollar and Herr (2008)).

joints and dorsiflexion (positive direction) and plantarflexion (negative direction) for the ankle joint (Dollar and Herr, 2008).

The human walking gait cycle is typically represented as starting and ending at the point of heel strike on the same foot, with heel strike on the adjacent foot occurring at approximately 62% of gait cycle. Figure 2.3 (from Dollar and Herr (2008)) shows a simplified diagram of one gait cycle, with terms that will be used throughout this dissertation. The timing of the labeled events during the gait cycle is approximate and varies across individuals and conditions (Dollar and Herr, 2008).

2.2 Gait Rehabilitation

The goal of rehabilitation exercises is to perform specific movements that facilitate neural plasticity in order to improve motor recovery and minimize functional

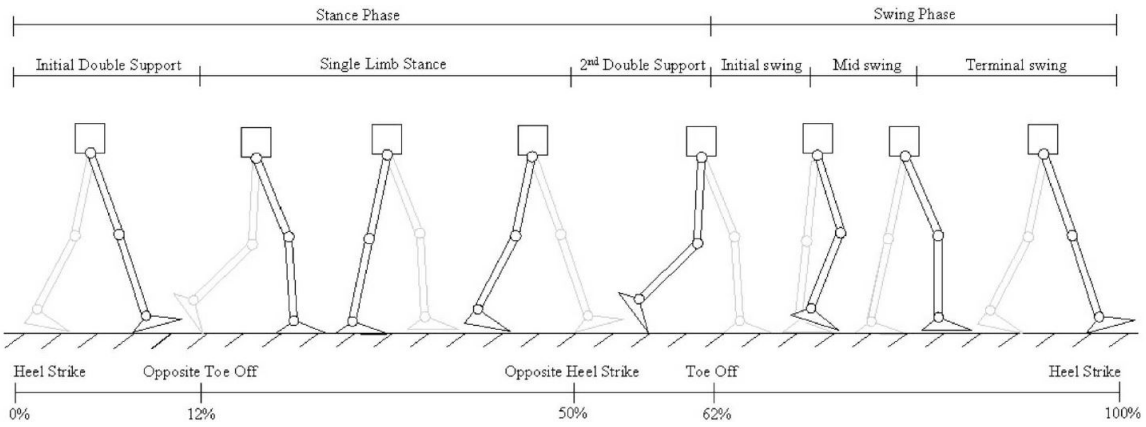

Figure 2.3: Human walking gait through one cycle, beginning and ending at heel strike. Percentages showing contact events are given at their approximate location in the cycle (Dollar and Herr, 2008).

deficits (Díaz *et al.*, 2011). The rehabilitation process toward regaining a meaningful mobility can be divided into three phases: (1) the bedridden patient is mobilized into a wheelchair as soon as possible, (2) restoration of gait, and (3) improvement of gait through walking exercises (Carr and Roberta, 1982; Chan *et al.*, 2006; Schmidt *et al.*, 2007). Thus, movement is a key to rehabilitation of gait impairments.

2.2.1 Conventional Approaches

Traditional therapies usually focus on treadmill training to improve functional mobility (Díaz *et al.*, 2011; Wernig *et al.*, 1995). This rehabilitation technique known as body-weight-supported treadmill training (BWSTT) has been widely used and standardized for rehabilitation of patients with gait impairments (Behrman and Harkema, 2000; Hesse *et al.*, 1995). In this technique three therapists assist the legs and hip of the patient walking on a treadmill while part of the patients body weight is supported by an overhead harness (Díaz *et al.*, 2011). A picture (from Helen Hayes Hospital, West Haverstraw, New York, USA) demonstrating BWSTT is shown in Figure 2.4. The advantages of BWSTT include adequate mobility of the walker, partial body-

Figure 2.4: Body-weight supported treadmill training. (Picture from Helen Hayes Hospital, West Haverstraw, New York, USA).

weight support, as well as controlled experimental environment equipped with many monitoring devices (Skidmore and Artemiadis (2016c), ©2016 IEEE). However, this traditional rehabilitation therapy is very labor intensive which limits the amount of training that the patient receives. Moreover, while some progress is made for many patients using this technique, one third of surviving stroke patients do not regain the ability to walk independently and those who are ambulatory, walk in a typical asymmetric manner (AHA, 2010).

2.2.2 Robot-assisted Gait Training

Many robotic systems have been developed with the aim to automate and improve gait training (Banala *et al.*, 2007; Galvez and Reinkensmeyer, 2005; Hesse *et al.*, 2000; Jezernik *et al.*, 2003; Morbi *et al.*, 2012; Peshkin *et al.*, 2005; Veneman *et al.*, 2007). Not only will automating existing therapies reduce the required manual labor of therapists (Galvez and Reinkensmeyer, 2005), but it will also facilitate more intense and repetitive training sessions that are important for stimulating neural plasticity (Kleim and Jones, 2008) which is the basic mechanism underlying improvement in functional

outcome after stroke (Belda-Lois *et al.*, 2011; Pekna *et al.*, 2012). While other groups of robotic systems for gait training exist (such as overground gait trainers (Goffer, 2006; Kawamoto *et al.*, 2009; Peshkin *et al.*, 2005)) and stationary gait trainers (Bouri *et al.*, 2009; Homma *et al.*, 2003; Schmitt and Métrailler, 2004)), only treadmill-based rehabilitation devices will be presented here because of the direct relationship with the treadmill experiments presented in this dissertation.

2.2.3 Treadmill-based Gait Trainers

Treadmill-based robotic training devices are mostly a combination of a body-weight support system, an exoskeleton type robot, and a controllable treadmill (Díaz *et al.*, 2011). Table 2.1 (adapted from Díaz *et al.* (2011)) summarizes the systems available in literature. Of the ten systems shown in the table, only three of them have been commercialized: the Lokomat, the LokoHelp, and the ReoAmbulator.

Commercial Systems

The Lokomat (Hocoma), shown in Figure 2.5, is the most clinically evaluated robotic gait-training system and arguably the most well known system of its type (Díaz *et al.*, 2011). It consists of a robotic gait orthosis, a body weight support system, and a treadmill. It uses computer controlled motors at each hip and knee joint that are precisely synchronized with the speed of the treadmill to assure a precise match between the speed of the gait orthosis and the treadmill (Colombo *et al.*, 2000).

The LokoHelp (LokoHelp Group), shown in Figure 2.6, is an electromechanical device developed for improving gait after brain injury (Freivogel *et al.*, 2008). The LokoHelp is placed on the treadmill and fixed to the front of the treadmill with a clamp. A body weight support system is also included to provide body weight support for the patient.

Table 2.1: Robotic systems for treadmill gait training (adapted from Díaz *et al.* (2011))

Robotic system	Company	Reference
Lokomat	Hocoma	Colombo *et al.* (2000)
LokoHelp	LokoHelp Group	Freivogel *et al.* (2008)
ReoAmbulator	Motorika Ltd.	West (2004)
ARTHuR	-	Reinkensmeyer *et al.* (2002)
POGO and PAM	-	Reinkensmeyer *et al.* (2006)
ALEX	-	Banala *et al.* (2007)
LOPES	-	Veneman *et al.* (2007)
ALTACRO	-	Beyl *et al.* (2008)
RGR	-	Pietrusinski *et al.* (2010)
String-Man	-	Surdilovic and Bernhardt (2004)

Figure 2.5: Lokomat by Hocoma.

Figure 2.6: LokoHelp by LokoHelp Group.

The ReoAmbulator (Motorika Ltd.), shown in Figure 2.7, is another commercialized body-weight-supported treadmill robotic system. Robotic arms are strapped to the patient's legs at the thigh and ankle and drive the legs through a prescribed walking pattern (West, 2004).

Systems Under Development

Other robotic systems for gait rehabilitation are still in a state of research or under development (Díaz *et al.*, 2011). The Biomechatronics Lab at the University of California has developed several robotic devices for locomotor training after spinal cord injury. These include the Ambulation-assisting Robotic Tool for Human Rehabilitation (ARTHuR), a device designed to measure and manipulate human stepping on a treadmill (Reinkensmeyer *et al.*, 2002); the Pneumatically Operated Gait Orthosis

Figure 2.7: ReoAmbulator by Motorika Ltd.

(POGO), an improved leg-robot design; and the Pelvic Assist Manipulator (PAM), a device that can accommodate and control naturalistic pelvic motion (Reinkensmeyer *et al.*, 2006).

The Active Leg Exoskeleton (ALEX) is a powered leg orthosis with linear actuators at the hip and knee joints. The device implements an assist-as-needed approach by providing assistance to the patient based a force-field controller that minimizes the error from a target motion (Banala *et al.*, 2007).

The LOwer-extremity Powered ExoSkeleton (LOPES) is a gait rehabilitation robot that can move in parallel with the legs of a person walking on a treadmill. Bowden-

cable driven series elastic actuators reduce the moving mass on the exoskeleton by separating the motors from the frame (Veneman *et al.*, 2007).

The Automated Locomotion Training using an Actuated Compliant Robotic Orthosis (ALTACRO) rehabilitation exoskeleton is a step rehabilitation robot that utilizes lightweight, compliant, pneumatic actuators. The device consists of a unilateral exoskeleton and a supportive arm that passively gravity-balances the device (Beyl *et al.*, 2008).

The Robotic Gait Rehabilitation (RGR) Trainer uses an impedance control strategy and a linear electromagnetic actuator to apply a force field to correct secondary gait deviations in pelvic motion. The device is coupled to the patient via an orthopedic brace which interacts with the patient in a way that mimics the interaction with a therapist (Pietrusinski *et al.*, 2010).

Finally, the String-Man (Surdilovic and Bernhardt, 2004), is a unique robotic system for supporting gait rehabilitation and restoration of motor functions. Based on the "string-puppet" principle, it has a particular kinematic structure with 7 wires attached to the trunk of the patient which provides the capability to control the posture of the subject in 6 degrees of freedom, as well as to balance the weight on the legs according to different gait patterns and training programs. Moreover, by sensing the interaction forces, the system can quantify the effort of the patient and control the force interactions.

Limitations

Despite the design of several robotic devices for rehabilitation of sensorimotor function, their widespread use remains somewhat limited by a number of factors, including the assessment of the true cost-to-benefit ratio relative to other types of rehabilitation approaches. Moreover, there have been conflicting results from recent studies about

the effectiveness of these robotic devices. Some studies report that when compared to conventional therapy, robotic rehabilitation achieves greater functional outcome (Mayr *et al.*, 2007; Pohl *et al.*, 2007), while others indicate less improvement (Hidler *et al.*, 2009; Hornby *et al.*, 2008). The general consensus is that there is only is no clear evidence of improvement in walking and motor recovery using robotic devices, including systems for (BWSTT), when compared to conventional therapy (Barbeau and Visintin, 2003; Bates *et al.*, 2005; Chang and Kim, 2013; Hidler *et al.*, 2009; Hornby *et al.*, 2008; Luft *et al.*, 2008; Mayr *et al.*, 2007; Riener *et al.*, 2005). Therefore, simply automating traditional therapy, which these robotic devices attempt to do, does not appear to be sufficient for improving therapy outcomes.

What previous methods fail to take advantage of is that locomotion can be mainly characterized as a dynamical process that involves inter-leg coordination and sensory feedback mechanisms from the environment. A limitation of the robotic devices used for gait therapy is that they consider locomotion as a kinematic process, and thus impose a prescribed motion. However, they do not consider mechanisms of inter-leg coordination and how the sensory feedback from one leg affects the motion of the other leg. Human walking, in addition to running and stair climbing, requires inter-limb coordination and neural coupling (Arya and Pandian, 2014). A recent review suggests that utilizing inter-limb coupling in stroke rehabilitation therapies will lead to improved functional outcome (Arya and Pandian, 2014). As an example, Johannsen *et al.* (2009) showed that chronic stroke patients performing seated bilateral leg exercises had increased step length during treadmill walking. Therefore, a fundamental understanding of underlying sensorimotor mechanisms of inter-leg coordination may facilitate improved robotic interventions in gait therapy (Skidmore and Artemiadis, 2016a).

2.3 Inter-leg Coordination

Inter-leg coordination can be defined as an interaction between segment kinematics, joint dynamics and muscle activity through time (Rose and Winstein, 2013). This coordination between legs is a fundamental mechanism of gait and has received increased attention during the last decade due to its implications on post-stroke therapy (Arya and Pandian, 2014). Inter-leg coordination is a process that involves multiple feedback channels and coupling mechanisms both in mechanical and neural levels. Neural coupling exists in poststroke patients as it does in healthy subjects (Arya and Pandian, 2014). In studies with poststroke subjects with hemiparesis, it was found that neural decoupling between the lower limbs perturbs the paretic lower limb function (Kautz and Patten, 2005). It has been also shown that forceful interaction with the non-paretic leg elicits involuntary tension of the resting paretic leg when subjects are supine (Poskanzer, 1972).

Investigation of the role of afferent sensory feedback to gait control mechanisms of inter-leg coordination usually involve sensory perturbations and the analysis of their effects (Skidmore and Artemiadis, 2016a). Various platforms and protocols have been used to investigate bilateral reflex mechanisms during different phases of the gait cycle (Artemiadis and Krebs, 2011a,b; Dietz *et al.*, 1989; Nakazawa *et al.*, 2004; van der Linden *et al.*, 2007), with the majority of the experimental protocols focusing on over-ground walking and dropping of the supportive surfaces at distinct gait phases (Artemiadis and Krebs, 2011a,b; Nakazawa *et al.*, 2004; van der Linden *et al.*, 2007). Perturbations to the load (i.e. force felt by the foot) feedback as well as the length of specific muscles during walking have been associated with evoked muscular activations of the unperturbed leg (Af Klint *et al.*, 2009; Berger *et al.*, 1987, 1984; Dietz *et al.*, 1989, 1994; Lam *et al.*, 2003). For example, unloading of the plantarflexor muscles by

unilaterally dropping the walking surface during stance phase significantly decreases soleus muscle activity of the contralateral leg (Af Klint *et al.*, 2009).

One significant limitation of the previous studies is that the sensory perturbations presented in the previous experiments were almost exclusively caused by dropping the walking surface, which causes a disruption in both force and kinesthetic feedback. When the walking surface is dropped there is a change in leg kinematics, and the force feedback on the bottom of the foot is lost as the foot loses contact with the walking surface. These types of perturbations do not provide any separation of those two sources of sensory feedback, and do not allow further in-depth investigation of the role of force and kinesthetic feedback in gait. In order to answer important questions on inter-leg coordination and sensorimotor control, it is desirable, therefore, to differentiate force and kinesthetic feedback. Adjustment of the stiffness of the walking surface is a unique way to achieve this differentiation, since stepping on a low stiffness platform continues to provide force feedback but affects leg kinematics (Skidmore and Artemiadis, 2016a).

A few studies have utilized compliant surfaces in researching sensorimotor mechanisms in human locomotion including while stepping on/off, hopping, or walking on a compliant surface (Dixon *et al.*, 2000; Ferris *et al.*, 1999; Hardin *et al.*, 2004; MacLellan and Patla, 2006; Marigold and Patla, 2005; Moritz *et al.*, 2004). The simplest setups include surfaces created out of foam of varying stiffness (MacLellan and Patla, 2006; Marigold and Patla, 2005), or collegiate gym mats (Chang *et al.*, 2010). However, inherent in these setups is the inability to utilize a large range of stiffness while maintaining high resolution – without employing an extreme number of materials. McMahon and Greene (1979) began the development of devices that allow for easy adjustment of stiffness between experiments decades ago with a setup that included simply supported plywood boards where the stiffness is changed by

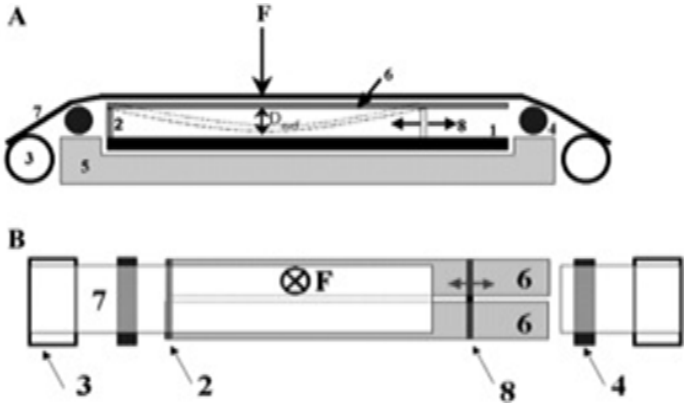

Figure 2.8: Side view (A) and top view (B) of adjustable compliant walking surface used by Kerdok *et al.* (2002)

adjusting the distance between the two supports. More recently, Kerdok *et al.* (2002) also utilized the concept of the deformation of a supported compliant beam in their development of a compliant track treadmill shown in Figure 2.8. While improving the easiness and resolution of compliant walking surfaces, these designs do not allow for the compliance of the surface to be changed in situ.

While the majority of these studies focus primarily on the perturbed leg or the center of mass of the walker (Dixon *et al.*, 2000; Ferris *et al.*, 1999; Hardin *et al.*, 2004; Moritz *et al.*, 2004), the bilateral response has also been investigated (MacLellan and Patla, 2006; Marigold and Patla, 2005). For example, Marigold and Patla (2005) showed that the contralateral tibialis anterior was activated 140 ms later than the normal condition when healthy subjects unexpectedly stepped onto a foam mat in the walkway. Another study has also shown that walking on a compliant surface creates activation of the tibialis anterior and soleus in both legs when compared to walking on a rigid surface (MacLellan and Patla, 2006). However, these studies lack the ability to vary the magnitude and timing of the walking surface stiffness perturbations within the gait cycle (Skidmore and Artemiadis, 2016a).

Moreover, another limitation of all of the previously mentioned works, including those utilizing compliant surfaces, is that the previous studies have failed to separate the mechanisms of inter-leg coordination from that of balance support. As a result, mechanical perturbations and sudden load changes would have likely triggered reflex mechanisms and vestibular responses to maintain balance and stability. However, little is known whether the bilateral activations are exclusively caused by the mechanisms required for body stabilization and balance maintenance, or if it is also brought about from inter-limb coordination and mechanisms of gait. This lack of knowledge leaves a significant gap in our understanding of sensorimotor control of gait and the effect of surface stiffness on gait mechanisms (Skidmore and Artemiadis, 2016a).

Chapter 3

EXPERIMENTAL PLATFORM: VARIABLE STIFFNESS TREADMILL

In this chapter the Variable Stiffness Treadmill (VST) system is developed and characterized in preparation for investigating the role of surface stiffness in inter-leg coordination mechanisms.

3.1 System Overview

The VST provides a unique platform for investigation of the role of walking surface stiffness in inter-leg coordination mechanisms. Advantages of the VST over other experimental platforms include (1) a wide range of controllable stiffness while maintaining high resolution, (2) the ability to apply low stiffness perturbations at any phase of the gait cycle and (3) body-weight support for the walker in order to suppress mechanisms of balance and posture (Skidmore and Artemiadis, 2016a). The VST achieves greater versatility and functionality than other devices by combining a variety of components into one unique system. The device is shown in Figure 3.1. The major components of the VST include a variable stiffness mechanism, a linear track (Thomson Linear Inc), a split belt treadmill, a DC treadmill motor (Anaheim Automation), a counter-weight system, and a custom-built body weight support (Lite-Gait) with two loadcells that measure the weight of the subject being supported by the system. Each component is important to the system for the overall function and proper investigation of gait and will be analyzed below (Barkan *et al.* (2014),).

3.1.1 Variable Stiffness Mechanism

The main novel feature of the VST is the ability to vary the vertical stiffness of the walking surface (i.e. treadmill), therefore controlling the kinetic and kinematic

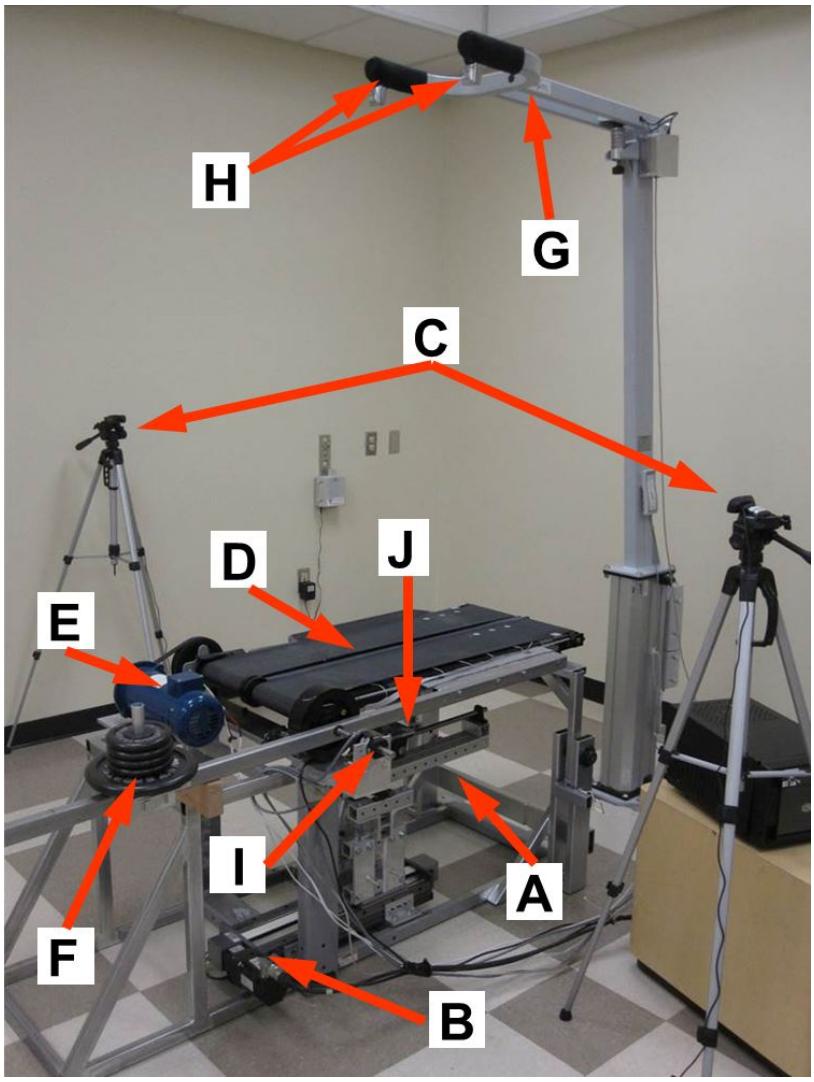

Figure 3.1: The Variable Stiffness Treadmill (VST) System. Subsystems shown include: A) Variable stiffness mechanism, B) Linear track, C) Motion capture system, D) Split-belt treadmill, E) Treadmill motor, F) Counter-weight system, G) Custom-made harness-based body-weight support, H) BWS loadcells, I) Rotary encoder for treadmill inclination measurement, J) Loadcell for walker foot force measurement (adapted from (Skidmore *et al.* (2015), ©2015 IEEE)).

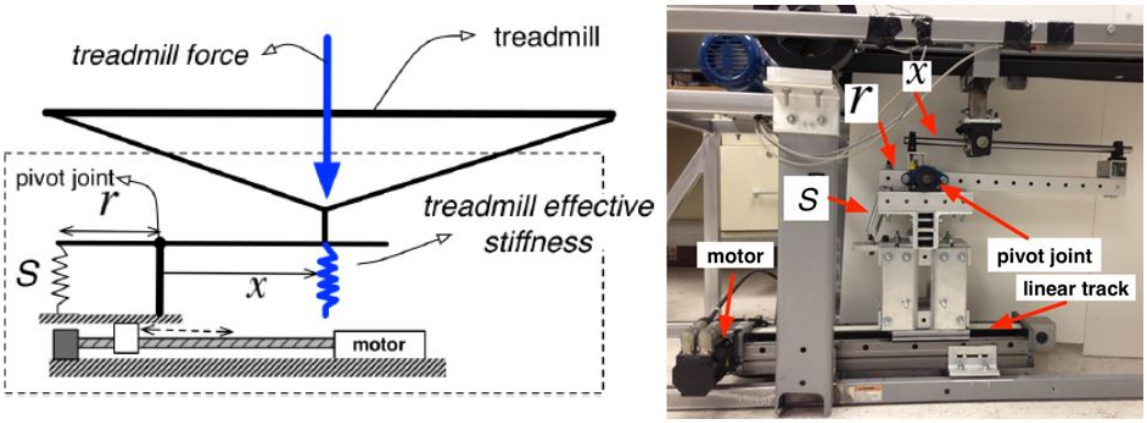

Figure 3.2: The variable stiffness mechanism. Conceptual diagram (left) and actual setup (right) (adapted from (Skidmore *et al.* (2015), ©2015 IEEE)).

interaction between the walker and the walking surface. The capability of the VST to achieve a large range of controllable stiffness with high resolution comes from a novel variable stiffness mechanism. In its most simplified form, the variable stiffness mechanism is a spring-loaded lever mounted on a translational track, as shown in Figure 3.2. The effective stiffness of the treadmill, located at a distance x from the pivot joint, is dependent on the coefficient of stiffness S of the linear spring and the moment arm r through which it exerts a force (Jafari *et al.*, 2011). By design, S and r remain constant, therefore, the effective stiffness of the treadmill can be controlled by changing the distance x (Skidmore *et al.* (2015), ©2015 IEEE).

In order to achieve the desired range of stiffness, the variable stiffness mechanism was built with two extension springs of stiffness $k = 5122$ N/m, rest length $l_0 = 12.7$ cm, and outside diameter $OD = 2.54$ cm (LE 135J 06 M, Lee Spring Co.). The two springs are combined in parallel, and are attached to the lever arm at a distance of 7.5 cm from the pivot point. The spring stiffness was chosen to meet the specification for the range of effective treadmill stiffness, which is analyzed below (Skidmore *et al.* (2015), ©2015 IEEE).

This entire assembly sits on the carriage of a high-capacity linear track (Thomson Linear, Part Number: 2RE16-150537) which is controlled by a high-precision drive (Kollmorgen, Part Number: AKD-P00606-NAEC-0000) and has a translational resolution of 0.01 mm. This results in a high resolution for the adjustment of effective stiffness, which is discussed below (Skidmore *et al.* (2015), ©2015 IEEE).

In addition to achieving the desired range and resolution of stiffness with the variable stiffness mechanism, the treadmill stiffness can also be varied actively throughout the gait cycle. In the most extreme scenario of going from a rigid surface, i.e. treadmill stiffness of $k_t = \infty$, to the minimum achievable stiffness, the linear track will have to move across its entire range (0 to 0.40 m). Considering that the linear track can move as fast as 3 m/s, the system could make this extreme change in stiffness in 0.13 s. Assuming that the subject is walking at a normal pace of 1.4 m/s (Browning *et al.*, 2006; Levine and Norenzayan, 1999), with a stride length (the distance between consecutive points of initial contact by the same foot) of 1.4 m (Perry and Burnfield, 1992), the stance phase would last approximately 0.5 s. This means that the variable stiffness mechanism can make this extreme change in stiffness three times during the stance phase. Therefore, it can easily change stiffness many times throughout the gait cycle when the desired change in stiffness is smaller than the two extreme values. The ability to change stiffness at a high rate throughout the stance phase of the gait cycle adds to the unique capabilities of the VST (Skidmore *et al.* (2015), ©2015 IEEE).

3.1.2 Additional Components

Motion capture

Another important component of the VST is a low-cost and portable motion capture system comprised of infrared cameras (Code Laboratories Inc, model: DUO MINI

LX) and infrared LEDs (Super Bright LEDs Inc, model: IR-1WS-850). The motion capture is important for tracking the location of the subject's foot in order to maintain the desired stiffness underneath the walker, and for precise timing of stiffness perturbations within the gait cycle. The motion capture system is also used for recording lower-limb joint angles throughout the gait cycle. The two cameras tracking the two legs are shown in Figure 3.1, part C (Skidmore and Artemiadis, 2016a).

Split-belt treadmill

The VST employs a split-belt treadmill configuration in order to allow each belt to deflect different amounts. This will allow different force perturbations to be applied to each leg. The treadmill belts are supported at 0.70 m above the floor on a frame of steel tubing that permits each belt to independently deflect downward to a maximum of 30° from the horizontal position. The adjustability of the treadmill stiffness is currently limited to only one belt, but can be applied to both sides by installing another variable stiffness mechanism. The split belt treadmill is shown in Figure 3.1, part D (Skidmore *et al.* (2015), ©2015 IEEE).

Treadmill motor

A 1-HP variable speed DC motor (Anaheim Automation, Part Number: BDA-56C-100-90V-1800) drives the treadmill belts. Speeds of up to 1.85 m/s at a resolution of 7 mm/s can be achieved. This includes the average preferred walking speed of 1.2-1.4 m/s (Browning *et al.*, 2006; Levine and Norenzayan, 1999), but can be slowed for individuals in therapy or rehabilitation applications. The treadmill motor is shown in Figure 3.1, part E (Skidmore *et al.* (2015), ©2015 IEEE).

Counterweight

One necessary component to ensure accurate control of treadmill stiffness is a counterweight system to eliminate moments created by the weight of the treadmill belts. This is achieved by fastening a weighted slider at the precise location along a co-linear beam which will induce an equal and opposite moment to that of the treadmill. This beam is attached to the side of the treadmill platform so that the counterweight system will cancel out the weight of the treadmill at any inclination of the treadmill. The counterweight is shown in Figure 3.1, part F (Skidmore *et al.* (2015), ©2015 IEEE).

Body weight support

Separate from the treadmill structure, there is a custom-built body weight support designed by LiteGait. By adjusting the height of the support system, full or partial body-weight support can be provided. This is an important capability for controlling the ground reaction forces created by the weight of the subject. In addition, the support increases safety and extends the system's capabilities to stroke patients and other individuals with decreased mobility and stability. Two loadcells attached on the body-weight support harness measure the subject's weight supported by the mechanism from each side. The body weight support and the loadcells are shown in Figure 3.1, parts G and H respectively (Skidmore *et al.* (2015), ©2015 IEEE).

Rotary encoder

The angular deflection of the walking surface is measured with a rotary encoder (Encoder Products Company, Model Number: 260-N-T-11-S-1024-Q-HV-1-S-SF-1-N) in order to calculate the actual stiffness of the treadmill walking surface. The encoder has 1024 cycles per revolution resulting in an angular resolution of 0.35°.

The rotary encoder is shown in Figure 3.1, part I (Skidmore *et al.* (2014), ©2014 IEEE).

Loadcell

The force exerted by the foot of the walker is calculated from the force measured by a 500 kg S Type Loadcell (RobotShop, Part Number RB-Phi-204) which is placed at the junction of the treadmill belt and the variable stiffness mechanism. This force is also used in the calculation of the measured stiffness of the treadmill. The loadcell is shown in Figure 3.1, part J (Skidmore *et al.* (2014), ©2014 IEEE).

3.2 System Modeling

The relationship between a desired stiffness and the actual effective stiffness of the treadmill is described by the governing equations of the system and the plant dynamics. The system is displayed in block diagram form in Figure 3.3 where the desired treadmill stiffness (k_t^d) is the reference signal, the desired linear track position (x_{track}^d) is the control input, the angular deflection of the treadmill (θ_1) under an applied load is the result of the track movement, and the actual measured stiffness (k_t) is the final output. The transfer functions (G_1, G_2) are relationships between variables of the system and are determined by the governing equations. The plant is the combination of the dynamics of the linear actuator and the treadmill platform. The governing equations (reprinted with permission from Barkan *et al.* (2014), ©2014 IEEE) and dynamics of the system (reprinted with permission from Skidmore *et al.* (2015), ©2015 IEEE) are discussed separately below (Skidmore *et al.* (2015), ©2015 IEEE).

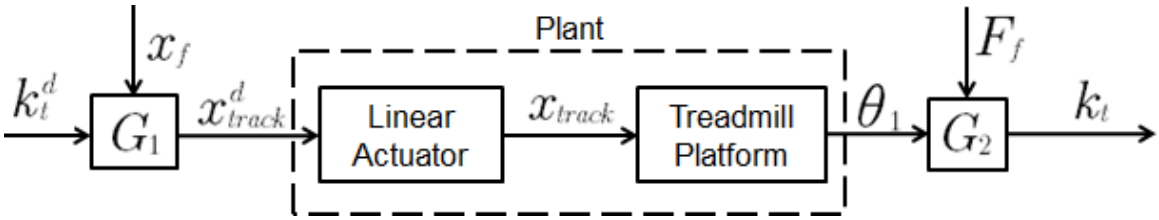

Figure 3.3: Block diagram of the open loop system (reprinted with permission from Skidmore *et al.* (2015), ©2015 IEEE).

3.2.1 Governing Equations

Both of the transfer functions of the system mentioned above are solutions to the governing equations and are used to relate the inputs and outputs of the system. The transfer function G_1 was found by performing a kinematic and kinetic analysis of the VST in order to create a mathematical model relating the desired treadmill stiffness k_t^d and the foot position x_f to the desired track position x_{track}^d.

3.2.1.1 Kinematics

To begin, the vector loop shown in Figure 3.4 was created based off of the rigid body structure of the VST. The vector loop equations are given by:

$$\mathbf{R_1}+\mathbf{R_2}=\mathbf{R_8}+\mathbf{R_7}+\mathbf{R_6}+\mathbf{R_5}+\mathbf{R_4}+\mathbf{R_3} \tag{3.1}$$

where $\mathbf{R_i}$, $i = 1, 2, \ldots, 8$ are the vectors shown in Figure 3.4. Resolving this vector equation into its x and y components using the reference system shown in Figure 3.4, we have:

$$\begin{aligned} \sum_{i=1,2} \|\mathbf{R}_i\| \cos(\theta_i) &= \sum_{m=3,4,5,6,7,8} \|\mathbf{R}_m\| \cos(\theta_m) \\ \sum_{i=1,2} \|\mathbf{R}_i\| \sin(\theta_i) &= \sum_{m=3,4,5,6,7,8} \|\mathbf{R}_m\| \sin(\theta_m) \end{aligned} \tag{3.2}$$

where θ_i, $i = 1, 2, \ldots, 8$ are the angles of the vectors $\mathbf{R_i}$, $i = 1, 2, \ldots, 8$ from the positive x-axis, measured counterclockwise. Some of the vectors are not rotating due

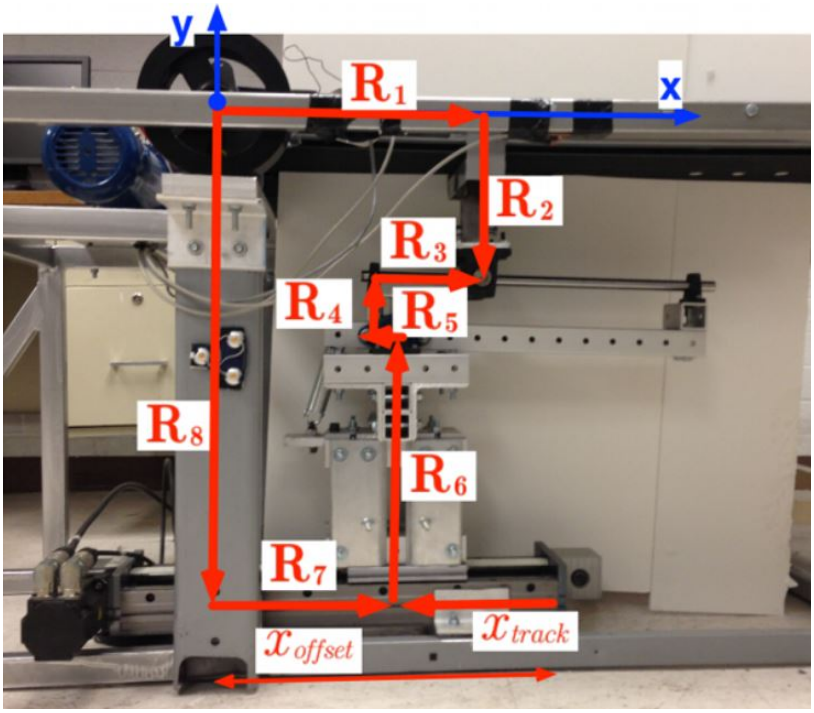

Figure 3.4: Kinematic analysis of variable stiffness mechanism (reprinted with permission from Barkan *et al.* (2014), ©2014 IEEE)

to structural constraints that are listed in Table 3.1. Because of this, the kinematic equations in (3.2) are simplified to:

$$\begin{aligned} \|\mathbf{R_1}\|\, c_1 + \|\mathbf{R_2}\|\, s_1 &= \quad x_{offset} - x_{track} - \|\mathbf{R_5}\|\, c_3 - \|\mathbf{R_4}\|\, s_3 + \|\mathbf{R_3}\|\, c_3 \\ \|\mathbf{R_1}\|\, s_1 - \|\mathbf{R_2}\|\, c_1 &= \quad -\|\mathbf{R_8}\| + \|\mathbf{R_6}\| - \|\mathbf{R_5}\|\, s_3 + \|\mathbf{R_4}\|\, c_3 + \|\mathbf{R_3}\|\, s_3 \end{aligned} \tag{3.3}$$

where c_i, s_i correspond to $\cos(\theta_\mathbf{i})$ and $\sin(\theta_\mathbf{i})$ respectively, and x_{offset} is the known horizontal distance from the rotation point of the treadmill to the zero position of the linear track.

These two equations were then solved for the two unknown variables $\|\mathbf{R_3}\|$ and θ_3 in terms of the inputs θ_1 and x_{track}. It must be noted that a rotary encoder (Encoder Products Company, Model Number: 260-N-T-11-S-1024-Q-HV-1-S-SF-1-N, 1024 cycles per revolution) was used in order to measure the treadmill angular

Table 3.1: Kinematic Constraints (reprinted with permission from Barkan *et al.* (2014), ©2014 IEEE).

Vector magnitudes (m)		Vector angles (rad)	
$\|\mathbf{R_1}\|$	0.33	θ_6	$\frac{\pi}{2}$
$\|\mathbf{R_2}\|$	0.18	θ_7	0
$\|\mathbf{R_4}\|$	0.085	θ_8	$\frac{-\pi}{2}$
$\|\mathbf{R_5}\|$	0.02	θ_{3a}	0
$\|\mathbf{R_6}\|$	0.44	θ_{4a}	$\frac{\pi}{2}$
$\|\mathbf{R_8}\|$	0.705	θ_2	$\theta_1 - \frac{\pi}{2}$
$\|\mathbf{R_{2a}}\|$	0.075	θ_5	$\theta_3 - \pi$
$\|\mathbf{R_{3a}}\|$	0.11	θ_4	$\theta_3 + \frac{\pi}{2}$
x_{offset}	0.325		
$\|\mathbf{R_{4a}}\|$	0.12	θ_{2a}	θ_3
$\|\mathbf{R_7}\|$	$x_{offset} - x_{track}$		

deflection θ_1, while the position of the linear track x_{track} is controlled in real-time via a dedicated controller in order to achieve the desired stiffness.

The same method was used in order to describe the kinematics of the spring mechanism shown in Figure 3.5. The final equations that were solved for the two unknowns $\|\mathbf{R_{1a}}\|$ and θ_{1a} are given by:

$$\begin{aligned} \|\mathbf{R_{1a}}\| \cos(\theta_{\mathbf{1a}}) + \|\mathbf{R_{2a}}\| \cos(\theta_{\mathbf{3}}) &= \|\mathbf{R_{3a}}\| \\ \|\mathbf{R_{1a}}\| \sin(\theta_{\mathbf{1a}}) + \|\mathbf{R_{2a}}\| \sin(\theta_{\mathbf{3}}) &= \|\mathbf{R_{4a}}\| \end{aligned} \tag{3.4}$$

where all vectors are shown in Figure 3.5, along with their correspondence to the real platform features.

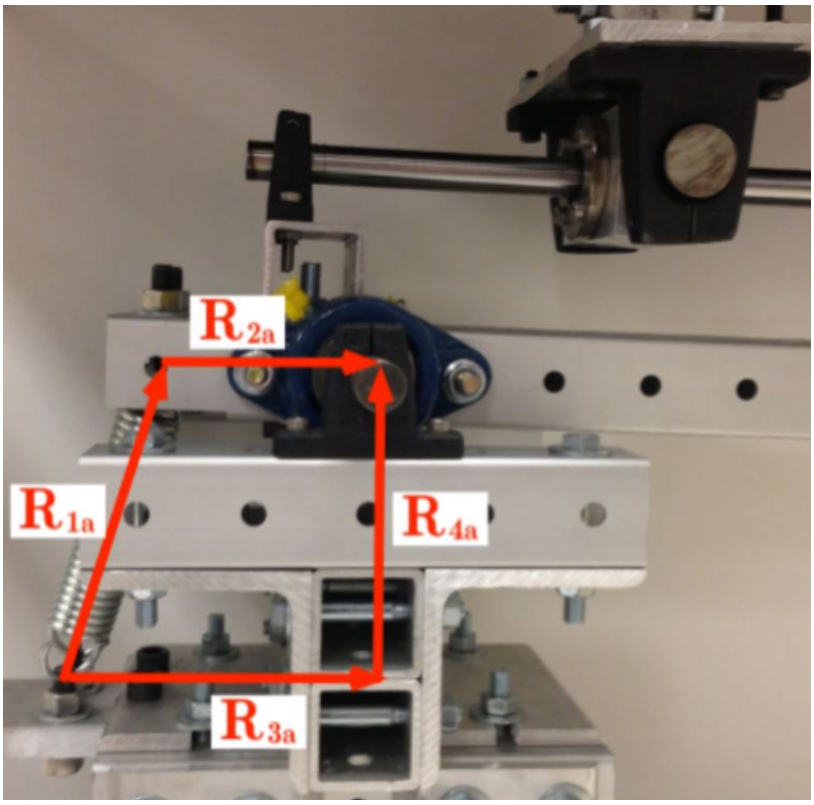

Figure 3.5: Kinematic analysis of the spring mechanism(reprinted with permission from Barkan *et al.* (2014), ©2014 IEEE).

3.2.1.2 Kinetics

The final step in the mathematical model of the VST was to use the solutions of unknown variables from the kinematic analysis and apply them to the equilibrium equations for the free body diagrams of the VST, shown in Figure 3.6, where F_s is the force exerted by the spring. Since the connection point at B is a sliding joint, the force that it transmits at mechanical equilibrium can only be perpendicular to the sliding axis along $\mathbf{R_3}$. This allowed for the calculation of the transmitted force F_B with the following moment equation about location D.

$$\sum \mathrm{M_D} = F_s \|\mathbf{R_{2a}}\| sin(\theta_{\mathbf{3}} - \theta_{\mathbf{1a}}) - F_B(\|\mathbf{R_3}\| - \|\mathbf{R_5}\|) = 0 \tag{3.5}$$

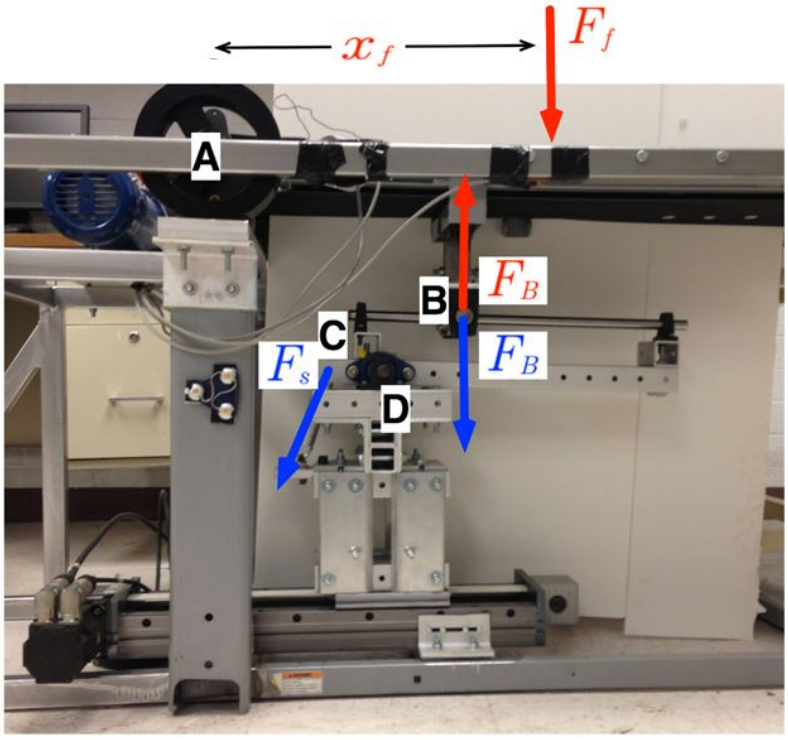

Figure 3.6: VST kinetics. F_f is the force exerted by the subject's foot at a distance x_f from the rotation point of the treadmill (location A). F_s is the spring force and F_B the force at the sliding joint B (reprinted with permission from Barkan *et al.* (2014), ©2014 IEEE).

where F_s=$2k(\|\mathbf{R_{1a}}\| - \mathrm{l}_0)$ is the force from the springs and l_0 is the rest length of the two springs, each one having a stiffness k. The calculated value for F_B was used to solve for the force of the foot F_f in the equilibrium equation about point A:

$$\sum \mathrm{M_A}=F_B\|\mathbf{R_1}\|cos(\theta_\mathbf{3}-\theta_\mathbf{1})-F_B\|\mathbf{R_2}\|sin(\theta_\mathbf{3}-\theta_\mathbf{1})-F_f x_f cos(\theta_\mathbf{1})=0 \tag{3.6}$$

Then, the effective stiffness of the treadmill k_t is computed by:

$$k_t=\frac{dF_f}{dy} \tag{3.7}$$

which is a function of x_f, x_{track}, and θ_1. Although θ_1 is one of the equation variables, it was observed that the difference in the solution to this equation with

$\theta_1 = 0$ instead of being a variable was negligible. Therefore, setting $\theta_1 = 0$ resulted in x_{track} as a function of k_t^d and x_f, which could easily put into a two dimensional lookup table to increase computational efficiency.

In the end, this system of equations results in a known relationship (G_1) that gives x_{track}^d based on input values k_t^d and x_f:

$$G_1{=}x_{track}^d{=}f\left(k_t^d,\, x_f\right). \tag{3.8}$$

The results obtained from the mathematical model were compared to experimental data for validation. The apparent stiffness of the treadmill for 0.01 m interval displacements of the linear track was found by placing a known mass (3.9 kg) at an arbitrary distance (0.66 m) along the treadmill and measuring the angular displacement of the treadmill. This process resulted in a plot of stiffness vs the track position. The resulting curve was compared to the theoretical model where the foot position x_f was defined as 0.66 m to match the experimental setup. The results are shown in Figure 3.7.

It can be observed that both models achieve the same type of inverse square power profile and converge at low stiffness. The slightly higher stiffness values from the experimental data in parts of the domain may reflect the fact that friction is not accounted for in the theoretical model. Friction would cause a decrease in deflection for a given force resulting in higher stiffness values than a frictionless model. However, the theoretical model matched the experimental data very well, proving the validity of our system. This plot also gives an indication of the range of achievable stiffness as a function of the linear track position.

The range of the control of the track position defines the range of the treadmill effective stiffness that can be achieved. For $x_{track} = 0$, the treadmill stiffness is infinite, since the treadmill cannot be deflected. For the maximum displacement of the track

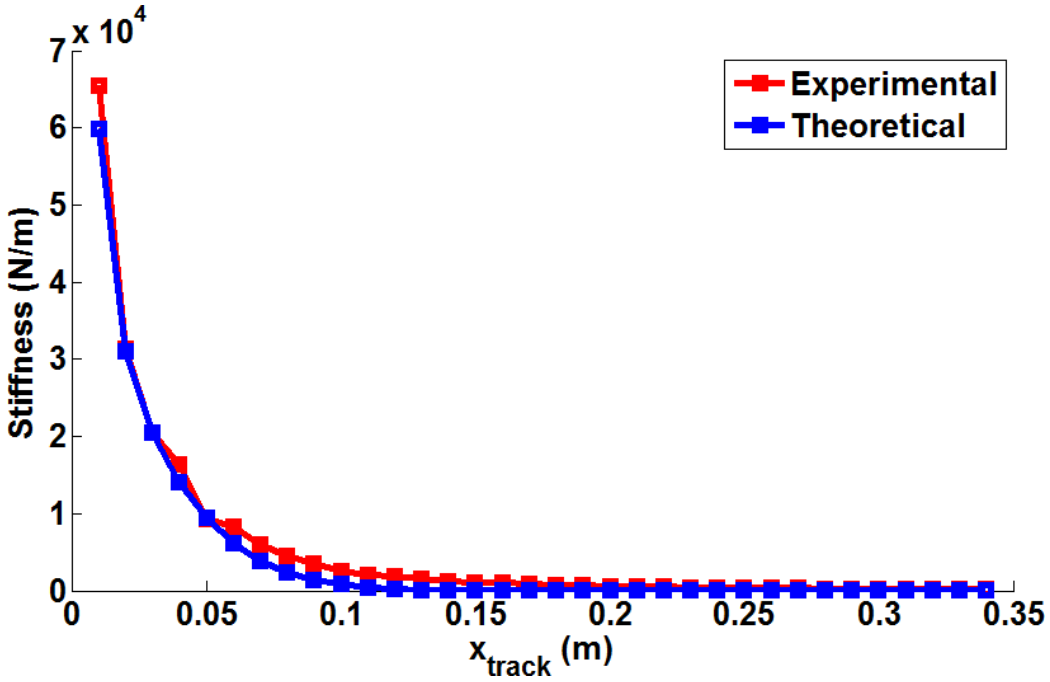

Figure 3.7: Experimental vs theoretical values of treadmill effective stiffness.

of 0.40 m, the computed treadmill stiffness, assuming that the foot of the subject is approximately in the middle of the treadmill (i.e. during mid-stance), is 585.5 N/m. At the end of the treadmill (i.e. at toe-off phase), the minimum achievable stiffness is 61.7 N/m.

The resolution of achievable displacement of the linear track is 0.01 mm. Since the relationship between the linear track position and the treadmill effective stiffness is non-linear, the resolution of achievable treadmill stiffness is dependent on the linear track position. By solving the equations derived above and using the given linear track resolution, the resolution of stiffness for any given linear track position can be computed. This solution curve is depicted in Figure 3.8, where it is shown that the resolution of stiffness can range from 9.06 N/m when the linear track is at 0.05 m, to 0.038 N/m when the linear track is at its maximum displacement of 0.40 m. Higher values for resolution are achieved for a position between 0 and 0.05 m of the linear track, as stiffness grows to infinity.

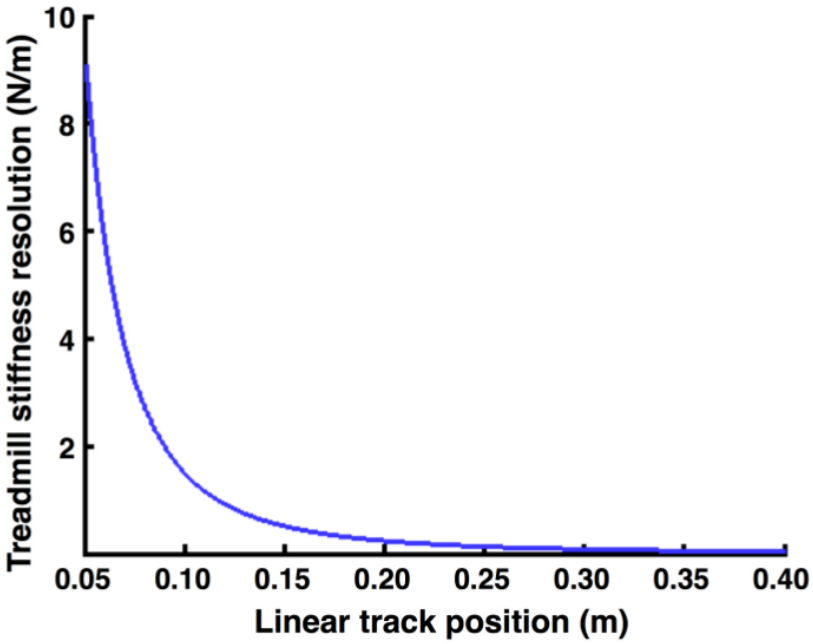

Figure 3.8: Treadmill stiffness resolution as a function of the linear track position(reprinted with permission from Barkan *et al.* (2014), ©2014 IEEE).

The transfer function G_2 describes the relationship between the actual treadmill stiffness, the force exerted by the foot and the deflection of the treadmill. This is found by application of Hooke's Law where the actual treadmill stiffness k_t is computed by the ratio of the vertical force F_f of the foot to the vertical deflection dy of the treadmill:

$$k_t = \frac{F_f}{dy} = \frac{F_f}{x_f \tan(\theta_1)} \tag{3.9}$$

3.2.2 Plant Dynamics

The dynamics of the system are governed by the combined dynamics of the linear actuator and the treadmill platform. The dynamics of the linear actuator are observed to be very fast compared to the treadmill. More specifically, the linear actuator is able to reach the desired position in approximately 20 ms, with a steady state error less than 0.01 mm. Therefore, the dominant open loop poles are assumed to be given

by the dynamics of the treadmill. While the system operates in discrete time, it is modeled here in continuous time to demonstrate some important characteristics of the system. Approximating the treadmill with second-order dynamics, the final open loop transfer function between the actual and desired treadmill stiffness is given by:

$$\frac{K_t(s)}{K_t^d(s)} = G_1 G_2 \frac{K}{s^2 + 2\zeta\omega_n s + \omega_n^2} \tag{3.10}$$

Although the system has been represented so far as linear (therefore the use of transfer functions), the system is actually nonlinear, since the value of K, as well as the damping ratio and natural frequency of the system will change as the input x_{track} changes. In other words, since the input x_{track} is used to change the effective stiffness of the treadmill, the dynamics of the treadmill will change for different values of x_{track}. This will in turn change the pole locations of the system. Therefore, a linear model will not accurately describe this system for its entire range of stiffness. To understand the nonlinearity of the system and the effect of changing the stiffness, the open loop poles were found at a variety of x_{track} positions and plotted in the s-plane, as shown in Figure 3.9.

The poles were found by identifying key parameters from the step response of the system. A known mass of 11.71 kg was placed at 0.33 m from the pivot point, and x_{track}^d was suddenly changed from 0 to an arbitrary value. The angular deflection of the treadmill was measured with an encoder to find the second order system response. The damping ratio ζ was calculated from the maximum overshoot and the undamped natural frequency ω_n was calculated from the damped natural frequency and the rise time of the step response. The poles of the system were finally calculated by solving for $s_p = -\zeta\omega_n \pm j\omega_n\sqrt{1-\zeta^2}$.

Based on the pole locations in the s-plane it is seen that the system is highly damped ($\zeta > 0.8$) and has a quick response (rise time: $t_r \leq 0.25\,s$) for all track posi-

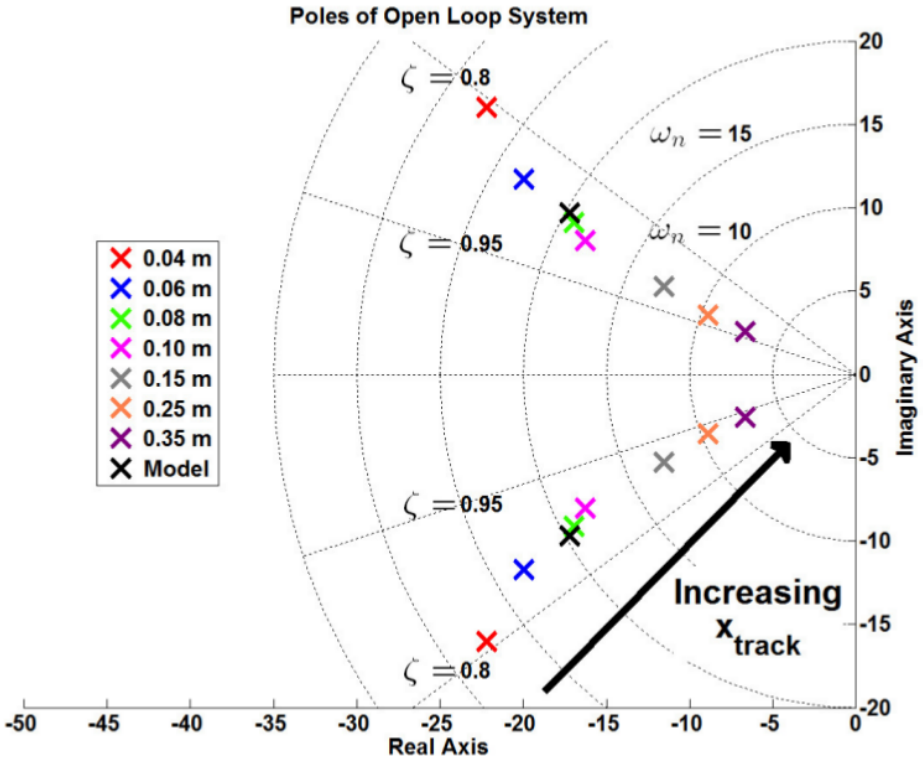

Figure 3.9: Plot of the open loop poles for different x_{track} positions in the s-plane (reprinted with permission from Skidmore *et al.* (2015), ©2015 IEEE).

tions. As x_{track} increases, the damping ratio also increases and the natural frequency decreases. The variability of the pole locations with changing stiffness prevents the entire system from being described with only one linear model. However, the above analysis gives an overview of the dynamics of the system.

3.2.3 Linear Model

A linear model about a reference input of $k_t^d = 20$ kN/m was created to further investigate the dynamic response of the system (Skidmore *et al.* (2015), ©2015 IEEE). A value of $k_t^d = 20$ kN/m was chosen because it is a stiffness that is similar to other studies that have been performed (Farley *et al.*, 1998; Ferris and Farley, 1997; Ferris *et al.*, 1999), and because it is within the desired operating range. The linear model was identified by placing a known mass (11.7 kg) at a constant distance (0.33 m)

from the treadmill pivot point, and commanding a step input by holding the desired stiffness at 2 MN/m and then suddenly dropping it to 20 kN/m. This corresponds to x^d_{track} changing from 0 to 0.065 m. This resulted in a damping ratio of $\zeta = 0.87$ and natural frequency $\omega_n = 19.74$ rad/s. By creating a bode plot based on the transfer function calculated from these system parameters, the system bandwidth frequency (defined here as the first frequency where the gain drops below -3 dB of its DC value) for the linear model is 2.45 Hz.

The identified linear model is useful for understanding the treadmill system but, as shown above, is not sufficient for controlling the stiffness of the treadmill due to inherent nonlinear relationships of the system. However, the errors in the linear model can be reduced by implementing a feedback control law. Implementing a Proportional Integral (PI) feedback controller will not only allow the transient dynamics to be shaped and drive the steady state error to zero, but the PI controller will also compensate for the nonlinearities that are neglected by the linear model.

3.3 Performance Characterization

A PI feedback controller was designed and implemented in order to achieve a zero steady state error of the actual treadmill stiffness in response to a desired stiffness reference signal (Skidmore *et al.* (2015), ©2015 IEEE). A block diagram representing the closed loop system is shown in Figure 3.10 where *err* is the error signal and u_{FF} and u_{FB} are the feedforward and feedback control efforts, respectively. The transfer function G_1 is the same as described previously and is placed in the feedforward path to get the control input close to its final value. The feedback controller then makes the corrections necessary to eliminate the steady state error. The actual stiffness is calculated based on the force exerted by the walker on the treadmill (F_f in the block diagram) and the actual vertical displacement of the treadmill, computed through the

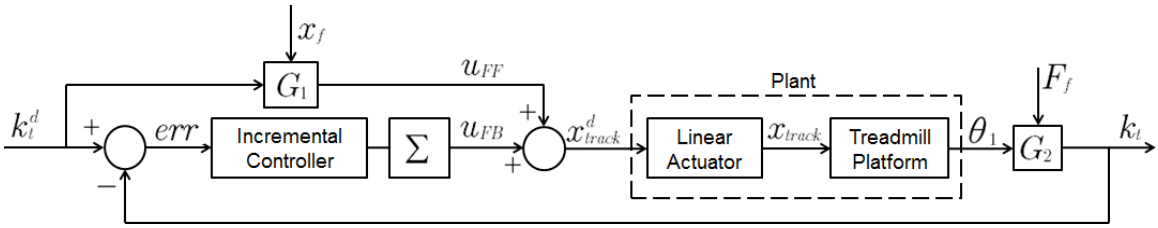

Figure 3.10: Block diagram of closed loop system (reprinted with permission from Skidmore *et al.* (2015), ©2015 IEEE).

rotary encoder measurements (θ_1). The walker force F_f is measured in real-time via a 500 kg S-type load cell (RobotShop, Product Code: RB-Phi-204) mounted between the treadmill platform and the variable stiffness mechanism, as shown in Figure 3.1, part J.

The design of the PI controller was performed in the continuous time domain by placing poles in the s-plane to decrease the rise time of the response and eliminate the steady state error. The control law was implemented in the discrete time domain with an incremental, or velocity, algorithm (shown in (3.11)), where err^p is the error calculated at the previous sample, k_p and k_i are the P and I gains respectively, and Δt is the sample period.

$$\Delta u_{FB} = k_p\,(err - err^p) + k_i err\,\Delta t \tag{3.11}$$

This change in feedback control effort is summed over time and results in the desired track position when added to the feedforward control. The proportional and integral gains were tuned to the linear model and then reduced to compensate for the implementation in discrete time instead of continuous time.

The feedback control structure was validated with two different reference stiffness values. First, a constant mass was placed at 0.33 m from the treadmill pivot point and the desired stiffness was changed from rigid ($k_t^d > 2$ MN/m) to 20 kN/m. A plot of the step response is shown in Figure 3.11. A steady state error (e_{ss}) of 7 N/m was obtained which is within the resolution of the system at that stiffness (see Figure 3.8).

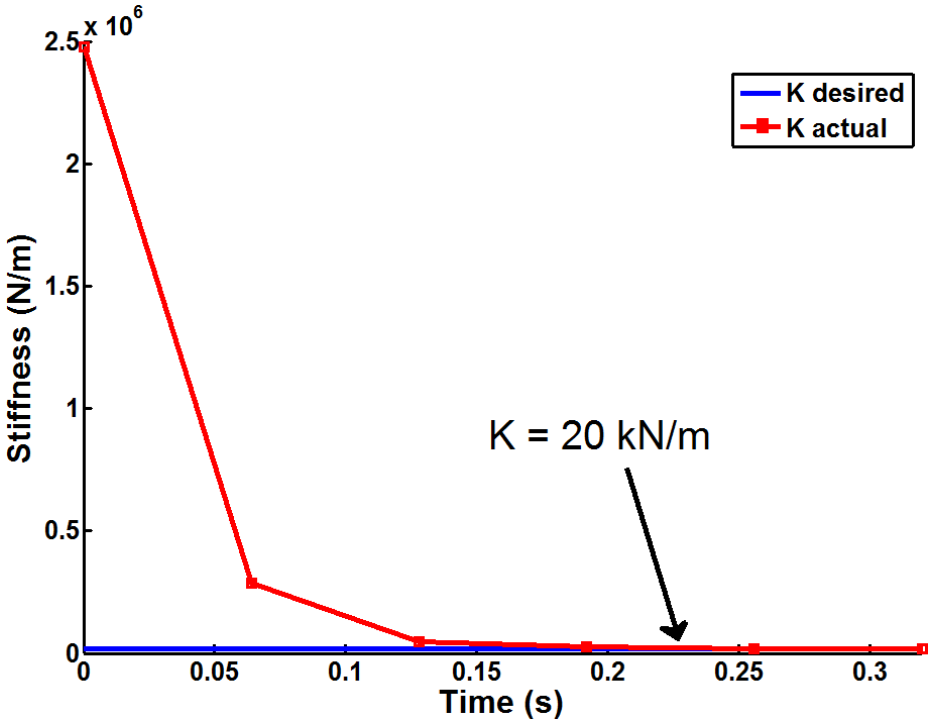

Figure 3.11: System response to step change in desired stiffness (reprinted with permission from Skidmore *et al.* (2015), ©2015 IEEE).

Moreover, this error is still only a fraction of one percent as shown in Table 3.2 along with the rise time (t_r) and 1% settling time (t_s), averaged from 3 repeated trials.

Second, in order to verify that the controller is robust to nonlinearities not modeled in the linear system, the exact same controller and gain values were tested with a step input to 56 kN/m. Results are shown in Table 3.2. As seen in Figure 3.9, the poles of the 20 and 56 kN/m systems are significantly far apart. However, the closed-loop feedback achieved essentially zero steady state error. This shows that the controller is robust enough to compensate for nonlinearities of the system. Therefore, the controller that was tuned to the 20 kN/m system is sufficient to achieve the desired stiffnesses within the range of interest.

In order to test the system in dynamic inputs and demonstrate the unique capabilities of the VST to create variable stiffness profiles, a reference sinusoidal input stiffness was created for the system to track. The signal oscillates about a mean of

Table 3.2: Closed Loop Response (reprinted with permission from Skidmore *et al.* (2015), ©2015 IEEE).

k_t^d (kN/m)	t_r (sec)	t_s (sec)	e_{ss} (%)
20	0.062	0.146	< 0.02
56	0.057	0.479	< 0.05

20 kN/m at a frequency of 0.77 Hz. The mean value of 20 kN/m was selected to correspond to the linear model that was created, and the frequency of oscillation was chosen so that one period of the sinusoid would be approximately the duration of the stance phase. The system response is shown in Figure 3.12. It can be seen that the actual stiffness profile matches the desired stiffness fairly well with some phase shift and attenuation. The magnitude attenuation is expected because it matches what the bode plot of the linear system (described above) would suggest. The phase shift is approx. 50°, which is very close to what the Bode plot would indicate.

3.4 Summary

The Variable Stiffness Treadmill (VST) system, presented and characterized in this chapter, has been developed with several advantages over existing devices for gait research. The system constitutes the first mechanical device that can alter the walking surface stiffness in real-time, with high accuracy, resolution and robustness. These characteristics make the VST a unique research platform which can be used for investigating sensorimotor mechanisms of inter-leg coordination (Skidmore *et al.* (2015), ©2015 IEEE). The VST is utilized in this dissertation to investigate the effect of walking surface stiffness on inter-leg coordination, but it can also be used for investigating the interplay of visual and proprioceptive feedback during human walking (Frost *et al.*, 2015).

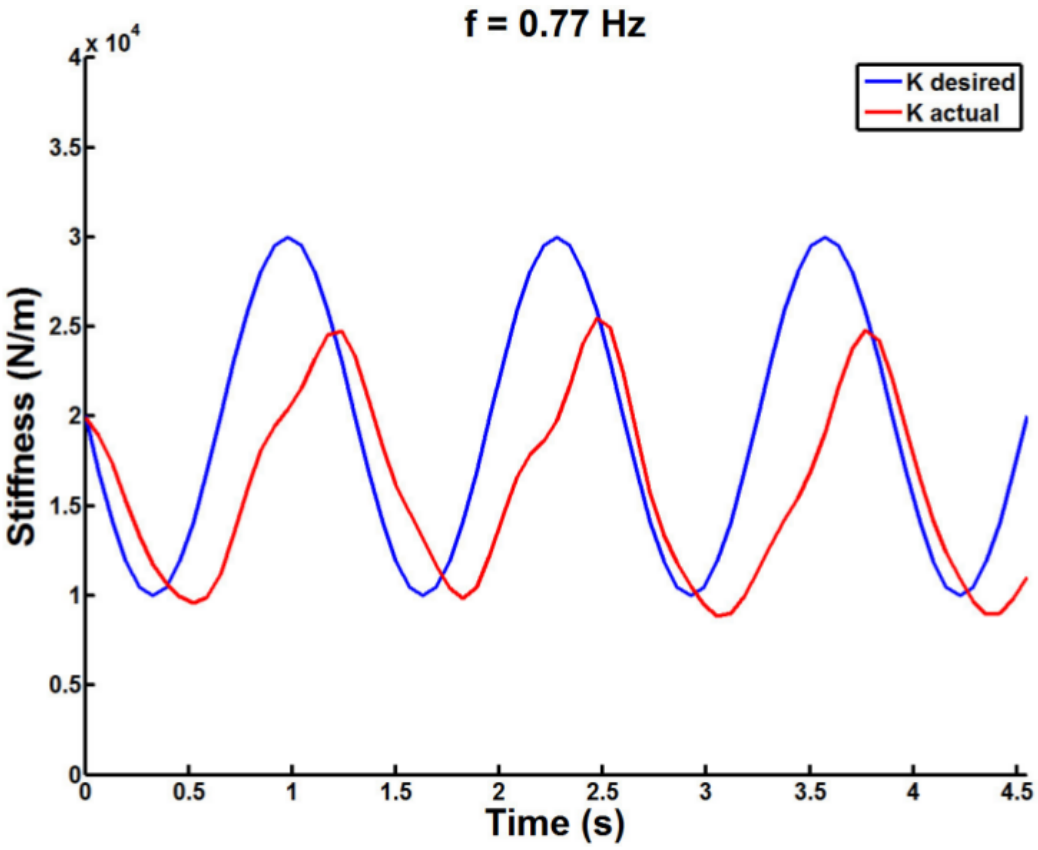

Figure 3.12: Closed loop system response to sinusoidal input (reprinted with permission from Skidmore *et al.* (2015), ©2015 IEEE).

Chapter 4

CONTRALATERAL EFFECTS OF UNILATERAL STIFFNESS PERTURBATIONS

In order to investigate the role of walking surface stiffness in inter-leg coordination, the response of the contralateral (unperturbed) leg to unilateral stiffness perturbations was investigated while varying three different experimental parameters. The variables that were changed in three separate experiments were (1) the magnitude of the stiffness perturbation, (2) the level of supplied BWS and (3) the timing of the stiffness perturbation within the gait cycle (Skidmore and Artemiadis, 2016a). This chapter comes from portions of a journal publication in the Journal of NeuroEngineering and Rehabilitation (Skidmore and Artemiadis, 2016a) with slight modification, except for sections that are otherwise cited.

4.1 Experimental Protocol

In each experiment the subject walked on the treadmill at a speed of 0.60 m/s and the differentiating aspects of the protocol for each experiment will be discussed below. For each experiment, five healthy subjects with no known neurological or gait impairments participated, where the five subjects were different for each experiment. Informed consent from the subject was obtained at the time of each experiment, and each experimental protocol is approved by the Arizona State University Institutional Review Board (IRB ID#: STUDY00001001).

4.1.1 Experiment 1: Altered Stiffness Magnitude

For this experiment, five healthy subjects [age 25 $\pm$ 5.4 years, weight 190 $\pm$ 35 lbs] walked on the treadmill for at least 200 gait cycles while being supported with approximately 30% BWS. A value of 30% BWS was chosen because this level of

support has been given in other studies (Af Klint *et al.*, 2010; Finch *et al.*, 1991) and effectively provides balance support without eliminating somatosensory feedback by unloading too much of the subject's weight. The right treadmill belt was not allowed to deflect for the duration of the experiment thus preventing any direct perturbation of the right leg. The surface underneath the left leg was commanded to maintain a stiffness of 1 MN/m, which makes the treadmill very stiff (i.e. considered to be rigid), for 30 gait cycles at the beginning of the experiment. Then, after a random number n of steps, where $n \in [3, 7]$, the stiffness was immediately dropped to 1 of 3 values: 10, 50 or 100 kN/m. The low stiffness perturbation began approximately 130 ms after heel-strike and lasted for the duration of the left leg stance phase (i.e. until toe-off) after which the stiffness was commanded back to 1 MN/m for the next n number of steps. A graphical representation of the timing and magnitude of the stiffness perturbations is shown in Figure 4.1(a). An average of 17 $\pm$ 2.3 perturbations at each stiffness level were experienced by all subjects.

4.1.2 Experiment 2: Altered BWS

This experiment was broken up into four sub-experiments, where the only difference between each sub-experiment was the level of BWS (0, 10, 20 or 30%) provided to the subject. Five healthy subjects [age 24 $\pm$ 2.4 years, weight 161 $\pm$ 24 lbs] walked on the treadmill for at least 100 gait cycles while being supported with the selected level of BWS. Similar to the previous experiment, the surface underneath the left leg was commanded to maintain a stiffness of 1 MN/m and then, after a random number n of steps, where $n \in [3, 7]$, the stiffness was immediately dropped to 60 kN/m approximately 130 ms after heel-strike. The perturbation lasted for the duration of the left leg stance phase after which the stiffness was commanded back to 1 MN/m for the next n number of steps. A walking surface stiffness of 60 kN/m was used for

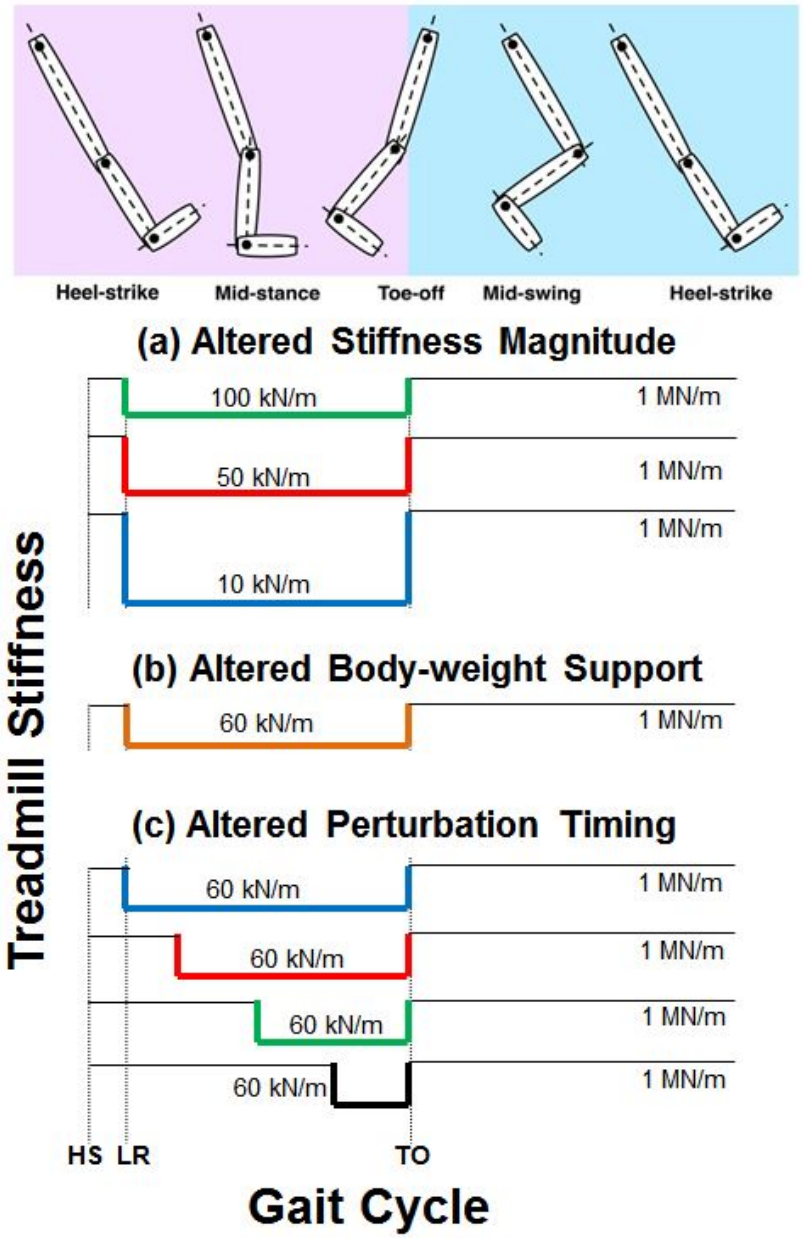

Figure 4.1: A diagram indicating the timing and magnitude of unilateral stiffness perturbations for three experiments: (a) Altered Stiffness Magnitude, (b) Altered BWS and (c) Altered Perturbation Timing. Heel strike, loading response and toe-off are represented by HS, LR and TO, respectively (Skidmore and Artemiadis, 2016a).

each level of BWS and was chosen because it is an intermediate value in the range of stiffness perturbations used in the first experiment. A graphical representation of the timing and magnitude of the stiffness perturbation for this experiment is shown in Figure 4.1(b). All subjects experienced 15 perturbations of the walking surface stiffness at each level of BWS. Again, the right treadmill belt was not allowed to deflect for the duration of the experiment thus preventing any direct perturbation of the right leg kinematics.

4.1.3 Experiment 3: Altered Perturbation Timing

This experiment was similar to the first experiment, except that instead of changing the magnitude of the stiffness perturbation, the timing of a stiffness perturbation of constant magnitude (60 kN/m) was altered. In this experiment, five healthy subjects [age 25 $\pm$ 3.6 years, weight 170 $\pm$ 37 lbs] walked on the treadmill for at least 150 gait cycles while being supported with approximately 30% BWS. A value of 30% BWS was chosen to provide some balance support and to allow for comparison with the first experiment. The surface underneath the left leg was commanded to maintain a stiffness of 1 MN/m for 30 gait cycles at the beginning of the experiment. Then, after a random number n of steps, where $n \in [5, 7]$, the stiffness immediately dropped to a level of 60 kN/m when the middle of the subject's left foot reached a certain percentage of the left stance phase. A stiffness magnitude of 60 kN/m was chosen in order to be consistent with the second experiment. The perturbation began at one of four locations (12, 30, 55 or 80% of the stance phase) that was randomly selected and lasted until the end of the left leg stance phase after which the stiffness was commanded back to 1 MN/m for the next n number of steps. A graphical representation of the timing and magnitude of the stiffness perturbations for this experiment is shown in Figure 4.1(c). An average of 9 $\pm$ 2.8 perturbations at each of the four

timing instances were experienced by all subjects. Again, the right treadmill belt was not allowed to deflect for the duration of the experiment thus preventing any direct perturbation of the right leg.

4.2 Data Analysis

The data analysis of the kinematic and muscular response of the unperturbed leg was the same for each of the three experiments described above. In all of the experiments, kinematic data for both legs were obtained at 140 Hz using the previously mentioned infrared camera system that tracked 12 (6 on each leg) infrared LEDs placed as pairs on the thigh, shank, and foot. The muscle activity of the legs were obtained using surface electromyography (EMG) via a wireless surface EMG system (Delsys, Trigno Wireless EMG) and recorded at 2000 Hz. Electrodes were placed on the tibialis anterior (TA) and soleus (SOL) of both legs. Raw EMG signals were processed by finding the moving root mean square envelope of each signal with a 250 ms window. After computing the EMG linear envelope, the data were normalized to the maximum value of that EMG signal.

The kinematic and EMG data corresponding to the gait cycles of normal conditions and the cycles pertaining to the perturbations were found and normalized temporally to percent gait cycle in order to eliminate discrepancies due to natural variations in gait patterns (i.e. stride length, cycle duration, etc). The data of each gait cycle were resampled at each 0.1% of the gait cycle (approximately 1.5 ms). The first 30 gait cycles and the cycles in between perturbations during the normal conditions are included in the unperturbed data set. One or two cycles (depending on which of the three experiments) following a perturbation are not included in the unperturbed set in order to eliminate any residual effects from the perturbation. This

results in normalized kinematic and EMG signals as a function of percent gait cycle, where 0 and 100% correspond to the heel-strike of the left leg.

Two different t-tests were utilized to establish statistical significance of the results. In order to evaluate the significance of recorded responses in both kinematics and EMG when compared to the normal condition, statistical significance was determined using an unadjusted *unpaired* t-test at each time instance. The unpaired t-test was selected in this case because it is a comparison of two independent distributions (i.e. gait cycles with and without perturbation) which have similar variances but different sample sizes. In order to evaluate the significance of perturbations across subjects, the *paired* t-test was used. Two values (the mean amplitude of cycles with and without perturbations) from each subject were used to test the significance of response to the perturbation at each time instance. Each test was performed at the 95% confidence level and any potential Type I errors from tests being performed at each 0.1% of the gait cycle were eliminated by only concluding significance if at least 40 tests (i.e. 4% of the gait cycle) in a row indicated significance.

A latency of response in each experiment is calculated from the beginning of the perturbation until there is a statistically significant difference between the TA EMG magnitude recorded during the perturbation and normal conditions.

4.3 Results

4.3.1 Experiment 1: Altered Stiffness Magnitude

The kinematic and muscular response to unilateral low stiffness perturbations of the walking surface of different magnitudes for a representative subject is shown in Figure 4.2. The normalized EMG amplitude for the TA and SOL, along with the hip flexion-extension, knee flexion-extension and dorsi-plantar flexion (mean and

standard deviation) for all gait cycles pertaining to each surface stiffness is shown for both the perturbed (left) and unperturbed (right) legs. The data are plotted as a function of the gait cycle percentage, where heel-strike and toe-off of each leg are indicated on the figure as HS and TO, respectively. Colored bars underneath an asterisk are included to indicate when statistically significant changes are observed. Both the muscular and kinematic profiles of walking on a rigid surface resemble that of what would be expected for normal human gait (Perry, 1992), showing that the system and experimental protocol did not alter normal gait patterns. Only data for a representative subject is shown in Figure 4.2 for clarify of presentation, but the contralateral response was consistent across subjects (Skidmore and Artemiadis (2015b), ©2015 IEEE).

Although the left leg was directly perturbed through the left treadmill stiffness change, the focus of this work is to understand inter-leg coordination by investigating the response of the unperturbed leg to the stiffness perturbations (Skidmore and Artemiadis (2015b), ©2015 IEEE). Therefore, the analyses for the majority of the dissertation will be primarily focused on the effects of the perturbation on the contralateral leg response. However, the change in left leg kinematics is important to understanding how the body perceives and therefore responds to the change in walking surface stiffness. A detailed investigation of the change in ipsilateral kinematics will be discussed in Chapter 5, and therefore will not be discussed here.

The experimental data of the response of the unperturbed leg shows a systematic evoked response in both kinematics and muscular activity. The majority of these evoked changes begin near 22% of the gait cycle and then converge back to the normal walking pattern later in the gait cycle. The evoked response was statistically significant at the 95% confidence level for a two sample unpaired t-test when comparing the data for each perturbation level to the rigid (i.e. normal) condition. Colored

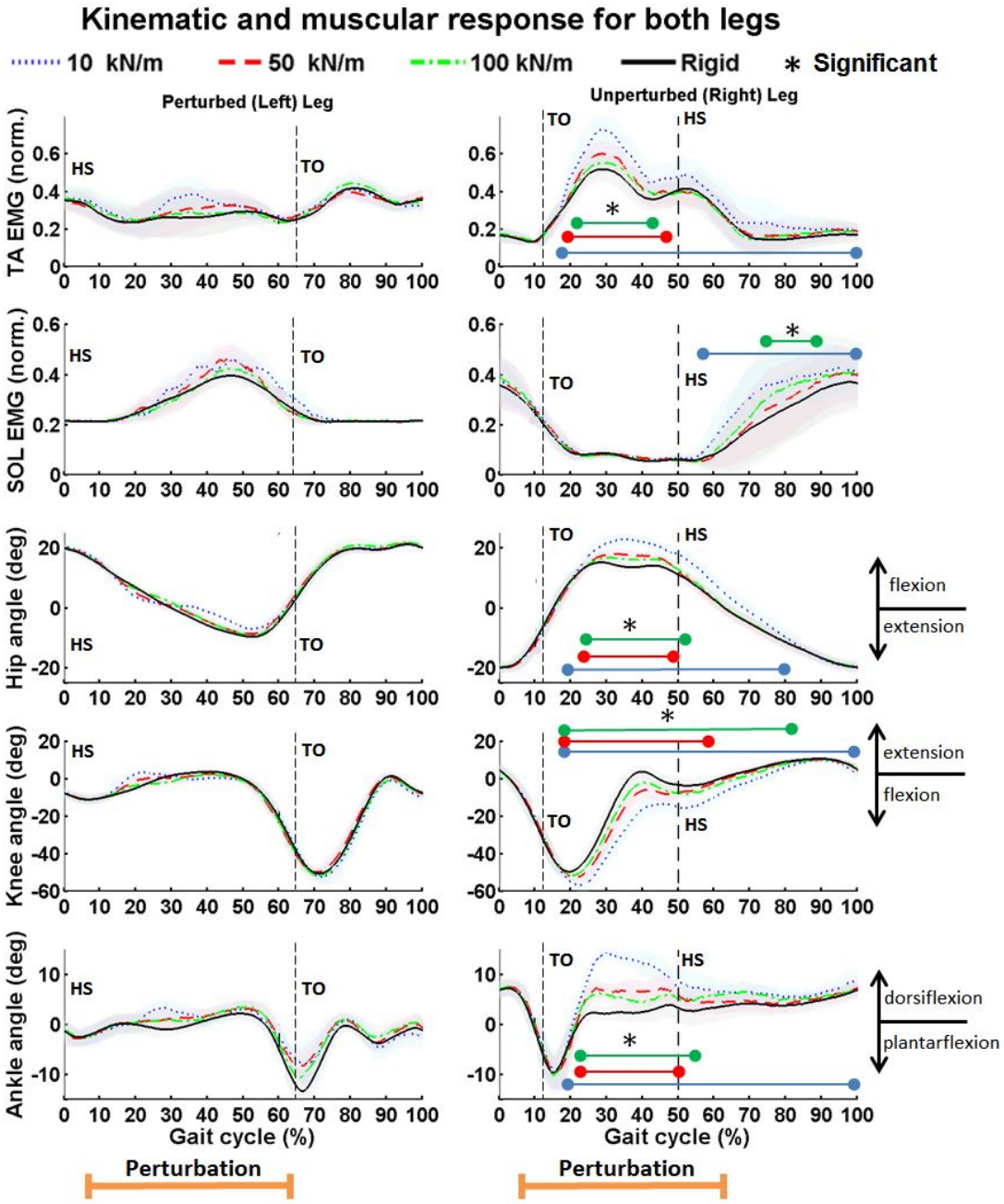

Figure 4.2: Averaged muscle activity and joint kinematics of the perturbed (left) and unpertubed (right) legs for a representative subject. Plotted from top to bottom is the normalized TA EMG, normalized SOL EMG, hip flexion (+) - extension (-), knee flexion (-) - extension (+) and ankle dorsi (+) - plantar (-) flexion for gait cycles at each of four surface stiffness levels. Mean (darker lines) and standard deviations (lightly shaded areas) values are shown along with an indication of the timing of the perturbation. Statistically significant changes are indicated by colored bars (corresponding to each stiffness level, aligned vertically from highest to lowest stiffness) that are placed beneath a black asterisk. Heel-strike and toe-off of each leg are indicated by HS and TO, respectively. The duration of the gait cycles shown is approximately 1.8 s (Skidmore and Artemiadis (2015b), ©2015 IEEE).

bars indicating when significant changes are observed in the right leg are included in Figure 4.2. As can be seen, the significance of the response is dependent on the magnitude of the stiffness perturbation where lower stiffness values result in greater contralateral response.

Moreover, the response in the contralateral TA is scalable such that as the magnitude of the perturbation increases (i.e. lower stiffness values), there are increased changes in TA activation. The significant increase in TA activation with lower walking surface stiffness is shown by using a paired t-test to compare the mean TA values at two levels of stiffness for all subjects. For example, the evoked TA EMG during the lowest stiffness perturbations (10 kN/m) is significantly greater than the medium stiffness perturbations (50 kN/m) from 16.8 to 42.5 percent of the gait cycle. This is shown in the first row of Table 4.1. The time period (in percent gait cycle) when the evoked TA EMG is significant when comparing the other levels of stiffness is also shown in Table 4.1. As calculated from the last column in the table, the TA activation significantly increases at each level of stiffness for at least 13% of the gait cycle. Therefore, there is a scalable response of the contralateral TA in response to unilateral stiffness perturbations. While the same systematic and scalable evoked response is not apparent in the SOL, there is significant evoked activity in the SOL during stance phase of the right leg.

4.3.2 Experiment 2: Altered BWS

The evoked muscle activity of the TA in the perturbed leg for all levels of BWS is first presented for comparison and validation with the first experiment. The normalized EMG amplitude for the TA (mean and standard deviation) for all perturbed and unperturbed gait cycles pertaining to each level of BWS for a representative subject is shown in Figure 4.3.

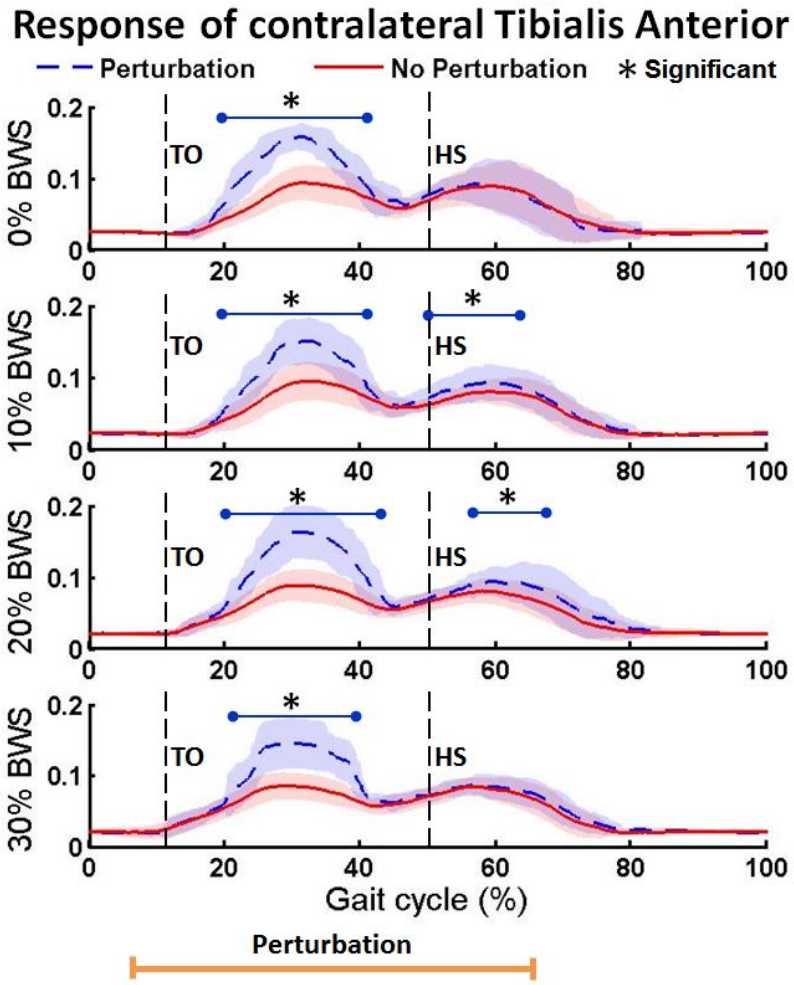

Figure 4.3: Averaged TA muscle activity for perturbed and unperturbed gait cycles at each of the four levels of BWS for a representative subject. Mean (darker lines) and standard deviation (lightly shaded areas) values are shown along with an indication of the timing of the perturbation. Statistically significant changes in perturbed gait cycles are indicated by a blue bar and a black asterisk. Heel-strike and toe-off of the right leg are indicated by HS and TO, respectively (Skidmore and Artemiadis, 2016a).

Table 4.1: Timing of evoked tibialis anterior activation for experiment 1. This table contains the range in percent gait cycle when the statistically significant evoked tibialis anterior EMG is seen when comparing two levels of stiffness.

Stiffness level 1 (kN/m)	Stiffness level 2 (kN/m)	Range of significance (% gait cycle)
10	50	16.8 - 42.5
50	100	25.3 - 38.8
100	1000	21.0 - 36.0

Similar to experiment 1, there is a statistically significant increase in TA activity between approx. 20 to 40% of the gait cycle, as well as occasionally at other times later in the gait cycle (such as shortly after heel-strike of the right leg). The significant evoked muscle activity during swing phase is observed for all levels of BWS and is consistent across subjects. The time (in percent gait cycle) of when significant TA EMG is first seen (mean and standard deviation across all levels of BWS) for all subjects is shown in Table 4.2. While there is some variability in the onset of evoked activity, all subjects show evoked TA activity during the swing phase of the gait cycle and at all levels of BWS. Of significant importance is that there is no statistically different response between the evoked TA activity at each level of BWS. The TA activation (mean and standard deviation) during perturbation cycles for all levels of BWS (i.e. all of the blue lines from Figure 4.3) is shown in Figure 4.4. As can be seen, the responses are very similar and there is no statistically significant difference at any time during the gait cycle. Therefore, the level of evoked muscle activity for a constant stiffness perturbation of 60 kN/m is independent of the level of BWS.

Table 4.2: Timing of evoked tibialis anterior activation for experiment 2. This table contains the mean and standard deviation in percent gait cycle across all levels of body weight support for when the statistically significant evoked tibialis anterior EMG is first seen for all subjects.

Subject 1	Subject 2	Subject 3	Subject 4	Subject 5
$26\% \pm 1.7$	$19\% \pm 0.8$	$21\% \pm 2.0$	$20\% \pm 5.0$	$28\% \pm 1.6$

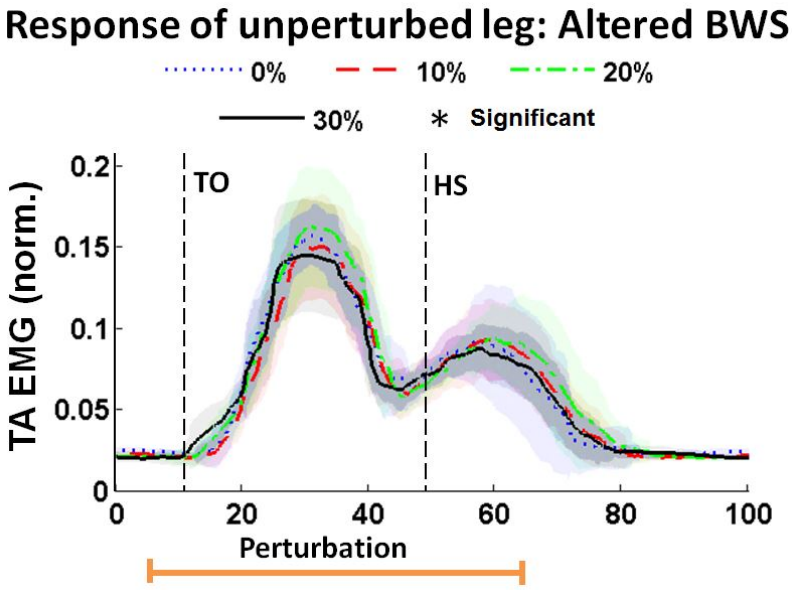

Figure 4.4: Averaged TA muscle activity for gait cycles at each of the four levels of BWS for a representative subject. Mean (darker lines) and standard deviation (lightly shaded areas) values are shown along with an indication of the timing of the perturbation. The timing of toe-off and heel-strike of the right leg within the gait cycle are represented by TO and HS, respectively (Skidmore and Artemiadis, 2016a).

4.3.3 Experiment 3: Altered Perturbation Timing

The kinematic and muscular response due to variation in the onset of the low stiffness perturbations for a representative subject is shown in Figure 4.5. The results from this experiment indicate that the timing of the low stiffness perturbation affects the timing of the muscular and kinematic response of the unperturbed leg. As would be expected, the data show that the altered response is only seen after the perturbation, independent of the onset of the perturbation. Of importance to note is that

Table 4.3: Timing of statistically significant changes for experiment 3. This table contains the mean and standard deviation in percent gait cycle across all subjects for when statistically significant response is first seen for the TA and SOL at all timing instances of the perturbations. No significant evoked response was seen with perturbations beginning at 80% of the stance phase which is indicated with a dash.

Muscle	Timing of perturbation (% stance phase)			
	12%	30%	55%	80%
Tibialis Anterior	$23\% \pm 3.6$	$42\% \pm 1.4$	$56\% \pm 5.7$	-
Soleus	$34\% \pm 14$	$50\% \pm 23$	$58\% \pm 4.6$	-

statistically significant evoked muscle activity is primarily seen when the muscle is normally active, independent of the timing of the perturbation. As seen in Figs. 4.2, 4.3 and 4.5, the majority of the evoked TA and SOL activity is seen during the swing and stance phases, respectively, which is when these muscles have higher activity during human walking. The timing of the evoked response in both the TA and SOL is consistent across subjects. The time (in percent gait cycle) of when significant TA and SOL EMG begin (mean and standard deviation across all subjects) for all timing instances of the perturbation is shown in Table 4.3. Only the beginning and not the end is shown because the durations of the significance varied between subjects. The important result here is that the onset of evoked contralateral response is consistent across subjects independent of when the timing of the perturbation begins.

4.4 Summary

This chapter presents results of evoking kinematic and muscular changes in the contralateral leg of healthy subjects using unilateral low stiffness perturbations of the walking surface. By systematically altering the magnitude and timing of the stiffness perturbations, along with the level of body-weight support, the effect of surface stiffness in inter-leg coordination during human walking is investigated. The

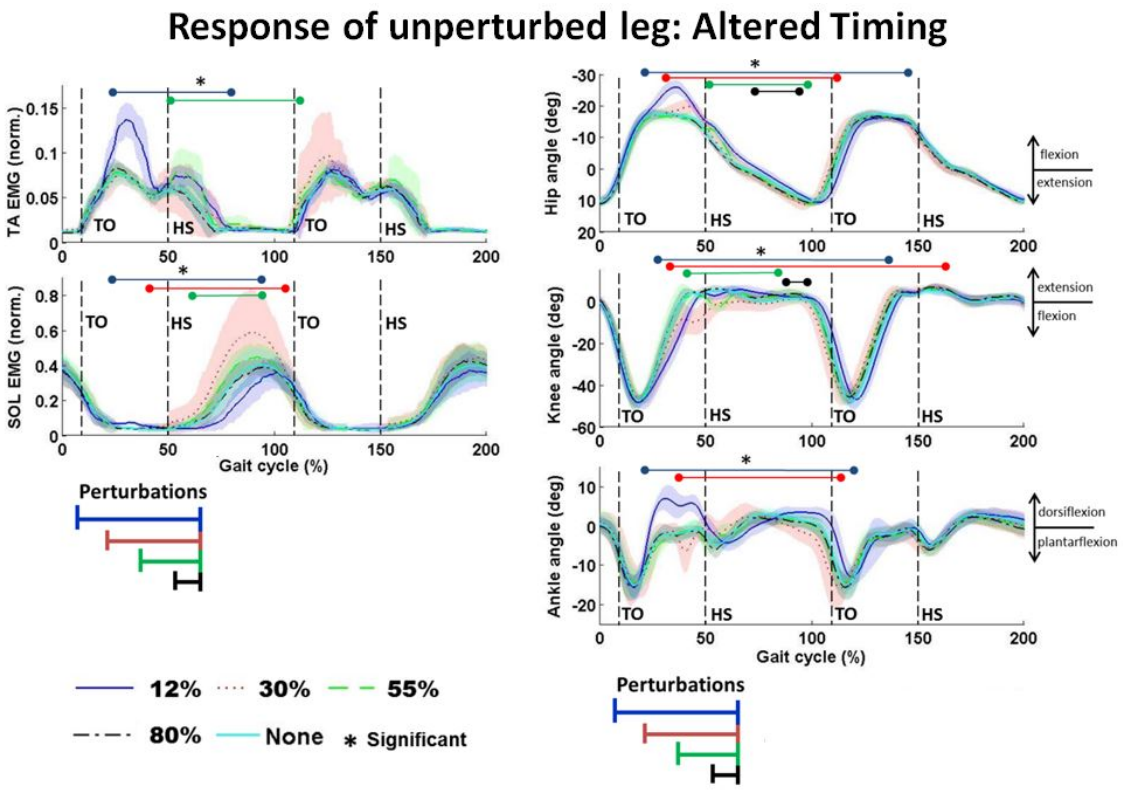

Figure 4.5: Averaged muscle activity and joint kinematics of the unperturbed (right) leg for a representative subject. Plotted from top to bottom is the normalized TA EMG and normalized SOL EMG (in left column), and hip flexion (+) - extension (-), knee flexion (-) - extension (+) and ankle dorsi (+) - plantar (-) flexion (in right column). Mean (darker lines) and standard deviations (lightly shaded areas) values for gait cycles pertaining each timing of the perturbation are shown along with an indication of the timing of each perturbation. Statistically significant changes are indicated by colored bars (corresponding to each perturbation timing, aligned vertically from earliest to latest in the gait cycle) that are placed beneath a black asterisk. Heel-strike and toe-off of the right leg are indicated by HS and TO, respectively. The duration of the data plotted is approximately 3.3 s (Skidmore and Artemiadis, 2016a).

repeatability (consistency across subjects and experiments) and scalability (significant increase in EMG activity with decreasing stiffness) of the results demonstrate the importance of the stiffness of the walking surface as a stimulus in human gait (Skidmore and Artemiadis, 2016a). Moreover, the latency of evoked response and the timing of evoked muscle activity in the contralateral leg suggests that the feedback may be modulated by supra-spinal neural circuits. A detailed investigation into the sensorimotor mechanism involved in the observed contralateral effect to unilateral stiffness perturbations will be provided in Chapter 5.

Chapter 5

INVESTIGATION OF RELATED SENSORIMOTOR MECHANISM

As was explained in Section 2.1, locomotion results from intricate dynamic interactions between a central program and feedback mechanisms (Rossignol *et al.*, 2006). The feedback from muscle and skin afferents (somesthetic senses) and from the visual, auditory, and vestibular systems (special senses) adapts the locomotor pattern to the requirements of the environment (Rossignol *et al.*, 2006). Thus, the response of the body to unexpected perturbations to the environment, such as low stiffness perturbations, is triggered by and related to the change in sensory feedback. In order to understand the sensorimotor mechanism underlying the contralateral response seen in Chapter 4, the potential contribution of each sensory modality to the perception (and therefore the response) of the perturbation will be investigated. Additionally, the neural pathway that relays the sensory signal into the motor output will be investigated in order to fully characterize this sensorimotor mechanism of inter-leg coordination.

5.1 Somesthetic Senses

5.1.1 Muscle Afferents

Muscle afferents from muscle spindles and Golgi Tendon Organs (GTOs) are a key contribution to the proprioceptive sense. Proprioception is the sense of relative positioning of parts of the body and is important in gait by regulating the amplitude of muscle output in various phases of the gait cycle and by facilitating the switch between phases (Rossignol *et al.*, 2006). Muscle spindles are situated in parallel with the muscle and provide feedback to the central nervous system by encoding the length of the muscle as well as its change over time (i.e. muscle velocity). GTOs are in series with the tendons of the muscles and sense the tension (i.e. muscle force) in the muscle.

As was shown in Section 4.3.1 there are distinct changes in ipsilateral kinematics due to the unilateral stiffness perturbations. In fact, this effect was by design and is a unique feature of this work. Stiffness perturbations were chosen for investigating sensorimotor mechanisms of inter-leg coordination because they allow for changes in leg kinematics while still allowing the subject to maintain contact with the walking surface. Thus stiffness perturbations allow for the investigation of the effect of a change in kinematics during walking while still maintaining force feedback from the walking surface (see Section 2.3 for more details).

However, the body does not detect change in joint angles directly, but rather through muscle length and velocity sensed by muscle spindles. Therefore, ipsilateral kinematics will not be discussed directly, but they will be used in biomechanical simulations to understand the proprioceptive feedback. The OpenSim software package (Delp *et al.*, 2007) was used to perform these analyses. A bipedal, 10 DOF model with 18 muscles (9 for each leg), shown in Figure 5.1, was chosen in order to calculate ipsilateral changes in muscle length. First of all, the model parameters were scaled with anatomical measurements (i.e. length of limb segments and total weight) of the subject. The bilateral kinematic data and ground reaction forces recorded during the experiment were then loaded in the software. The Inverse Dynamics Tool calculated the joint torques required to achieve the loaded motion. The Static Optimization Tool was then run to resolve the net joint torques into individual muscle activations by minimizing the total activation energy required to achieve the required joint torques. Finally, the Muscle Analysis tool provided detailed information regarding the muscle lengths and velocities.

In order to understand the difference in feedback information being relayed to the central nervous system by the muscle afferents, the average change in muscle length was calculated when comparing gait cycles with perturbations and gait cycles

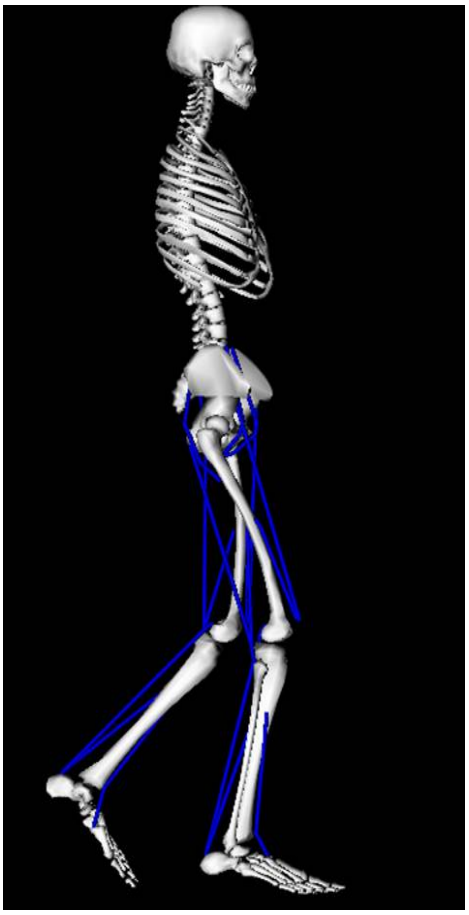

Figure 5.1: 10 DOF biomechanical model in OpenSim (Delp *et al.*, 2007) for calculating ipsilateral changes in muscle length.

without perturbations. In order to do this, the average muscle length across all normal cycles preceding a perturbation cycle (i.e. up to the gait cycle immediately after the previous perturbation) were subtracted from the muscle length during that perturbation cycle. This difference was then averaged across all perturbations of the same type (i.e. magnitude and timing). The change in muscle length (mean and standard deviation) of all nine modeled muscles on the ipsilateral leg for one type of stiffness perturbation (20 kN/m during the loading response) is shown in Figure 5.2.

As expected, due to changes in all three ipsilateral joint angles (hip, knee, ankle), as seen in Figure 4.2, there are changes in all nine of the muscles. Moreover, antagonistic muscles have reciprocal changes in muscle lengths. This can be seen

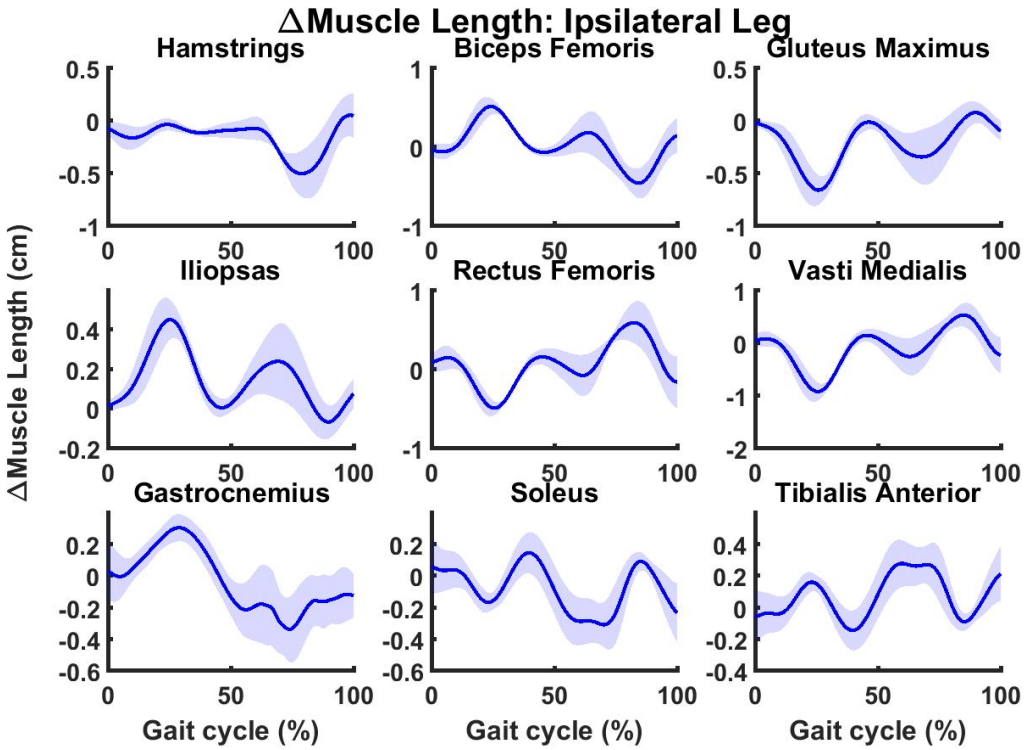

Figure 5.2: Average (mean and standard deviation) change in ipsilateral muscle lengths due to unilateral stiffness perturbations.

clearly in the soleus and tibialis anterior, as well as the gluteus maximus and iliopsas. Therefore, the simulation data matches the experimental data. The main conclusion from this analysis is that proprioception is definitely affected due to the stiffness perturbations, and must be accounted for in understanding the observed sensorimotor mechanism.

5.1.2 Skin Afferents

Cutaneous feedback from skin afferents is utilized for correcting the placement of the foot during gait and provides information with regards to foot contact and interaction with the walking surface (Zehr *et al.*, 1997). Stiffness perturbations were chosen for this research because they allow the subject to maintain contact with the walking surface, thus preventing a total loss of force feedback and high impact forces

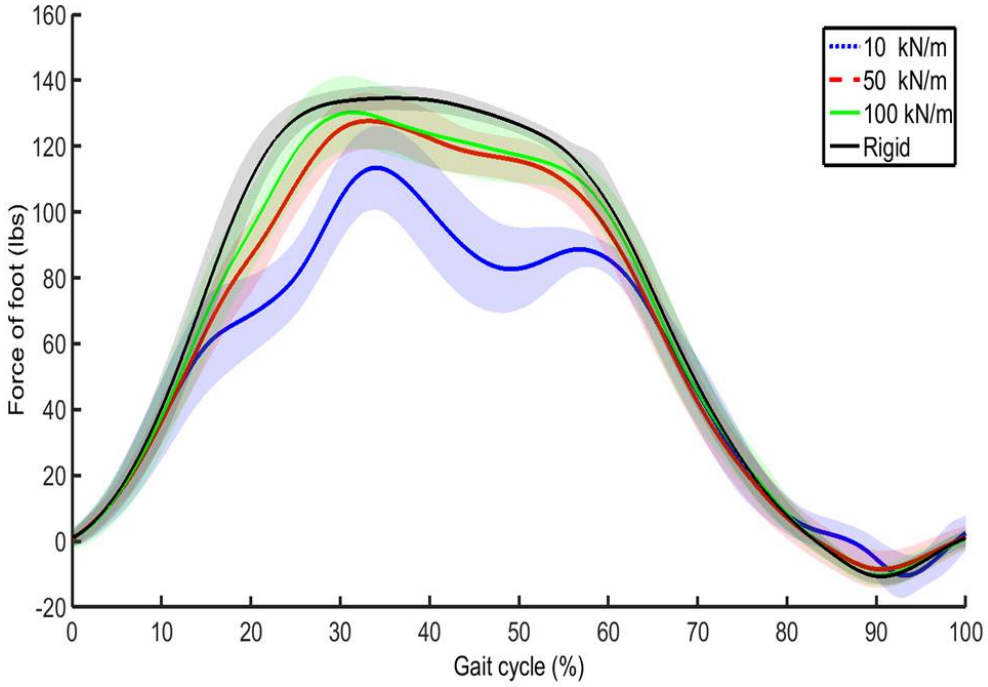

Figure 5.3: Foot force (mean and standard deviation) over one gait cycle at four levels of walking surface stiffness.

upon reestablishing contact with the walking surface. The force exerted by the left leg on the treadmill is measured with a loadcell during all experiments (see Section 3.1.2). The average force over one gait cycle is shown for the four levels of walking surface stiffness described in 4.3.1 is shown in Figure 5.3.

As can be seen, there are only slight deviations from the normal force profile during the high and medium stiffness perturbations of 100 and 50 kN/m, respectively. The force during the low stiffness perturbation of 10 kN/m is significantly less than the normal profile during the single support phase of the left leg. This difference is explained by the compliance in the BWS that was implemented by design. A spring is mounted on the body-weight system which allows the subject's body to lower with the treadmill deflection. This allows the foot to continue to apply a similar force to the treadmill for most levels of stiffness, as shown by the 100 and 50 kN/m profiles. However, with larger deflections of the treadmill, such as those seen with low stiffness

perturbations (i.e. 10 kN/m), the spring on the BWS is completely compressed by the weight of the subject, and acts like a hard stop. Therefore, the harness will carry a greater load as it prevents the subjects from falling. Nevertheless, there is continuous contact with the walking surface during stiffness perturbations, thus the body can always detect that a surface is present (as evidenced by the nonzero force profile). Therefore, any changes in cutaneous feedback due to the stiffness perturbations are assumed to be negligible during the stiffness perturbations.

5.2 Special Senses

5.2.1 Vision

The visual system is used to choose a direction and avoid obstacles during locomotion (Rossignol *et al.*, 2006). In the experiments with stiffness perturbations, there are no indications preceding a perturbation that would alert the subject to an upcoming perturbation. The first visual indication of a perturbation is when the lever arm attached to the treadmill platform deflects upward due to the rotation of the treadmill platform about its pivot point under the load of the subject. However, this is a minor change in the optical flow field and assumed not to be involved in the perception of the perturbation. Moreover, the latencies from the commanded perturbation to the contralateral response are shorter than what would be required for processing the visual information and sending commands to the leg muscles (Di Lollo *et al.*, 2000). Therefore, vision is concluded to not be influential in the contralateral effect seen in Chapter 4.

5.2.2 Audition

Sound can be incorporated in locomotion by utilizing rhythmic sounds to organize movement and mark time. The use of rhythmic acoustic stimuli, such as metronomes or music, has gained popularity in gait rehabilitation of various movement disorders, including stroke and Parkinson's disease (Roerdink *et al.*, 2011; Thaut *et al.*, 1997). While there is no auditory indication of an upcoming perturbation during an experiment, a sound is created when the linear actuator moves to create a change in walking surface stiffness. A couple of investigations were performed in order to investigate the contribution of auditory feedback in the observed contralateral response.

First, an investigation was performed in which a subject walked on the VST with and without noise canceling headphones and experienced the same stiffness perturbations. The perturbations for this investigation were applied during the loading response with a magnitude of 60 kN/m, in the same manner as was described in Section 4.1.1. Moreover, the subject walked at a speed of 0.6 m/s and was provided with 30% BWS, to be consistent with previous experiments. The subject experienced 20 perturbations for each experimental condition (i.e. with and without headphones).

The average TA activation while wearing and not wearing the noise canceling headphones are plotted on top of each other for comparison in Figure 5.4 for both normal and perturbed gait cycles. The plot on the left of the TA activation with and without noise canceling headphones serves as a validation that the same muscle activation is seen during both trials. The plot on the right shows that there is no change in evoked contralateral TA activation due to the noise canceling headphones. Therefore, it is concluded that the noise of the linear actuator during a perturbation does not contribute to the evoked contralateral response. However, comparing the level of TA activation from the perturbed gait cycles (right plot) with the normal gait

cycles (left plot) confirms the previously presented result that unilateral low stiffness perturbations applied during the loading response result in increased contralateral TA activation.

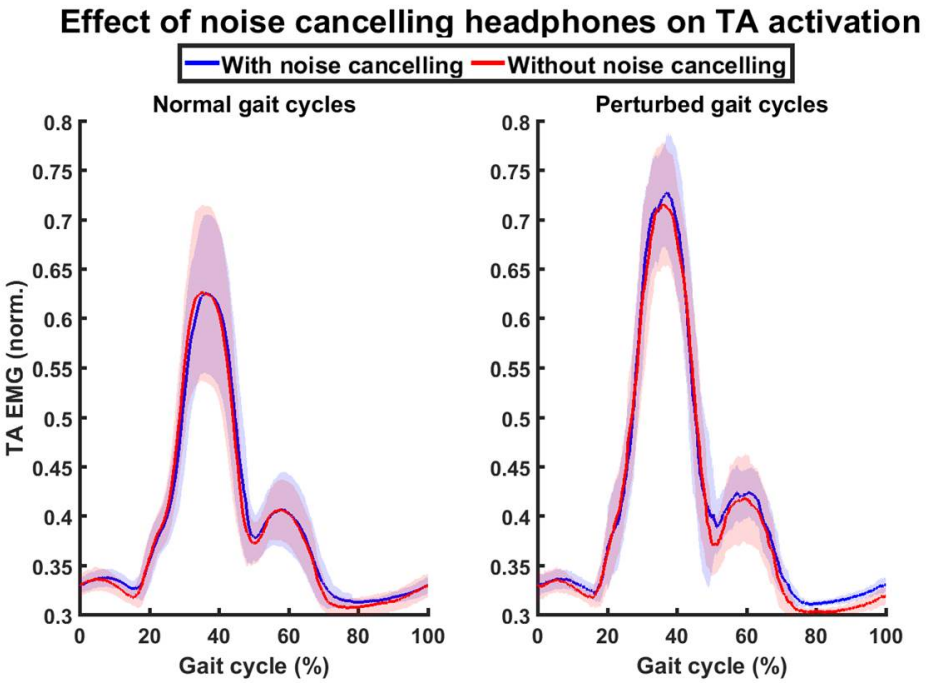

Figure 5.4: Normalized TA EMG with and without noise canceling headphones for both normal (left) and perturbed (right) gait cycles.

Second, an intense auditory stimulus can generate a startle response in humans that is partially seen in legs (Rossignol *et al.*, 2006; Sanders *et al.*, 2015). Subjects report that they do not feel startled when experiencing a perturbation, but in order to verify objectively that a startle response is not occurring, EMG electrodes were placed bilaterally on the the sternocleidomastoid (SCM) muscles while subjects experienced low stiffness perturbations. Three subjects participated in this investigation and each subject experienced 50 perturbations that were applied during the loading response with a magnitude of 20 kN/m, in the same manner as was described in Section 4.1.1. Each subject walked at 0.6 m/s and was provided with 30% BWS to ensure consistency with previous experiments.

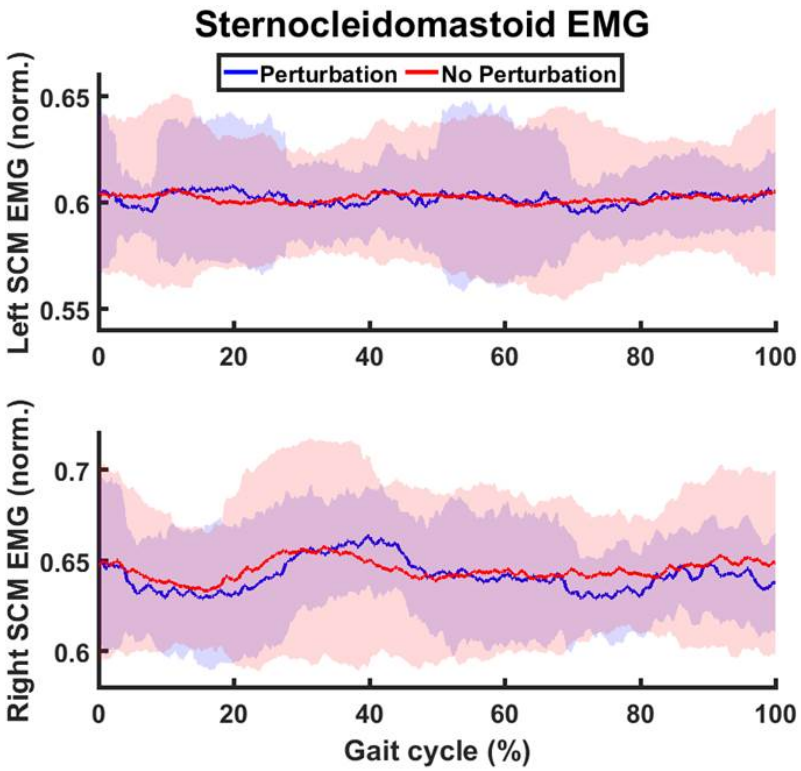

Figure 5.5: Averaged (mean and standard deviation) left sternocleidomastoid (top) EMG and right sternocleidomastoid (bottom) EMG during treadmill walking with random stiffness perturbations.

The normalized EMG of the left and right SCMs averaged across all gait cycles pertaining to normal walking and stiffness perturbations is shown in Figure 5.5 for a representative subject. There is no significant difference in EMG for either the left or right SCM. For comparison with voluntarily activated SCMs, the raw EMG from the experiment is plotted in Figure 5.6, where the data is plotted for 1 minute of experiment time followed by the subject looking left and then right for 6 seconds after the walking portion of the experiment. An indication of when stiffness perturbations occurred is also shown. This comparison reveals that there is no substantial activation of the SCMs during the experiment. Since startle responses are characterized by rapid bilateral sternocleidomastoid muscle activation within 80ms of stimulus onset (Sanders *et al.*, 2015), it is concluded that a startle response is not elicited by low

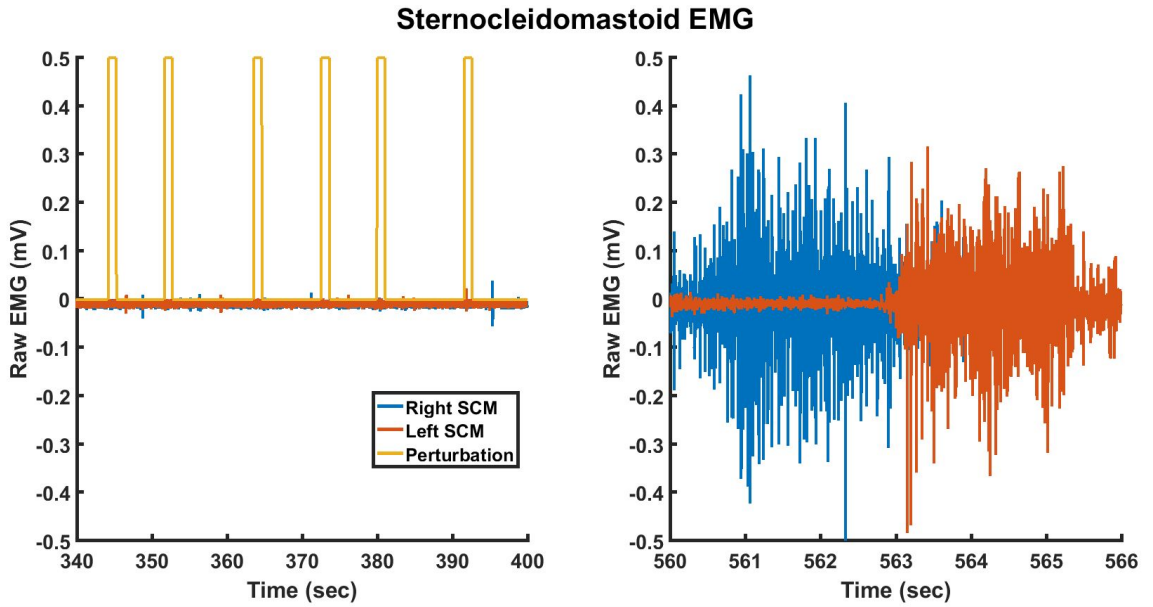

Figure 5.6: Raw sternocleidomastoid EMG during treadmill walking with random stiffness perturbations (left) and when voluntarily contracting muscles after walking by looking left and then right (right).

stiffness perturbations. Therefore, it is concluded that the audition has no effect on the contralateral response and is not a part of the related sensorimotor mechanism.

5.2.3 Vestibular

The vestibular system provides information that is used for orientation, balance, and posture (Rossignol *et al.*, 2006) and patients with vestibular deficiency show abnormal gait patterns (Mamoto *et al.*, 2002; Whitney *et al.*, 2009). The vestibular system is located inside each ear and is composed of the saccule and utricle that detect gravity and linear accelerations and three nearly orthogonal semicircular canals that detect rotational accelerations. The use of 30% BWS for the majority of this research was chosen to partially support the patient, thereby providing postural stability. This was intended to eliminate vestibular responses due to maintaining balance. However, inherent in a stiffness perturbation is the deflection of the treadmill under

the load of the subject. Therefore, some amount of vertical linear acceleration would be anticipated.

In order to experimentally verify the change in vestibular feedback during stiffness perturbations, an investigation was performed in which 3-axis accelerometers (Delsys Trigno) were placed bilaterally on the mandible (so as to roughly approximate the location and function of the saccule and utricle) and on the upper sternum. Two subjects walked on the treadmill at 0.6 m/s with 30% BWS for at least 250 gait cycles. The perturbations for this investigation were applied during the loading response with a magnitude of 20 kN/m, in the same manner as was described in Section 4.1.1. Each subject experienced the described perturbations 17 times.

The vertical acceleration of the body as recorded from the accelerometers is shown in Figure 5.7. As is expected for normal gait on a flat walking surface, there are small fluctuations in vertical acceleration during gait cycles without a perturbation (shown in red) as the center of mass of the subject rises and falls in a cyclic manner (Perry, 1992). Additionally, there are significant deviations from the normal profile during the stiffness perturbations which verifies that the vestibular feedback is perturbed during stiffness perturbations. An intense change in vestibular input could also elicit a startle response (Yeomans *et al.*, 2002), but the startle response has already been eliminated as a contributing factor as described above in Section 5.2.2.

5.3 Neural Pathway

As mentioned in Section 4.4, the results from the experiments in Chapter 4 suggest that the response is mediated through supra-spinal neural pathways. The latency of the contralateral response, the timing of the evoked muscle activation during the gait cycle, and a study with EEG recordings all provide support for this conclusion, and will be discussed below.

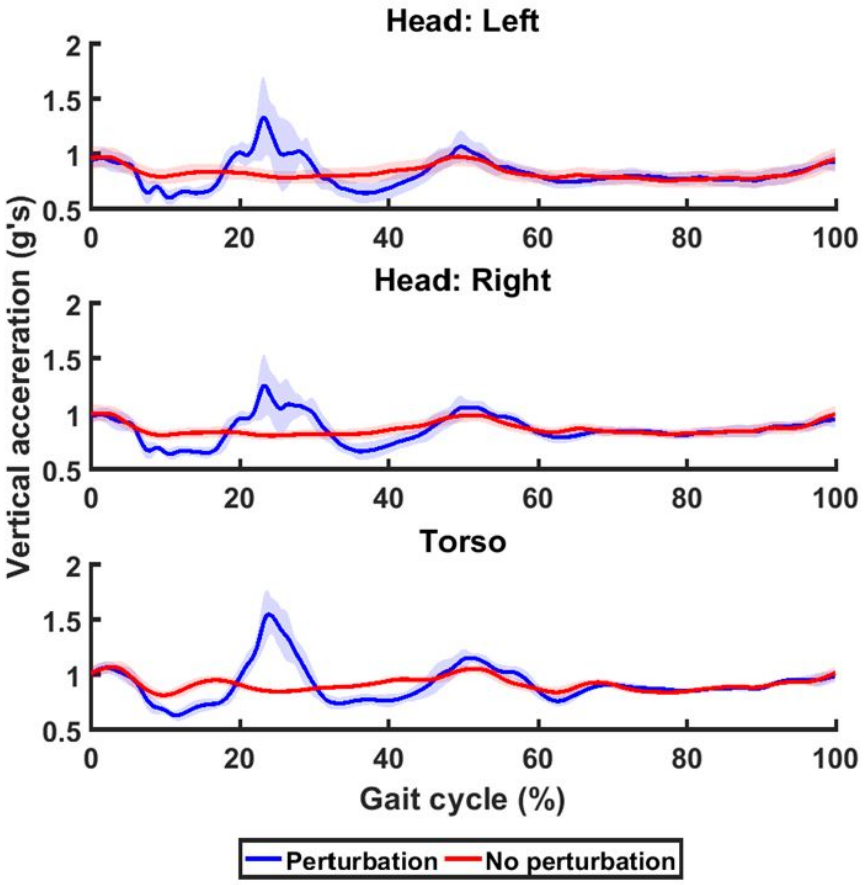

Figure 5.7: The average vertical acceleration (mean and standard deviation) of the body over the gait cycle from accelerometers placed on the left of the head (top), right of the head (middle), and torso (bottom), for a representative subject.

5.3.1 Latency of Response

The consistent latency of evoked muscle activity after the perturbation in the results of Chapter 4 suggest that supra-spinal neural circuitry, as opposed to a spinal reflex mechanism, is stimulated through sudden low stiffness perturbations. The latency averaged across subjects and experiments resulted in a mean of 202 ± 60 ms (Skidmore and Artemiadis, 2016a). A delay of this duration is longer than the 50-80 ms latency that would be seen for spinal reflexes (Darton *et al.*, 1985; Yavuz *et al.*, 2014). Rather delays greater than 125 ms correspond to transcortical circuitry

(Christensen *et al.*, 2000b; Shemmell *et al.*, 2009; Zuur *et al.*, 2009), suggesting that supra-spinal regions are stimulated through the low stiffness perturbations.

5.3.2 Timing of Response

In addition, the timing of the evoked EMG in both the TA and SOL within the gait cycle suggests that supraspinal structures modify the amplitude of the neuromuscular response to sensory stimuli created by sudden changes in surface stiffness but does not initiate activation of the muscles in gait. This is consistent with the theory that supraspinal structures are not responsible for generating basic gait motor patterns through cyclical flexion and extension of the joints, but rather in modulating these basic gait patterns with descending inputs (Rossignol *et al.*, 2006; Skidmore and Artemiadis, 2016a).

As can be seen in Figures 4.2, 4.3, and 4.5, the majority of the evoked muscle activity occurs only when the muscle is normally active. Specifically, evoked EMG in the TA is seen during the swing phase and beginning of the stance phase, with the greatest change in EMG occurring at the same time (approximately 30% of the gait cycle) as the peak EMG during normal walking. The same pattern is seen for the SOL. Even though the perturbation occurs from approximately 8 to 60% of the gait cycle, evoked muscle activity of the SOL is not seen until the stance phase later in the gait cycle, which is when the SOL is active in normal walking (Perry, 1992; Skidmore and Artemiadis, 2016a). This result also agrees with research that has shown motor evoked potentials (MEPs) in plantar- and dorsi-flexors evoked by TMS are only evident during phases of the gait cycle when a muscle is active (Belda-Lois *et al.*, 2011). For example, MEPs in the soleus are present during stance and absent during swing (Capaday *et al.*, 1999; Schubert *et al.*, 1997).

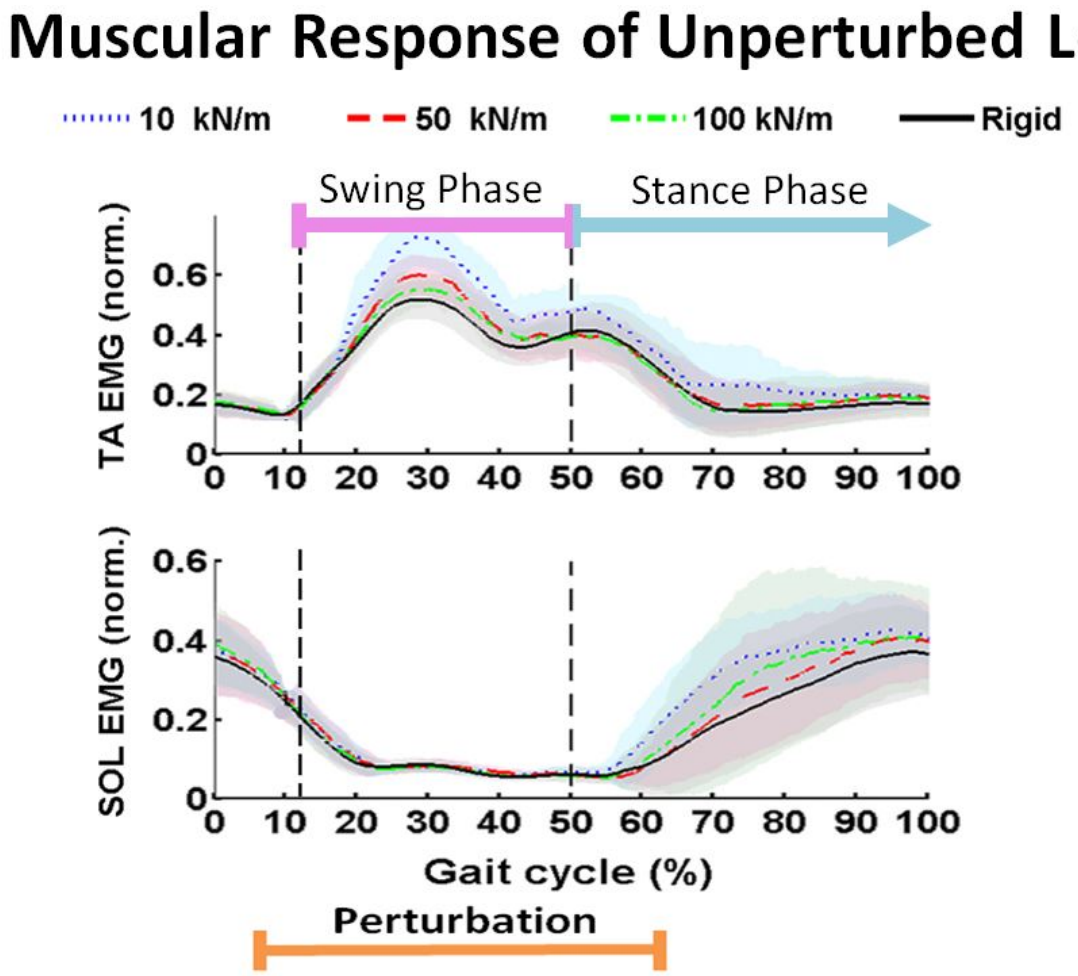

Figure 5.8: Averaged TA and SOL muscle activity for gait cycles at each of the four surface stiffness levels for a representative subject from experiment 1. Mean (darker lines) and standard deviation (lightly shaded areas) values are shown. An indication of the timing of the perturbation and the swing and stance phases are also shown (Skidmore and Artemiadis (2015b), ©2015 IEEE).

This result of the evoked TA and SOL activity occurring during swing and stance phase, respectively, for a representative subject from experiment 1 is demonstrated succinctly in Figure 5.8.

5.3.3 EEG Recordings

An experiment with low stiffness perturbations to healthy subjects while measuring brain activations with EEG and contralateral muscle activations with EMG

was performed to investigate the existence of supraspinal influences in inter-leg coordination. This section comes from part of a publication in the proceedings of the 2016 IEEE International Conference on Robotics and Automation (Skidmore and Artemiadis (2016c), ©2016 IEEE), with slight adaptation.

5.3.3.1 Experimental Protocol

For this study two healthy subjects [Subject 1: age 20 years, weight 130 lbs, height 70 in; Subject 2: age 25 years, weight 175 lbs, height 75 in] were supported by 30% BWS and walked on the treadmill at a speed of 0.60 m/s for at least 320 gait cycles. A speed of 0.60 m/s was chosen for comparison with the previous experiments. As with previous experiments, the right treadmill belt was not allowed to deflect for the duration of the experiment, thus preventing any direct perturbation of the right leg. The surface underneath the left leg was commanded to maintain a stiffness of 1 MN/m for 30 gait cycles at the beginning of the experiment. Then, after a random number n of steps, where $n \in [4, 7]$, the stiffness was immediately dropped to a constant value of 60 kN/m. A stiffness level of 60 kN/m was chosen because it resembles that of a gym mat (Chang *et al.*, 2010) and for comparison with experiments presented in Chapter 4. The low stiffness perturbation began shortly after heel strike (approximately 125 ms) and lasted for the duration of the left leg stance phase (i.e. until toe-off) after which the stiffness was commanded back to 1 MN/m for the next n number of steps. A graphical representation of the timing of the stiffness perturbation is included at the bottom of Figure 5.11. Each subject experienced 50 low stiffness perturbations. Informed consent from the subject was obtained at the time of the experiment, and the experimental protocol is approved by the Arizona State University Institutional Review Board (IRB ID#: STUDY00001001).

Figure 5.9: Subject on the VST wearing the EEG cap (Skidmore and Artemiadis (2016c), ©2016 IEEE).

5.3.3.2 Data Collection and Processing

Kinematic data for both legs were obtained at 140 Hz using an infrared camera system that tracked 12 infrared LEDs (6 on each leg) placed as pairs on the thigh, shank, and foot. This data was also utilized in real time for timing of the stiffness perturbation.

The muscle activity of the unperturbed leg was obtained using surface electromyography (EMG) via a wireless surface EMG system (Delsys, Trigno Wireless EMG) and recorded at 2000 Hz. Electrodes were placed on the tibialis anterior (TA), gas-

trocnemius (GA) and soleus (SOL) of the right leg. After computing the EMG linear envelope, the data were normalized to the maximum value of that EMG signal. The EMG data corresponding to the gait cycles of walking on the rigid surface and the cycles pertaining to the low stiffness perturbations were found and categorized accordingly. Because muscle activity during walking is highly dependent on the phase of the gait cycle, the data were normalized temporally to percent gait cycle. The first 30 gait cycles and the cycles in between perturbations at rigid stiffness (except for one cycle following a perturbation to eliminate any residual effects from the perturbation) are included in the unperturbed data set. The normalized EMG signals were then resampled at the average duration of the gait cycle in order to plot the EMG activity over time, where time = 0 corresponds to the heel strike of the left leg.

The EEG data were collected using a BrainProducts ActiCHamp amplifier module and 128 active electrodes, as shown in Figure 5.9. The electrodes were placed on the subject's scalp based on the International 10-20 system using a BrainProducts ActiCAP cap. The data were recorded at 1000 Hz. The processing of the EEG data was done using the EEGLAB (Delorme and Makeig, 2004) and ERPLAB (Lopez-Calderon and Luck, 2014) packages which are available for the Matlab environment. First, a 6th order high-pass Butterworth filter at 1 Hz followed by a 6th order low-pass Butterworth filter at 40 Hz were applied to the data in order to remove any low frequency trends and high frequency noise, respectively. The filtered data were then re-referenced at average reference and epoched at 500 ms before and 1.2 s after the left heel-strike. Finally, channels and epochs that contained artifacts were removed from the data set. This was done using standard artifact rejection techniques implemented in EEGLAB that include detection of extremely large fluctuations in voltage levels, abnormal trends, improbable data and abnormal distributions.

5.3.3.3 Results

The results of the experiment show significant changes in EEG activity, as well as the kinematics and muscle activity of the right leg, in response to the low stiffness perturbations on the left leg. Since the changes in contralateral kinematics and muscle activity match the results that have been previously presented (see Chapter 4) and the focus of this section is to understand supraspinal influences on inter-leg coordination by investigating the response of the brain to stiffness perturbations, kinematic data will not be presented and muscle activation will only be included in support of understanding supraspinal influences on inter-leg coordination. However, the kinematic and muscular responses recorded during this study are consistent with what was shown in Chapter 4.

Significant changes in EEG activity were seen between the event related potentials (ERPs) of the perturbed and unperturbed gait cycles throughout the data epochs. Statistically significant differences between the two cases were calculated for all channels at every 1 ms of the epoch using a two sample unpaired t-test at the 95% confidence level. Topological plots of statistical significance are shown at 25 ms intervals from -50 to 1050 ms (where t = 0 ms corresponds to left heel strike) for both subjects in Figure 5.10. Significant differences are indicated in red while insignificant differences are designated by green. Other colors that are seen in the figure result from interpolation across the topology of values at the electrode locations.

As can be seen in the figure, there are time periods with little to no significant changes and but there are also noticeable regions with sustained levels of significance. Specifically, from approximately 150 to 575 ms for subject 1 and 350 to 525 ms for subject 2 there are generally sustained significant differences in the same regions of the brain. Generally speaking, these regions of activation are near the center of the

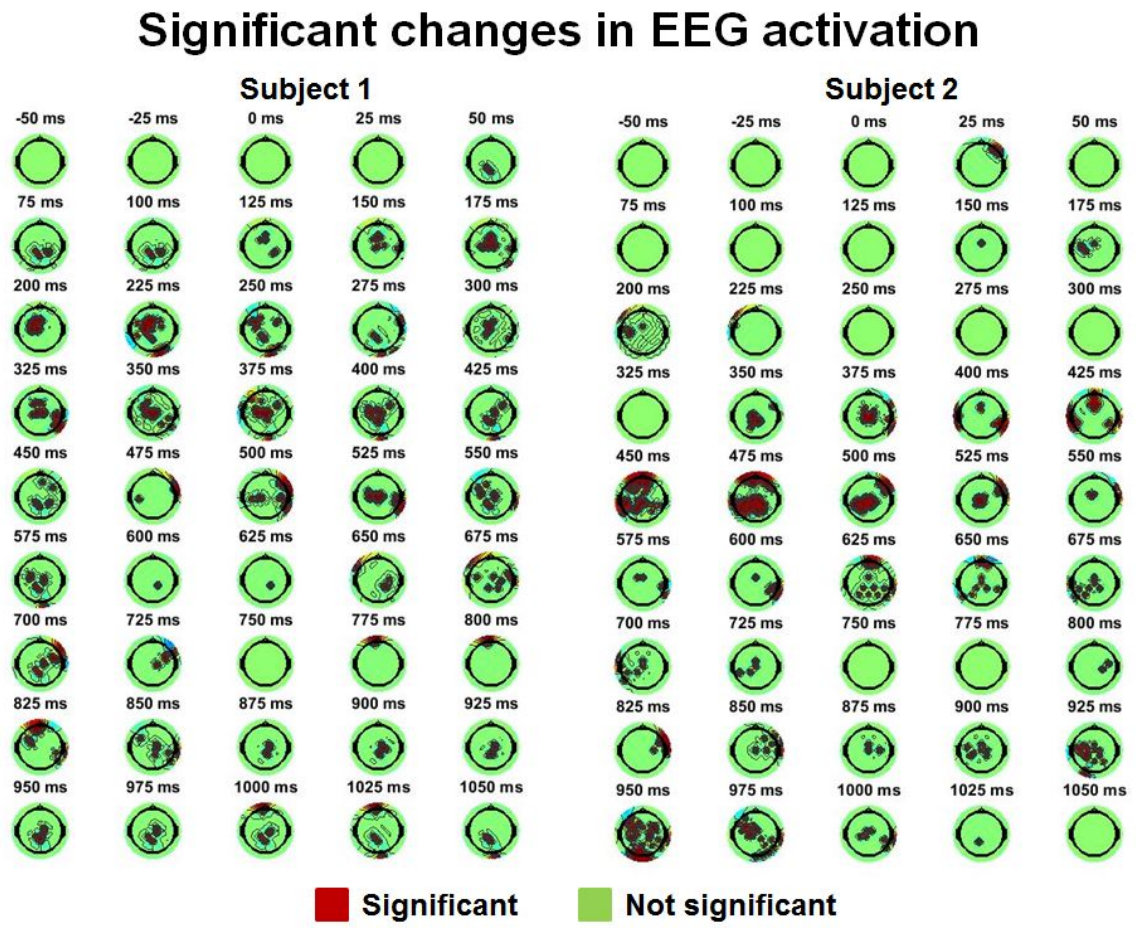

Figure 5.10: Topological plots of statistical significance at 25 ms intervals from -50 to 1050 ms (where t = 0 ms corresponds to left heel strike) for both subjects. Significant differences are indicated in red while insignificant differences are designated by green. Other colors result from interpolation across the topology of values at the electrode locations. The low stiffness perturbation began shortly after heel strike (approx. at 125ms) and lasted for the duration of the left leg stance phase (ie. until toe-off), which occurred at approx. 815 and 1150 ms for subject 1 and 2, respectively (Skidmore and Artemiadis (2016c), ©2016 IEEE).

brain with a bias to the left of the midline. This is the approximate location of the medial section of the primary motor and sensory cortices which lie just anterior and posterior of the central sulcus, respectively. Regions with concentrated significance and large gradients with very little activation elsewhere in the topology (ex. subject 1 at 800 ms) are also seen in the figure and are attributed to blinking artifacts and not actual brain activations.

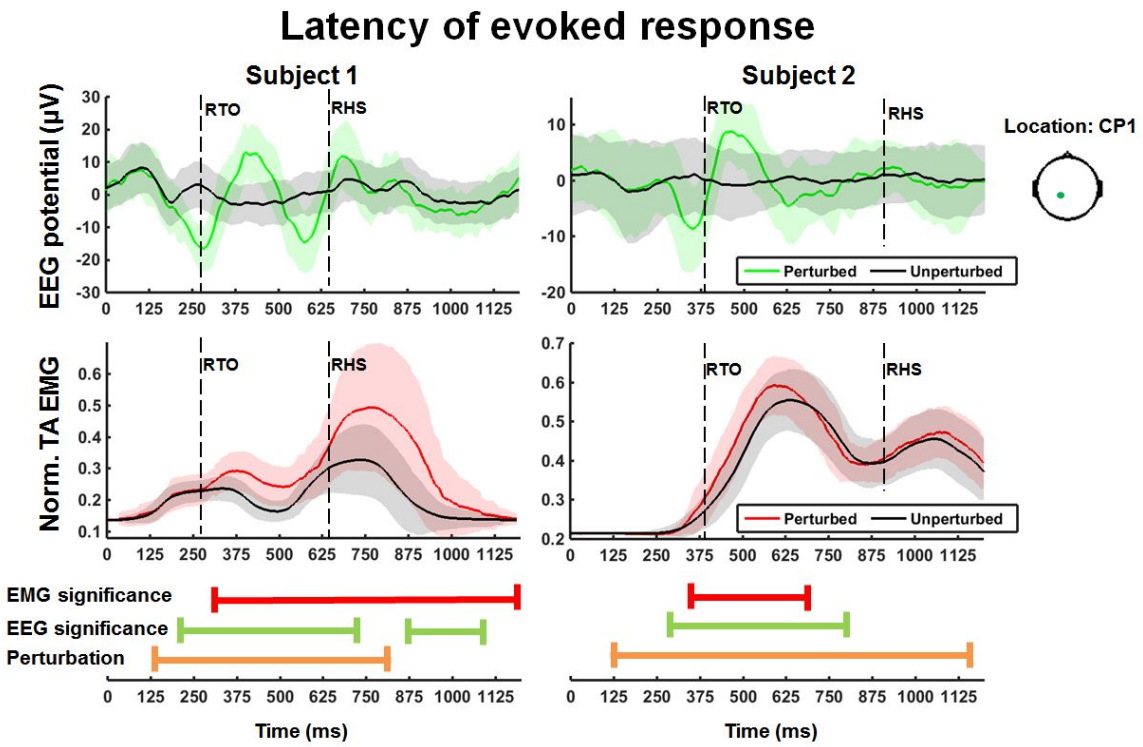

Figure 5.11: EEG potential at the CP1 location and normalized EMG for the tibialis anterior (TA) for both subjects. Mean (darker lines) and standard deviations (lightly shaded areas) values are shown for the perturbed and unperturbed gait cycles. Statistically significant changes are indicated by colored bars that correspond to the type of neural signal. An indication of the timing of the perturbation is also shown. RTO and RHS correspond to toe-off and heel-strike of the right leg, respectively (Skidmore and Artemiadis (2016c), ©2016 IEEE).

In order to visualize the actual ERPs, the EEG potential recorded at location CP1 of the International 10-20 system (mean and standard deviation) over time under both conditions (perturbed and unperturbed) for both subjects is shown in Figure 5.11. The normalized right leg TA EMG activity for both conditions and both subjects is also included for comparison between the central and peripheral neural activity.

As seen in the figure, there are statistically significant differences between the unperturbed and perturbed cases in both brain and muscle activation for both subjects. For subject 1 the EEG and EMG are significant from 200-729, 863-1083 and 291-1200 ms, respectively. For subject 2 the EEG and EMG are significant from 283-776 and

341-648 ms, respectively. Therefore, the latency from the onset of perturbation to significant changes in EEG and EMG are 71 and 162 ms, respectively, for subject 1, and 161 and 219 ms, respectively, for subject 2. The differences in onset of evoked muscle and brain activity between the two subjects results from subject 2 having a larger stride length than subject 1, and they walked at the same treadmill speed.

5.3.3.4 Discussion

The latency of response seen in Chapter 4 is again seen for both subjects (delay $>$ 150 ms) in the evoked TA activation shown in Figure 5.11, which supports the hypothesis of supra-spinal circuitry. Furthermore, significant changes in EEG activation are seen prior to the evoked TA activity for both subjects. The latency of EEG response at location CP1 shown in Figure 5.11 precedes the TA activation by 98 and 58 ms for subjects 1 and 2, respectively. Therefore, this finding provides stronger support that supraspinal mechanisms are involved in mechanisms of inter-leg coordination and participate in the evoked TA activation.

Moreover, as seen in Figure 5.10, the main concentration of significant changes is seen in the medial side of the left brain near the mid-coronal plane. This is the approximate location of the medial section of the primary motor and sensory cortices which lie just anterior and posterior of the central sulcus, respectively. These areas are primarily involved in motor commands and sensory responses to and from the right side of the body, respectively. Specifically, activations in the medial section of the primary motor cortex near the brain midline are associated with motor output in the lower limb of the right leg. Because the activation in the brain is seen before changes in muscle activity of the right leg (as described above), it is concluded that the activations are associated with the motor output signal as opposed to the input sensory signal. Therefore, this provides some indication that the brain is influenced

by the low stiffness stimulus to the left leg and then contributes to the evoked TA activity of the right leg.

5.4 Summary

A systematic investigation of the role of several sensory modalities (muscle afferents, skin afferents, vision, audition, vestibular) has shown that the body detects the stiffness perturbations through proprioceptive and vestibular feedback. Moreover, the latency of the contralateral response, the timing of the evoked muscle activation during the gait cycle, and a study with EEG recordings all support the hypothesis that the sensorimotor mechanism responsible for the response to these perturbations is mediated through the brain. In fact, it appears that this sensorimotor mechanism may pass through the motor cortex, and be considered as what has been defined as a "transcortical reflex loop" (Shemmell *et al.*, 2009).

This result agrees with other studies that have shown the existence of a long-loop transcortical reflex that can modulate a stretch reflex (Shemmell *et al.*, 2009; Zuur *et al.*, 2009). Zuur *et al.* (2009) have shown suppression of the tibialis anterior stretch reflex in early stance phase by repetitive transcranial magnetic stimulation over the motor cortex. This indicates that this reflex is modulated through the motor cortex which is in agreement with the EEG data presented in Section 5.3.3. With all of the above considerations, it is reasonable to assume that the repeatable contralateral response due to unilateral stiffness perturbations is due to a sensorimotor mechanism that is mediated through the motor cortex and may be considered a transcortical reflex.

Chapter 6

MODEL OF OBSERVED SENSORIMOTOR MECHANISM

A model which relates the vertical deflection of the left walking surface to the evoked contralateral muscle activation is developed in this chapter. This model was developed with the aims of 1) predicting contralateral muscle activation based on the timing and magnitude of the unilateral stiffness perturbations and 2) providing insight into the observed sensorimotor mechanism. A description of the experiment for obtaining the necessary data will be presented, followed by the formulation of the model. Results and validation of the model will then be presented and discussed.

6.1 Experiment

6.1.1 Experimental Protocol

Eight healthy subjects [age 24 $\pm$ 4 years, weight 150 $\pm$ 18 pounds, height 69 $\pm$ 3 inches] were supported by 30% BWS and walked on the VST at a speed of 0.60 m/s for 575 gait cycles. The surface underneath the left leg was commanded to maintain a stiffness of 1 MN/m, which is very high and considered to be rigid, for 30 gait cycles at the beginning of the experiment. Then, after a random number n of steps, where $n \in [4, 8]$, the stiffness of the left walking surface was lowered to 1 of 3 levels. For subjects who weighed less than 165 lbs (6 subjects) the three levels were 20, 40, and 60 kN/m. For subjects who weighed more than 165 lbs (2 subjects) the three levels were 40, 60, and 80 kN/m. The differentiation of stiffness levels for different subject weights was chosen in order to have similar deflection levels independent of body weight. Otherwise, for a given stiffness level, heavier subjects would create larger deflections than lighter subjects. The levels of stiffness will be designated as low, medium, and high for the remainder of this chapter. The stiffness perturbation

began randomly at either 10, 30, or 60% of the stance phase and will be referred to as loading response, mid-stance, and terminal stance perturbations, respectively. Each perturbation lasted for the duration of the left leg stance phase after which the stiffness was commanded back to 1 MN/m during the left leg swing phase in order to create a rigid walking surface for the next n number of steps. Each subject experienced 10 perturbations at each timing and magnitude for a total of 90 perturbations. The right treadmill belt was not allowed to deflect for the duration of the experiment, thus preventing any direct perturbation of the right leg. Informed consent from the subject was obtained at the time of the experiment, and the experimental protocol is approved by the Arizona State University Institutional Review Board (IRB ID#: STUDY00001001).

6.1.2 Data Collection and Processing

Kinematic data for both legs were obtained at 140 Hz using an infrared camera system that tracked 12 infrared LEDs (6 on each leg) placed as pairs on the thigh, shank, and foot. This real-time data was sampled at 20 Hz to be utilized for timing of the stiffness perturbation. The force exerted by the subject and the angular deflection of the left walking surface were also recorded at 20 Hz.

The muscle activity of the right leg was obtained using surface electromyography (EMG) via a wireless surface EMG system (Delsys, Trigno Wireless EMG) and recorded at 2000 Hz. Electrodes were placed on the tibialis anterior (TA), and soleus (SOL). Raw EMG signals were processed by finding the moving root mean square envelope of each signal with a sliding window of 250 ms. After computing the EMG linear envelope, the data were normalized to the maximum value of that EMG signal. Finally, the data was filtered using a 2nd order low-pass Butterworth filter with a cutoff frequency of 10 Hz.

The kinematic, force, deflection, and EMG data corresponding to the gait cycles of normal conditions and the cycles pertaining to each of the 9 types of perturbations were found and separated. The data of each gait cycle was truncated to the length of the shortest gait cycle and resampled at each 0.1% of the total cycle time for comparison of gait cycles over time. The first 30 gait cycles and the cycles in between perturbations during the normal conditions are included in the unperturbed data set. One gait cycle following a perturbation is not included in the unperturbed set in order to eliminate any residual effects from that may exist from the perturbation.

In order to evaluate the significance of recorded kinematic and muscular responses when compared to the normal condition, statistical significance was determined using an unadjusted unpaired t-test at each time instance. The unpaired t-test was selected in this case because it is a comparison of two independent distributions (ie. gait cycles with and without perturbation) which have similar variances but different sample sizes. Each statistical test was performed at the 95% confidence level and any potential Type I errors from tests being performed at each 0.1% of the gait cycle were eliminated by only concluding significance if at least 40 tests (i.e. 4% of the gait cycle) in a row indicated significance.

6.2 Model

After determining the sensory modalities that are involved (i.e. vestibular and proprioception) in the observed contralateral response, a simplified model of inter-leg coordination can be made that will relate this sensory feedback to the evoked muscle activity. Since the objective of this model is to capture and predict the effects of the low stiffness perturbations, the model will be created with input and output signals that represent deviations from normal operating conditions. In other words, instead of creating a model that utilizes measurements of sensory signals to predict measured

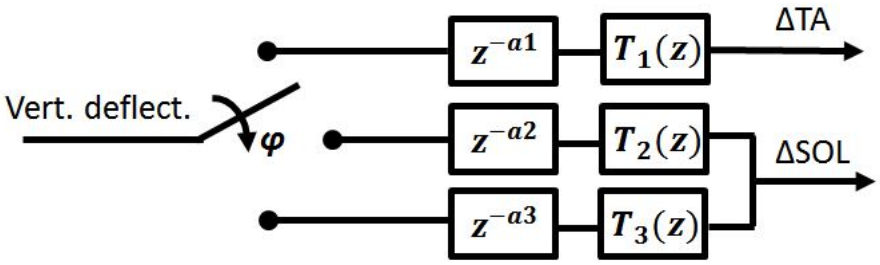

Figure 6.1: Block diagram of the simplified model of inter-leg coordination consisting of phase selected transfer functions with delays.

contralateral EMG during all (perturbed and unperturbed) cycles, the model will predict only evoked muscle activation (i.e. the recorded EMG during perturbation minus recorded EMG during cycles with no perturbation) with a representation of changes in sensory feedback. A block diagram of the simplified model is shown in Figure 6.1 and will be described below.

The input to the model was chosen to be the vertical deflection of the treadmill because it is a simple and appropriate representation of the combined change in proprioceptive and vestibular feedback. As the treadmill deflects under the load of the subject during a stiffness perturbation, there is a simultaneous change in both proprioceptive and vestibular feedback as indicated by changes in leg kinematics and body vertical acceleration. Both sensory modalities are encoding the change in the subject's vertical position, and since the subject always maintains contact with the treadmill surface, the change in vertical position can be described by the vertical deflection of the treadmill at the location of the foot. Moreover, the deflection of the treadmill is controllable by the operator through the choice of stiffness level, which would be beneficial for a therapy situation.

As mentioned above, the output of the model is evoked EMG. The recorded EMG during each perturbation gait cycle was subtracted from the mean of the EMG recordings from the last 25 unperturbed gait cycles that proceeded that perturbed gait cycle.

The mean was calculated with 25 gait cycles so as to include sufficient gait cycles for an accurate sample distribution mean and to not introduce any bias that could exist due to slight changes in experimental conditions (eg. small decrease in BWS over time due to harness slippage).

The relationship between the vertical deflection of the treadmill and the evoked muscle activity is highly nonlinear, time dependent, and has a latency of response. However, a nonlinear time-varying system can be approximated as a series of linear models at a variety of operating conditions. For this model, the system is approximated as three linear systems, each with an associated delay, at three different phases of the gait cycle. Each model is fit with 200 ms of data, which is approximately the duration between operating conditions. Another simplifying assumption, validated by the recorded data and discussed in the previous chapter, is that evoked muscle activation is only seen when the muscles are normally active. In response to the stiffness perturbations, the activity is only evoked in the TA during the loading response perturbation, within the first 500 ms. Conversely, the SOL is only evoked during the mid-stance and terminal stance perturbations. Therefore, each linear model is simplified to a linear single-input, single-output function with a delay.

6.2.1 Parameter identification

The delays ($a1$, $a2$, $a3$) were found by finding the latency between the beginning of the low stiffness perturbation to the evoked muscular response. The beginning of the perturbation was designated by the average time at which the treadmill deflection was first greater than zero. The time instance in which muscle activity was considered to have been evoked was determined when the data was significantly greater than zero, determined by a one-sample upper t-test at the 95% confidence level.

System identification techniques were used to identify the relationship between the evoked EMG activity (model output) to the vertical treadmill deflection (input). A variety of model orders and types were investigated as options to create a black box model. Eighty percent (80%) of the data cycles corresponding to low and high stiffness perturbations were randomly selected for fitting the models. The resultant models were then tested against the remaining 20% of the data from those data sets, and all of the medium stiffness data sets, as validation. The model was validated with the medium stiffness level to verify the generalization of the model to stiffness levels on which it was not trained. Expectation maximization (EM) algorithms were used for fitting the model, implemented in the System Identification Toolbox in MATLAB. Based on the normalized root mean square error between the model prediction and validation data, and the complexity of the model, a forth order polynomial model with Box-Jenkins structure was selected. This model structure is shown in Equation 6.1,

$$y(kT) = \frac{B(z)}{F(z)}u(kT) + \frac{C(z)}{F(z)}e(kT) \tag{6.1}$$

where $B(z)$, $F(z)$, $C(z)$, and $F(z)$ are 4th order polynomials and $y(kT)$, $u(kT)$, and $e(kT)$ are the evoked muscle activity, vertical deflection, and white noise, respectively, at time kT.

The model prediction and experimental validation data were compared with the Pearson correlation coefficient and a fitness value derived from the normalized root mean square error shown in Equation 6.2

$$f = 1 - \frac{||y - \hat{y}||_2}{||y - mean(y)||_2} \tag{6.2}$$

where f is the fitness value, y is the experimental validation data and $\hat{y}$ is the model prediction.

6.3 Results

The results of the kinematic and muscular response for this experiment show a response that is scalable with the magnitude of the perturbation and dependent on the timing of the perturbation within the gait cycle. As this result has been shown in Chapter 4, it will not be shown nor discussed in this chapter. However, this data confirms the previous results and will be used to fit a model that predicts contralateral muscle activation based on the magnitude and timing of the vertical deflection of the treadmill.

The latencies (a_1, a_2, a_3) for each of the three models for all 8 subjects are shown in Table 6.1. The average and standard deviation across subjects is also shown. A dash indicates that there was not significant evoked EMG activity, and thus a latency could not be calculated. The TA EMG for subject 7 was very noisy and did not resemble appropriate activation of the TA during normal walking, presumably due to inadequate attachment or poor placement of the electrode. This made latency 1 incalculable and is indicated with an asterisk. The data for this subject are still included in the analysis because the SOL EMG, kinematics, deflection, and force data are accurate and useful for the purposes of this model.

The roots of the model polynomials in polar form, followed by the fitness values and the Pearson correlation coefficients (mean and standard deviation), for all 3 models (T_1, T_2, T_3) are shown below in Tables 6.2 - 6.10.

Table 6.1: Model Latency Values

	Latency 1 (ms)	Latency 2 (ms)	Latency 3 (ms)
Subject 1	163.1	271.6	-
Subject 2	96.4	401.3	181.0
Subject 3	98.5	-	-
Subject 4	146.0	196.8	-
Subject 5	139.8	246.0	193.3
Subject 6	136.1	-	-
Subject 7	*	285.7	-
Subject 8	106.8	237.8	-
Ave±std	126.7±26.0	273.2±69.9	187.2±8.7

6.4 Discussion

The main objectives in the creation of the presented model were to 1) predict contralateral muscle activation based on the timing and magnitude of the unilateral stiffness perturbations and 2) provide insight into the related sensorimotor mechanism. A discussion of how the model addresses each of these points will be presented below.

6.4.1 Model prediction

As shown in Tables 6.5 - 6.10, the model prediction matches the experimental data with high accuracy (average fitness value ≥ 0.66 and average correlation coefficient ≥ 0.91) for all models. Moreover, the accuracy of fit is high across all levels of stiffness. Since the model was trained with 80% of the data from the low and high stiffness perturbations, and with no data from the medium stiffness perturbation

Table 6.2: Roots of Model 1 Polynomials

	B(z)	F(z)	C(z)	D(z)
Subject 1	$0.04\angle 180°$ $1.01\angle \pm 177°$	$0.99\angle \pm 1°$ $0.54\angle \pm 63°$	$0.97\angle \pm 175°$ $0.97\angle \pm 179°$	$0.94\angle \pm 29°$ $1.00\angle \pm 1°$
Subject 2	$0.64\angle 180°$ $1.03\angle 180°$ $1.08\angle 180°$	$0.97\angle \pm 32°$ $0.97\angle \pm 3°$	$0.98\angle \pm 173°$ $0.98\angle \pm 179°$	$0.91\angle \pm 28°$ $0.99\angle \pm 0°$
Subject 3	$1.41\angle 0°$ $1.01\angle \pm 169°$	$0.97\angle \pm 5°$ $0.92\angle \pm 0°$	$0.95\angle \pm 174°$ $0.87\angle \pm 170°$	$0.90\angle \pm 27°$ $0.99\angle \pm 1°$
Subject 4	$0.53\angle 180°$ $1.06\angle \pm 175°$	$0.98\angle \pm 27°$ $0.96\angle \pm 1°$	$0.97\angle \pm 176°$ $0.96\angle \pm 179°$	$0.94\angle \pm 27°$ $0.99\angle \pm 1°$
Subject 5	$4.24\angle 0°$ $1.00\angle \pm 179°$	$0.99\angle \pm 32°$ $0.98\angle \pm 1°$	$0.97\angle \pm 177°$ $0.97\angle \pm 179°$	$0.89\angle \pm 26°$ $0.99\angle \pm 1°$
Subject 6	$2.44\angle 0°$ $0.98\angle \pm 178°$	$0.99\angle \pm 28°$ $0.99\angle \pm 2°$	$0.98\angle \pm 177°$ $0.97\angle \pm 179°$	$0.91\angle \pm 27°$ $1.00\angle 0°$ $0.99\angle 0°$
Subject 8	$1.06\angle 180°$ $0.92\angle \pm 169°$	$0.96\angle \pm 2°$ $0.96\angle 0°$ $0.31\angle 180°$	$0.96\angle \pm 174°$ $0.96\angle \pm 179°$	$0.89\angle \pm 27°$ $1.00\angle \pm 2°$

Table 6.3: Roots of Model 2 Polynomials

	B(z)	F(z)	C(z)	D(z)
Subject 1	$2.11\angle 0°$ $1.04\angle \pm 178°$	$0.97\angle \pm 3°$ $0.98\angle \pm 29°$	$0.97\angle \pm 176°$ $0.97\angle 180°$ $0.90\angle 180°$	$0.93\angle \pm 31°$ $1.00\angle \pm 0°$
Subject 2	$1.23\angle 0°$ $1.01\angle \pm 178°$	$0.96\angle \pm 4°$ $0.95\angle \pm 1°$	$0.97\angle \pm 175°$ $0.97\angle \pm 179°$	$0.95\angle \pm 31°$ $0.99\angle \pm 1°$
Subject 4	$0.98\angle 180°$ $0.79\angle 180°$ $0.15\angle 0°$	$0.98\angle \pm 27°$ $0.98\angle \pm 2°$	$0.98\angle \pm 175°$ $0.98\angle \pm 178°$	$0.91\angle \pm 28°$ $1.00\angle 0°$ $0.97\angle 0°$
Subject 5	$0.93\angle 0°$ $1.01\angle \pm 177°$	$0.90\angle \pm 22°$ $0.97\angle \pm 1°$	$0.98\angle \pm 176°$ $0.97\angle \pm 178°$	$0.93\angle \pm 24°$ $1.00\angle \pm 1°$
Subject 7	$1.10\angle 0°$ $1.02\angle 180°$ $0.87\angle 180°$	$0.95\angle \pm 35°$ $0.98\angle 0°$ $0.95\angle 0°$	$0.99\angle \pm 171°$ $0.99\angle 180°$ $0.58\angle 0°$	$0.99\angle \pm 0°$ $0.81\angle \pm 1°$
Subject 8	$803.79\angle 180°$ $1.02\angle \pm 174°$	$0.99\angle \pm 80°$ $0.97\angle \pm 2°$	$0.98\angle \pm 148°$ $0.97\angle \pm 178°$	$0.92\angle \pm 34°$ $1.01\angle \pm 1°$

Table 6.4: Roots of Model 3 Polynomials

	B(z)	F(z)	C(z)	D(z)
Subject 2	$1.11\angle 180°$ $1.02\angle 180°$ $0.00\angle 0°$	$0.98\angle \pm 27°$ $0.97\angle \pm 1°$	$0.97\angle \pm 177°$ $0.97\angle \pm 179°$	$0.95\angle \pm 31°$ $1.00\angle \pm 0°$
Subject 5	$0.66\angle 0°$ $1.04\angle \pm 180°$	$0.94\angle \pm 15°$ $0.95\angle \pm 3°$	$0.97\angle \pm 175°$ $0.96\angle \pm 179°$	$0.95\angle \pm 31°$ $1.00\angle \pm 0°$

Table 6.5: Model 1 Validation - Fitness Value

	Low	Medium	High	All
Subject 1	0.85 ± 0.04	0.81 ± 0.05	0.85 ± 0.03	0.82 ± 0.05
Subject 2	0.83 ± 0.05	0.76 ± 0.13	0.82 ± 0.11	0.78 ± 0.12
Subject 3	0.88 ± 0.06	0.76 ± 0.21	0.67 ± 0.22	0.76 ± 0.19
Subject 4	0.76 ± 0.03	0.69 ± 0.26	0.83 ± 0.00	0.72 ± 0.22
Subject 5	0.80 ± 0.19	0.76 ± 0.20	0.70 ± 0.05	0.76 ± 0.18
Subject 6	0.88 ± 0.03	0.73 ± 0.14	0.40 ± 0.16	0.71 ± 0.19
Subject 8	0.80 ± 0.22	0.79 ± 0.13	0.76 ± 0.07	0.79 ± 0.13
Average	0.83 ± 0.04	0.76 ± 0.04	0.72 ± 0.16	0.76 ± 0.04

Table 6.6: Model 1 Validation - Correlation Coefficient

	Low	Medium	High	All
Subject 1	0.99 ± 0.01	0.98 ± 0.01	0.99 ± 0.00	0.98 ± 0.01
Subject 2	0.99 ± 0.01	0.96 ± 0.04	0.98 ± 0.02	0.97 ± 0.03
Subject 3	0.99 ± 0.01	0.95 ± 0.07	0.93 ± 0.08	0.95 ± 0.06
Subject 4	0.97 ± 0.01	0.91 ± 0.11	0.99 ± 0.00	0.93 ± 0.10
Subject 5	0.97 ± 0.04	0.96 ± 0.07	0.95 ± 0.02	0.96 ± 0.06
Subject 6	0.99 ± 0.00	0.95 ± 0.04	0.79 ± 0.12	0.94 ± 0.09
Subject 8	0.97 ± 0.04	0.97 ± 0.04	0.97 ± 0.02	0.97 ± 0.03
Average	0.98 ± 0.01	0.95 ± 0.02	0.94 ± 0.07	0.96 ± 0.02

Table 6.7: Model 2 Validation - Fitness Value

	Low	Medium	High	All
Subject 1	0.87 ± 0.04	0.61 ± 0.20	0.26 ± 0.76	0.60 ± 0.32
Subject 2	0.86 ± 0.13	0.75 ± 0.17	0.76 ± 0.09	0.77 ± 0.15
Subject 4	0.93 ± 0.01	0.68 ± 0.22	0.71 ± 0.26	0.73 ± 0.21
Subject 5	0.80 ± 0.15	0.65 ± 0.19	0.63 ± 0.12	0.67 ± 0.18
Subject 7	0.37 ± 0.16	0.72 ± 0.18	0.72 ± 0.23	0.67 ± 0.22
Subject 8	0.86 ± 0.06	0.39 ± 0.24	0.73 ± 0.12	0.50 ± 0.28
Average	0.78 ± 0.21	0.63 ± 0.13	0.64 ± 0.19	0.66 ± 0.09

Table 6.8: Model 2 Validation - Correlation Coefficient

	Low	Medium	High	All
Subject 1	0.99 ± 0.01	0.90 ± 0.12	0.60 ± 0.54	0.87 ± 0.21
Subject 2	0.99 ± 0.02	0.96 ± 0.05	0.97 ± 0.00	0.97 ± 0.04
Subject 4	1.00 ± 0.00	0.92 ± 0.12	0.94 ± 0.08	0.93 ± 0.11
Subject 5	0.97 ± 0.03	0.92 ± 0.07	0.92 ± 0.05	0.93 ± 0.06
Subject 7	0.77 ± 0.12	0.94 ± 0.07	0.94 ± 0.07	0.92 ± 0.09
Subject 8	0.99 ± 0.01	0.74 ± 0.26	0.96 ± 0.03	0.81 ± 0.24
Average	0.95 ± 0.09	0.90 ± 0.08	0.89 ± 0.14	0.91 ± 0.06

Table 6.9: Model 3 Validation - Fitness Value

	Low	Medium	High	All
Subject 2	0.40 ± 0.62	0.74 ± 0.25	0.42 ± 0.06	0.64 ± 0.31
Subject 5	0.82 ± 0.04	0.78 ± 0.19	0.88 ± 0.09	0.80 ± 0.16
Average	0.61 ± 0.30	0.76 ± 0.03	0.65 ± 0.33	0.72 ± 0.11

Table 6.10: Model 3 Validation - Correlation Coefficient

	Low	Medium	High	All
Subject 2	0.58 ± 0.58	0.92 ± 0.16	0.81 ± 0.05	0.86 ± 0.25
Subject 5	0.98 ± 0.01	0.96 ± 0.08	0.99 ± 0.01	0.96 ± 0.07
Average	0.78 ± 0.28	0.94 ± 0.03	0.90 ± 0.13	0.91 ± 0.07

data set, accurate model predictions of the validation data indicates that the model is both repeatable and generalizable. The tables of validation data all show that the correlation coefficient values are consistently higher than the fitness values. This occurs because the model prediction follows the trend of the experimental data, but with small low-frequency oscillations. This results in the model being highly linearly correlated with the experimental data, but has some error accumulation as the model oscillates, as any deviation from the experimental data is penalized in the fitness calculation, shown in Equation 6.2. This can be visualized in Figure 6.2 where the experimental data and the simulation prediction of results with the highest correlation coefficient from model 1 for low (left column), medium (center column), and high (right column) stiffness perturbations for all subjects (rows).

6.4.2 Additional Considerations

6.4.2.1 Pole and Zero Locations

The location of the poles and zeros of the three models reveal additional insight about the observed mechanism of inter-leg coordination. First, all of the poles are either laying on or within the unit circle in the z-plane indicating that the system is not unstable. Moreover, the pole locations are very similar across subjects (see Figure 6.3) which indicates that the model, and therefore the contralateral response, is repeatable

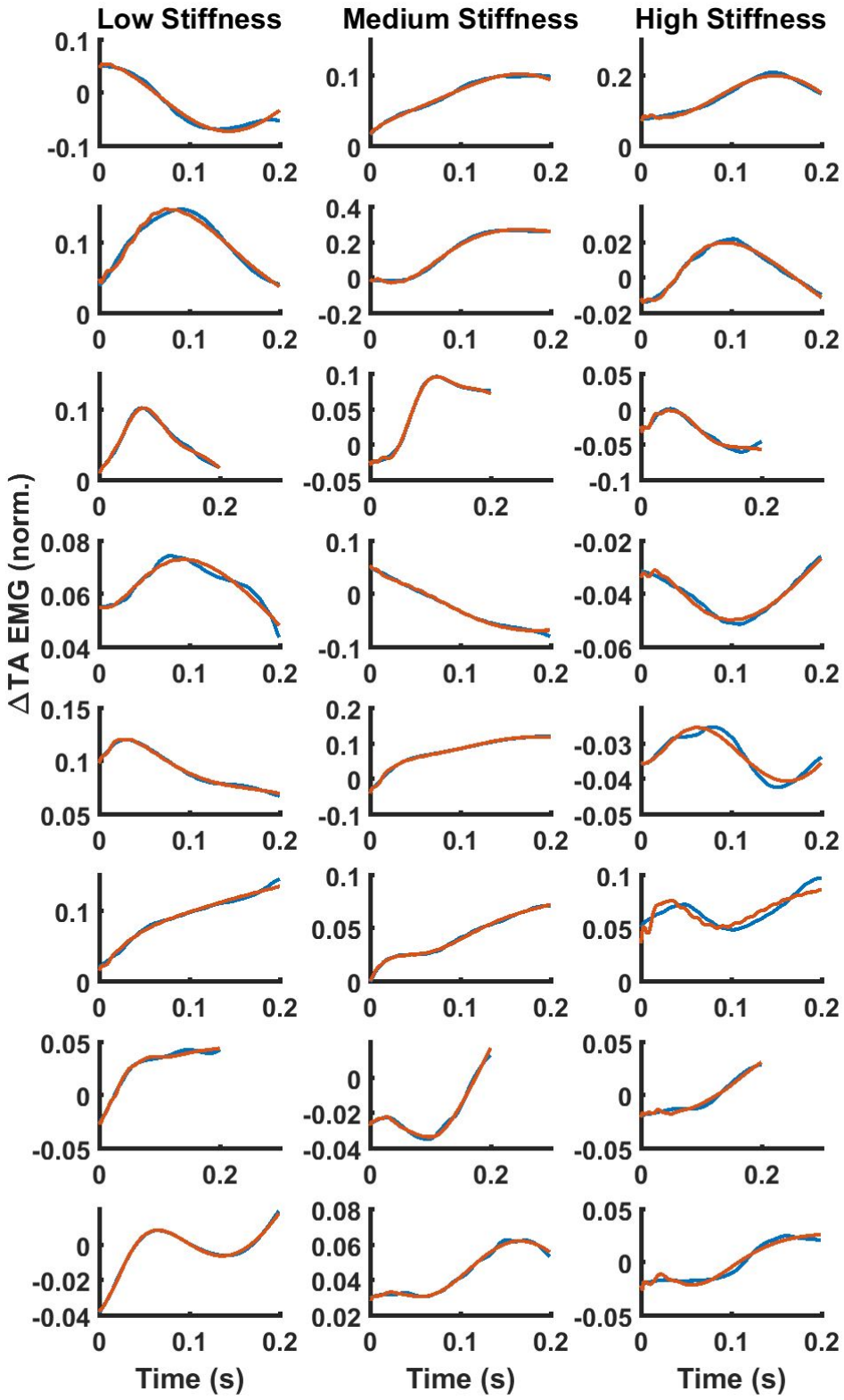

Figure 6.2: Experimental data and simulation prediction of results with the highest correlation coefficient from model 1 for low (left column), medium (center column), and high (right column) stiffness perturbations for all subjects (rows).

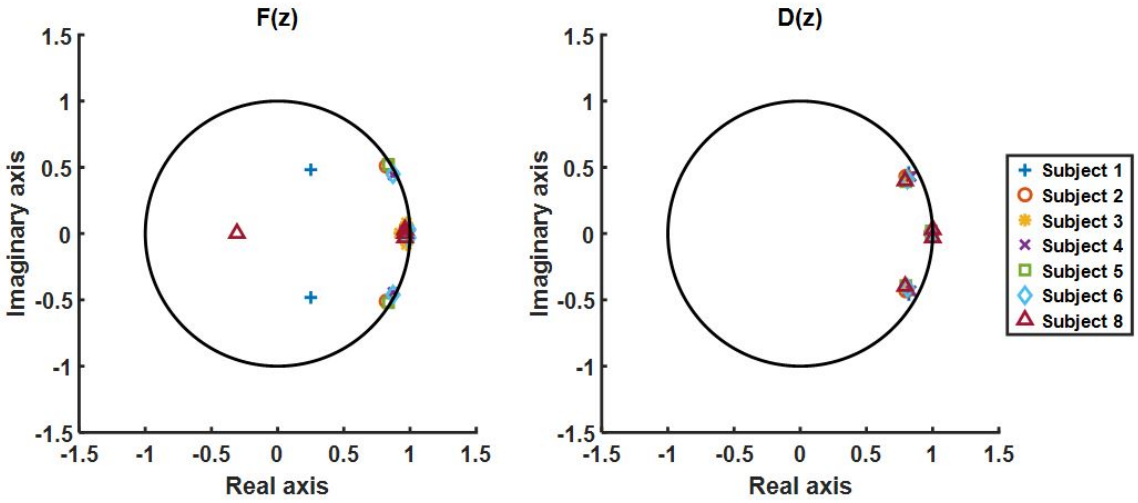

Figure 6.3: Map of poles from model 1 for all subjects.

across subjects. This is another validation of the repeatable experimental results of systematic increases in muscle activation for all subjects.

The poles and zeros are also similar across models (ie. phase of the gait cycle). A map of all poles and zeros for all three models for subject 5 is shown in Figure 6.4, with each model represented by a different color. There is very little change in pole location, indicated by x's and squares, but some movement in zeros from $B(z)$. Of special interest are the zeros from $B(z)$ that lay on the real axis. The zero decreases in magnitude from model 1 to model 3. In the step response, zeros lead to a change in rise time and overshoot. Since the poles are in the same regions, but there is a change in this zero, this indicates that within the series of linear models each model creates a similar overall response (ie. evoked muscular activity), with a slightly different speed of response.

6.4.2.2 Latency

The latency of response shown in Table 6.1 provides indications that the observed evoked muscle activity is mediated by supraspinal structures. The minimum latency

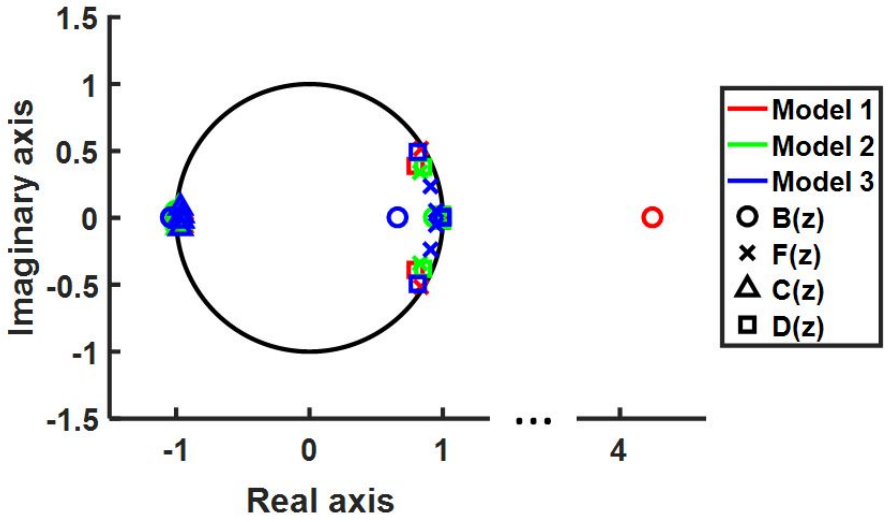

Figure 6.4: Map of roots of model polynomials for all three models for subject 5.

recorded for all subjects was 96.4 ms which is longer than the 50-80 ms latency that would be seen for spinal reflexes (Darton *et al.*, 1985; Yavuz *et al.*, 2014). Moreover, with average latencies greater than 125 ms, the results from this study suggest that the response is mediated through supraspinal neural structures (Shemmell *et al.*, 2009; Zuur *et al.*, 2009). This result agrees with the conclusion presented in Section 5.4 that the observed sensorimotor mechanism is modulated through the motor cortex.

6.5 Conclusions

In this chapter, a series of linear 4th order polynomial models with input delays were created that accurately predicts the evoked contralateral muscle activity based on the vertical deflection of the left walking surface. This model was also shown to be similar across subjects. Additionally, a latency of response was observed that provides support that the contralateral response to unilateral stiffness perturbations is mediated through the brain. This model is foundational for model-based, predictive and individualized robot-assisted gait therapy that utilizes this mechanism of inter-leg coordination. This type of therapy would involve a brief training session in which

a variety of timing and magnitudes of stiffness perturbations would be prescribed. This data would then be used to fit the model parameters for the specific patient. Then a therapy protocol could be designed in which perturbations are chosen and tuned to facilitate desired therapeutic outcomes.

Chapter 7

CASE STUDIES WITH HEMIPLEGIC WALKERS

The experimental results presented thus far have been with healthy subjects in order to identify and model sensorimotor mechanisms of inter-leg coordination during normal walking. As a major long-term objective of this research is to improve robot-assisted gait therapy for impaired walkers by utilizing mechanisms of inter-leg coordination, it is desirable to investigate the preservation of the identified sensorimotor mechanism after neurological injury. In this chapter, three case studies with hemiplegic walkers are presented.

7.1 Case Study I

7.1.1 Study Participant

The study participant was a 29 year old female (weight 123 lbs) who had an hemorrhagic stroke 5.5 years prior to this study. The cerebrovascular accident occurred in the left hemisphere and resulted in right hemiparesis (dominant side). She has received physical therapy and occupational therapy, which was first focused on recovering her right arm function. She has minimal voluntarily controlled activation of her right TA, and no voluntary contraction of the other ankle muscles (i.e. GA and SOL). However, the subject is ambulatory because the muscles work in synergy such as when walking. A major impairment of the subject's gait includes insufficient activity in the right TA (which is the primary muscle creating dorsiflexion) in the swing phase which results in decreased dorsiflexion. Insufficient dorsiflexion during walking, referred to as drop-foot, is a problem that most impaired walkers suffer from, and is the leading cause of after-stroke falls (Knutsson and Richards, 1979; Takebe and Basmajian, 1976). The subject typically wears the NESS L300 Foot Drop System

(Bioness Inc.) to reduce drop-foot while walking. However, she wears an articulated ankle-foot orthosis (AFO) with a plantarflexion stop instead of the NESS L300 when wanting better ankle stabilization when walking. The subject wore her AFO while participating in this study.

7.1.2 Experimental Protocol

In order to investigate the existence of mechanisms of inter-leg coordination in this hemiparetic walker, unilateral stiffness perturbations were induced using the VST in the same manner as was described in Section 4.1.1. The subject participated in four sequential trials with a brief (approximately 5 minute) rest break in between trials. For all trials the subject was offloaded by 30% of her body weight to be consistent with the experiments with healthy subjects previously presented (see Chapters 4-6). In each trial she walked for approximately 7 minutes on the treadmill at a self selected speed of 0.51 m/s. Again for consistency with previous experiments, the right treadmill belt was not allowed to deflect for the duration of the experiment, thus preventing any direct perturbation of the right leg. The surface underneath the left leg was commanded to maintain a stiffness of 1 MN/m, which is very high and considered to be rigid, for 30 gait cycles at the beginning of the experiment. Then, after a random number n of steps, where $n \in [4, 8]$, the stiffness was immediately dropped to a constant value. The stiffness utilized in trials 1, 2, 3, and 4 were 80, 60, 40 and 20 kN/m, respectively. The low stiffness perturbation began shortly after heel strike (approximately 125 ms) and lasted for the duration of the right leg stance phase after which the stiffness was commanded back to 1 MN/m for the next n number of steps. The subject experienced a minimum of 30 perturbations at each level of stiffness. A picture of the subject experiencing a low stiffness perturbation is shown in Figure 7.1. Informed consent from the subject was obtained at the time

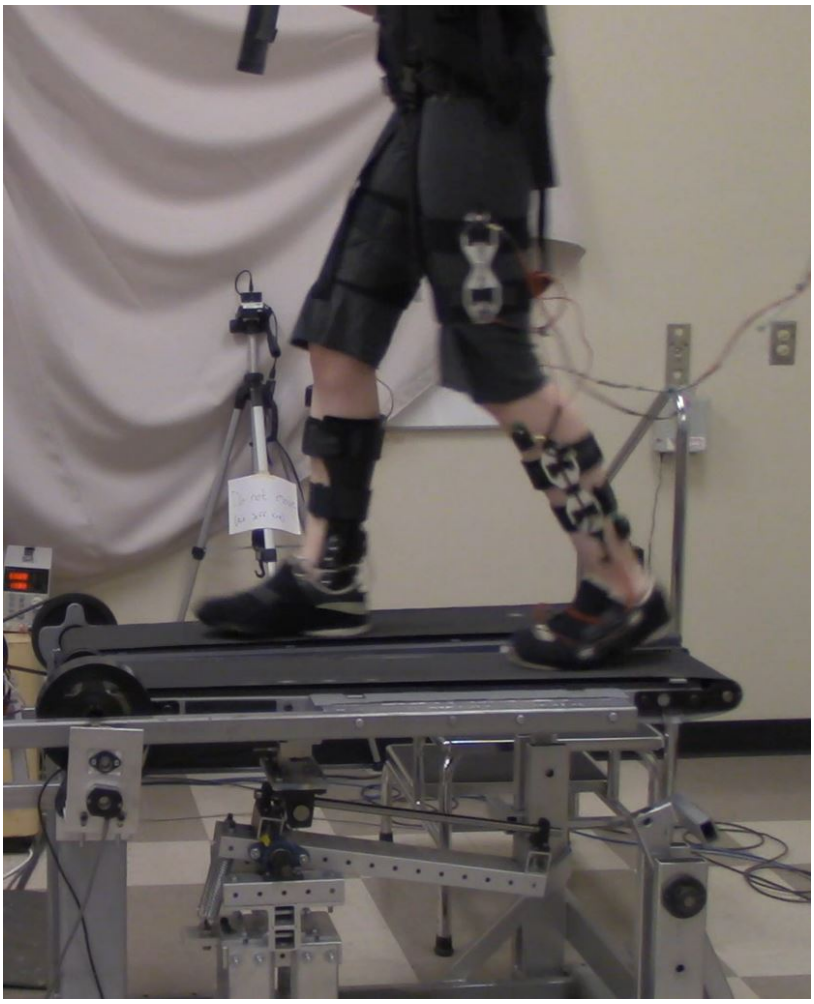

Figure 7.1: The subject experiencing a low stiffness perturbation to the left walking surface.

of the experiment, and the experimental protocol is approved by the Arizona State University Institutional Review Board (IRB ID#: STUDY00001001).

7.1.3 Data Collection and Processing

Kinematic data for both legs were obtained at 140 Hz using an infrared camera system that tracked 12 infrared LEDs (6 on each leg) placed as pairs on the thigh, shank, and foot. This data was also utilized in real time for timing of the stiffness perturbation.

The muscle activity of both legs were obtained using surface electromyography (EMG) via a wireless surface EMG system (Delsys, Trigno Wireless EMG) and recorded at 2000 Hz. Electrodes were placed on the tibialis anterior (TA), gastrocnemius (GA) and soleus (SOL) of both legs. Raw EMG signals were processed by finding the moving root mean square envelope of each signal with a 250 ms window. After computing the EMG linear envelope, the data were normalized to the maximum value of that EMG signal.

The kinematic and EMG data corresponding to the gait cycles of normal conditions and the cycles pertaining to the perturbations were found and normalized temporally to percent gait cycle in order to eliminate discrepancies due to natural variations in gait patterns (i.e. stride length, cycle duration, etc). The data of each gait cycle was resampled at each 0.01% of the gait cycle (approximately 0.15 ms) during the normalization to percent gait cycle. The first 30 gait cycles and the cycles in between perturbations during the normal conditions are included in the unperturbed data set. One gait cycle following a perturbation is not included in the unperturbed set in order to eliminate any residual effects from the perturbation. This processing results in normalized EMG signals as a function of percent gait cycle, where 0 and 100% correspond to the heel-strike of the left (perturbed) leg.

In order to evaluate the significance of recorded EMG responses when compared to the normal condition, statistical significance was determined using an unadjusted unpaired t-test at each time instance. The unpaired t-test was selected in this case because it is a comparison of two independent distributions (i.e. gait cycles with and without perturbation) which have similar variances but different sample sizes. Each statistical test was performed at the 95% confidence level and any potential Type I errors from tests being performed at each 0.01% of the gait cycle were eliminated by

only concluding significance if at least 400 tests (i.e. 4% of the gait cycle) in a row indicated significance.

7.1.4 Results

The results of this case study show that significant changes in contralateral muscle activity can be evoked by unilateral perturbations to the stiffness of the walking surface. The muscular response of the affected (unperturbed) leg to the low stiffness perturbations of magnitudes 20 and 40 kN/m are shown in Figure 7.2. The normalized EMG amplitude for the TA, GA and SOL (mean and standard deviation) for all gait cycles pertaining to each of these two surface stiffness levels is shown. The data are plotted as a function of the gait cycle percentage, where heel-strike and toe-off of the right leg are indicated on the figure as HS and TO, respectively. Black bars underneath an asterisk are included to indicate when statistically significant changes are observed. An indication of the timing of the perturbation of the left walking surface is also shown.

As indicated by the black bars in Figure 7.2, there are significant increases in TA and GA activation during the swing and stance phases, respectively, for both levels of stiffness. There was no evoked activation in any muscle for either the 60 or 80 kN/m stiffness levels, and therefore, are not plotted for simplicity. The most significant result from this study is that there was muscle activity evoked in the paretic leg, showing the existence of mechanisms of inter-leg coordination after neurological injury. Moreover, the exact same result (i.e. increased TA activation during swing phase) is shown from this study as was seen with healthy subjects (see Section 4.3). This additional activation in the right TA also created significant dorsiflexion in the right ankle, as shown in Figure 7.3. Moreover, there are also increases in hip flexion

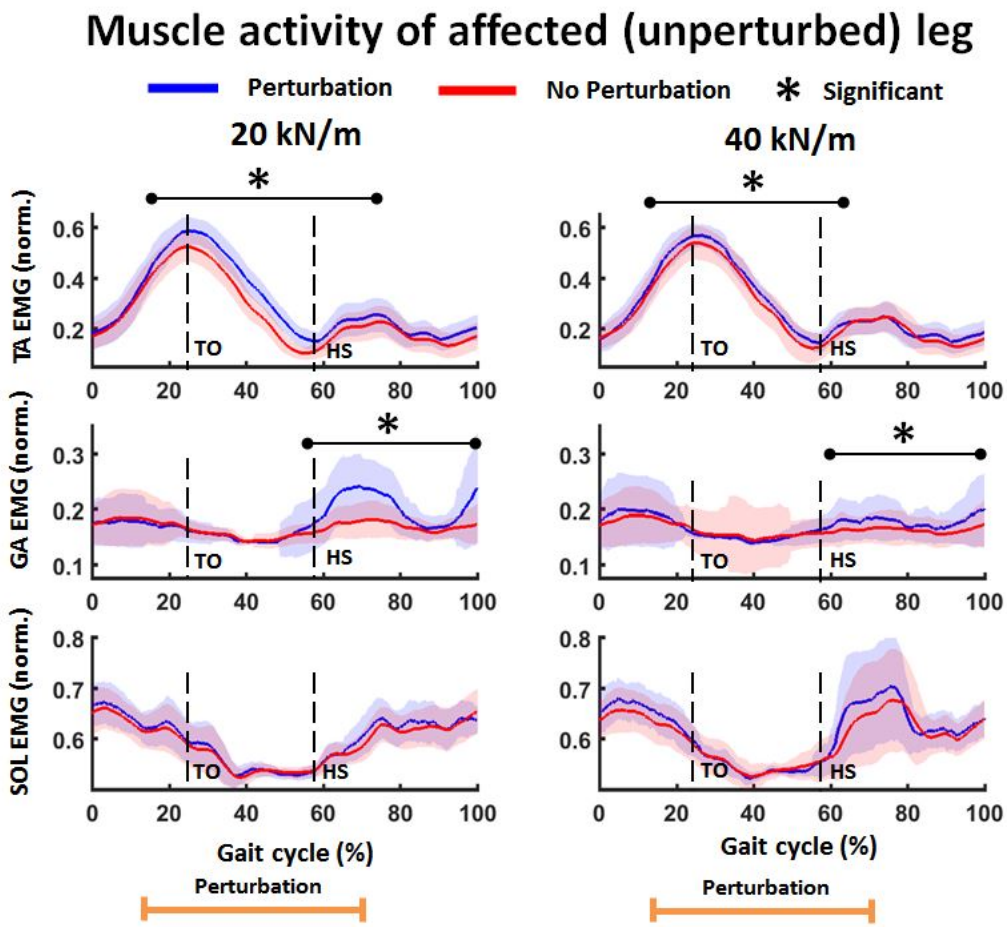

Figure 7.2: Averaged muscle activity of the unperturbed (affected) leg for a the participating subject as function of percent gait cycle, where 0% corresponds to heel-strike of the left (perturbed) leg. Plotted in rows from top to bottom are the normalized TA EMG, normalized GA EMG, and normalized SOL EMG for two levels of stiffness perturbation (20 and 40 kN/m), from left to right, respectively. Mean (darker lines) and standard deviations (lightly shaded areas) values are shown. Statistically significant changes are indicated by black bars placed beneath a black asterisk. Heel-strike and toe-off of the right leg are indicated by HS and TO, respectively. The duration of the gait cycle for this subject is approximately 1.4 s.

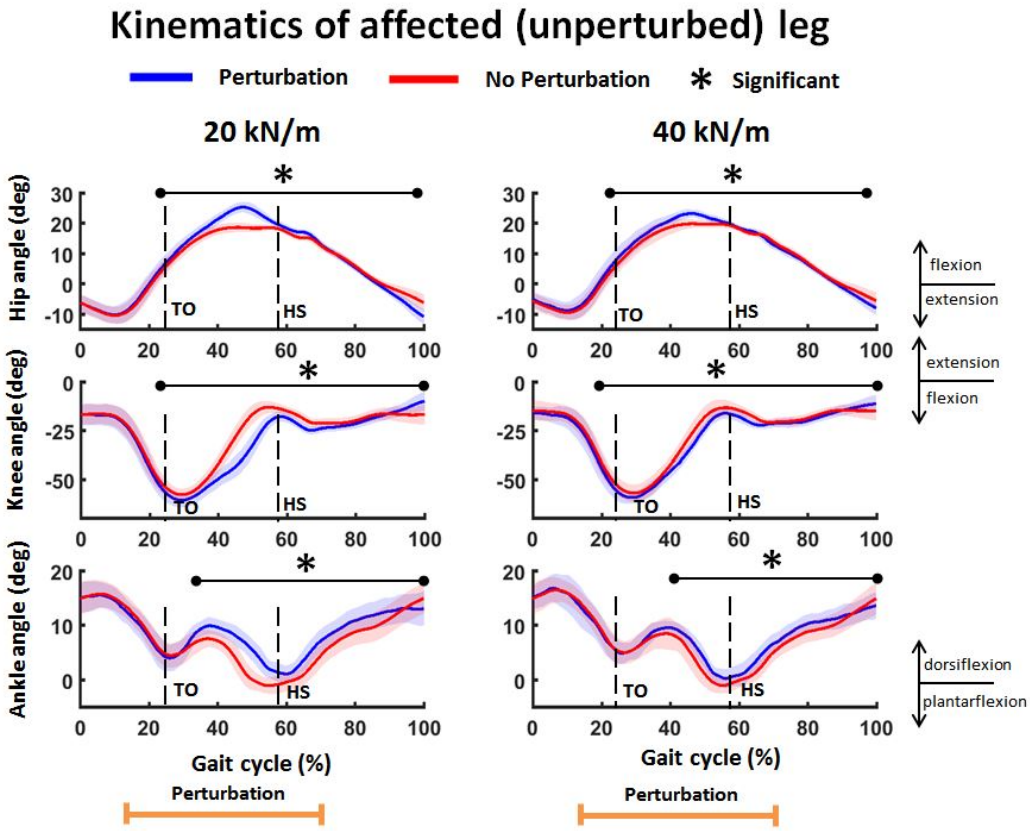

Figure 7.3: Averaged kinematics of the unperturbed (affected) leg for a the participating subject as function of percent gait cycle, where 0% corresponds to heel-strike of the left (perturbed) leg. Plotted in rows from top to bottom are the kip, knee, and ankle angles for two levels of stiffness perturbation (20 and 40 kN/m), from left to right, respectively. Mean (darker lines) and standard deviations (lightly shaded areas) values are shown. Statistically significant changes are indicated by black bars placed beneath a black asterisk. Heel-strike and toe-off of the right leg are indicated by HS and TO, respectively. The duration of the gait cycle for this subject is approximately 1.4 s.

and knee flexion for this subject, which was also seen in Section 4.3 with healthy subjects.

7.2 Case Study II

7.2.1 Study Participant

The study participant was a 17 year old male (weight 155 lbs) who had an traumatic brain injury 18 months prior to the study. A left basal ganglia hemorrhage with surrounding edema and left frontal hematoma resulted in hemiparesis in his right (dominant) side. He demonstrates decreased right ankle dorsiflexion and utilizes a right hip hike to clear his right foot during swing phase. He currently does not use any assistive devices for walking.

7.2.2 Experimental Protocol

The experimental protocol and data collection for this study was the same as presented in Case Study I (see Sections 7.1.2 and 7.1.3), with a few differences in order to accommodate the preferences and needs of this subject. The subject did not feel comfortable with the BWS and, therefore, walked with 0% BWS. The subject wore the harness and was safely attached to the BWS system but was not offloaded with any force. This subject only experienced perturbations at the 80 and 60 kN/m stiffness levels. A picture of the subject experiencing a perturbation is shown in Figure 7.4. Informed consent from the subject and his parents was obtained at the time of the experiment, and the experimental protocol is approved by the Arizona State University Institutional Review Board (IRB ID#: STUDY00001001).

7.2.3 Results

The results from this Case Study are similar to those from Case Study I (see Section 7.1.4). This includes no significant contralateral response due to stiffness perturbations of 80 kN/m, but significant TA activation and dosriflexion during swing

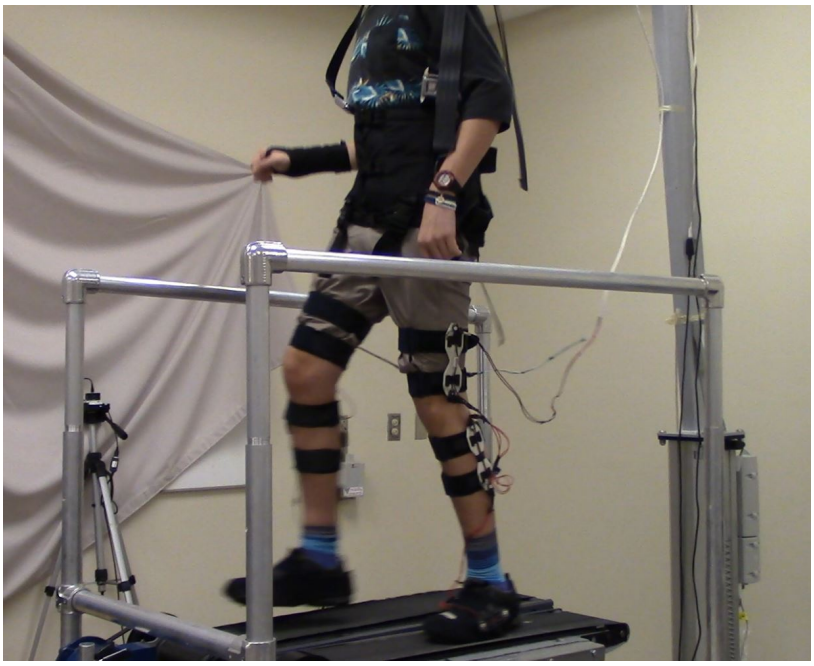

Figure 7.4: The subject experiencing a low stiffness perturbation to the left walking surface.

phase due to stiffness perturbations of 60 kN/m. The contralateral muscular and kinematic response to the 60 kN/m stiffness perturbations is shown in Figure 7.5. The data are plotted as a function of the gait cycle percentage, where heel-strike and toe-off of the left leg are indicated on the figure as HS and TO, respectively. Black bars underneath an asterisk are included to indicate when statistically significant changes are observed.

The results of this experiment confirm the results presented in Case Study I, thus providing additional support for the preservation of sensorimotor mechanisms of inter-leg coordination after neurological injury. Moreover, the contralateral response of increased TA activation and increased dosrsiflexion was consistent despite differences between the subjects. A few of these differences include the time after injury, level of impairment, and compensatory strategies. Therefore, this mechanism of inter-leg coordination appears to be robust across injuries and level of impairment.

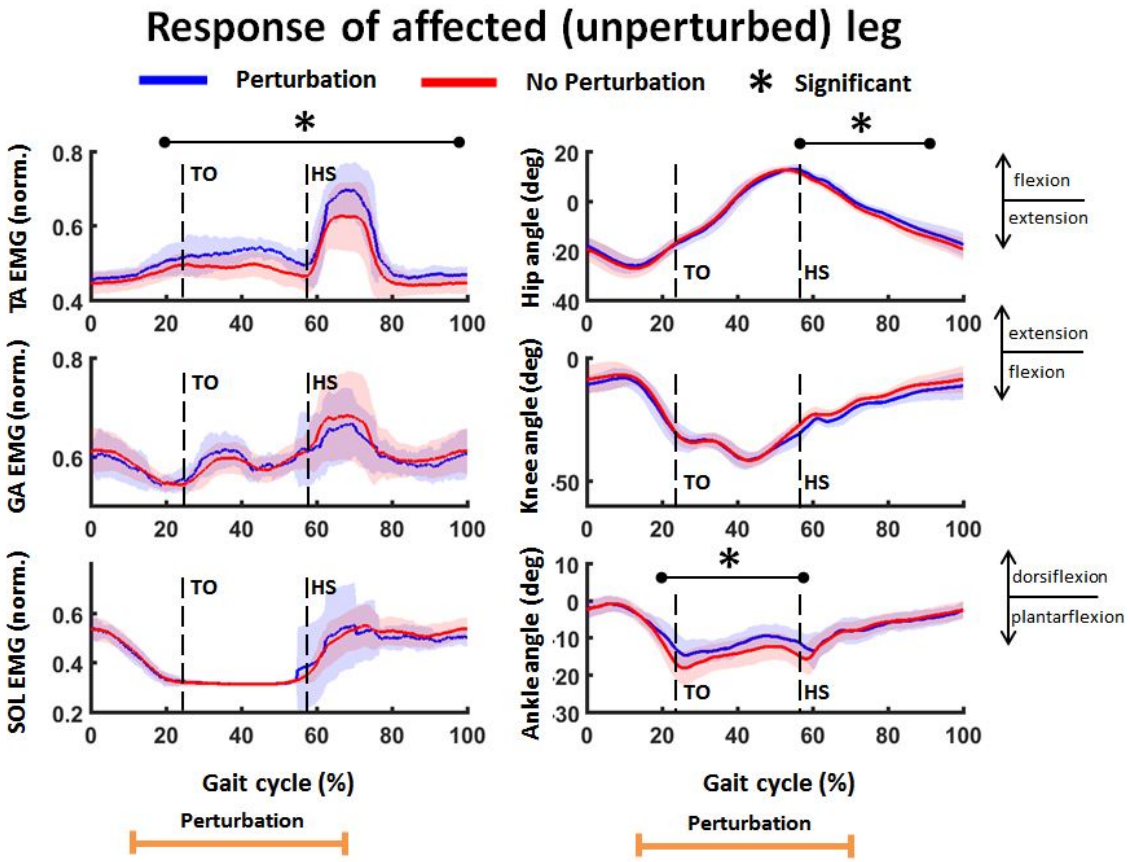

Figure 7.5: Response the affected (unperturbed) leg for the participating subject as function of percent gait cycle, where 0% corresponds to heel-strike of the left (perturbed) leg. Plotted in rows from top to bottom are the normalized TA EMG, normalized GA EMG, and normalized SOL EMG (left column) and hip, knee, and ankle angles (right column). Mean (darker lines) and standard deviations (lightly shaded areas) values are shown. Statistically significant changes are indicated by black bars placed beneath a black asterisk. Heel-strike and toe-off of the right leg are indicated by HS and TO, respectively. The duration of the gait cycle is approximately 1.8 s.

7.3 Case Study III

The case study presented here (up to the comparisons with the two previous case studies) comes from sections of a publication in the proceedings of the 2016 International Conference of the IEEE Engineering in Medicine and Biology Society (Skidmore and Artemiadis (2016b), ©2016 IEEE).

7.3.1 Study Participant

The study participant was a 41 year old male (weight 175 lbs) who experienced a traumatic brain injury at the age of 12. A 6-7 hour epidural arterial hematoma in the right hemisphere resulted in hemiplegia. His left leg (non-dominant) is the affected limb with gait impairments due to reduced motor control, limited range of motion, and the chronic influence of spasticity.

7.3.2 Experimental Protocol

The experimental protocol and data collection for this case study was the same as presented in Case Study I (see Sections 7.1.2 and 7.1.3), with one major difference. Due to the fact that this subject's affected limb is the left leg, and the VST system currently can only adjust the stiffness of one treadmill belt (see Section 3.1.2), this subject was required to walk on the treadmill facing the opposite direction than all of the previous subjects. The direction of the treadmill belt motion is reversible so he was able to walk forward, but was facing the opposite direction. A discussion of the significance of the direction of walking will be given below in Section 7.3.3.

This subject participated in three sequential trials with a brief (approximately 5 minutes) rest break in between trials. For each trial he was offloaded by 30% of his body weight and walked for approximately 7 minutes on the treadmill at a self selected speed of 0.51 m/s. For this experiment the treadmill belt underneath his left leg was not allowed to deflect and the perturbations were applied to the right walking surface. As in previous experiments, the walking surface maintained a stiffness of 1 MN/m for 30 gait cycles at the beginning of the experiment and then, after a random number n of steps, where $n \in [4, 7]$, the stiffness was immediately dropped to a constant value. The stiffness utilized in trials 1, 2, and 3 were 100, 80, and 60

Figure 7.6: The subject experiencing a low stiffness perturbation to the right walking surface (Skidmore and Artemiadis (2016b), ©2016 IEEE).

kN/m, respectively. The low stiffness perturbation began shortly after heel strike (approximately 125 ms) and lasted for the duration of the right leg stance phase (i.e. until toe-off) after which the stiffness was commanded back to 1 MN/m for the next n number of steps. The subject experienced 30 perturbations at each level of stiffness. A picture of the subject walking on the treadmill facing the opposite direction and experiencing a low stiffness perturbation to the right walking surface is shown in Figure 7.6. Informed consent from the subject was obtained at the time of the experiment, and the experimental protocol is approved by the Arizona State University Institutional Review Board (IRB ID#: STUDY00001001).

7.3.3 Results

The results of the experiment show significant changes in evoked contralateral muscle activity of the left leg in response to the low stiffness perturbations to the right walking surface, again showing the existence of mechanisms of inter-leg coordination after neurological injury. The muscular response of the affected (unperturbed) leg for all levels of stiffness for the impaired walker is shown in Figure 7.7. The normalized EMG amplitude for the TA, GA and SOL (mean and standard deviation) for all gait cycles pertaining to each surface stiffness is shown. The data are plotted as a function of the gait cycle percentage, where heel-strike and toe-off of the left leg are indicated on the figure as HS and TO, respectively. Black bars underneath an asterisk are included to indicate when statistically significant changes are observed.

The first thing to notice from Figure 7.7 is that the subject's muscle activations do not match that of what would be expected for normal human gait (Perry, 1992), confirming an impaired gait. Specifically, the GA is only active for a brief period of time. In healthy subjects, the GA is active with increasing amplitude throughout the stance phase, whereas this subject shows only brief activation at the beginning of the stance phase. Moreover, the SOL activity in this subject shows irregular fluctuations in the average muscle activation during the stance phase whereas normal muscle activity for healthy subjects is a smooth curve when averaged over several gait cycles.

The most significant result of this case study is that sudden changes in unilateral stiffness of the walking surface evoke significant changes in contralateral GA activity. As indicated in Figure 7.7, the increased GA activity in the affected leg occurred during the early stance phase of the gait cycle when the subject's GA was active during normal walking. This result (i.e. low stiffness perturbations only evoking muscle activity in muscles when normally active) agrees with the results presented

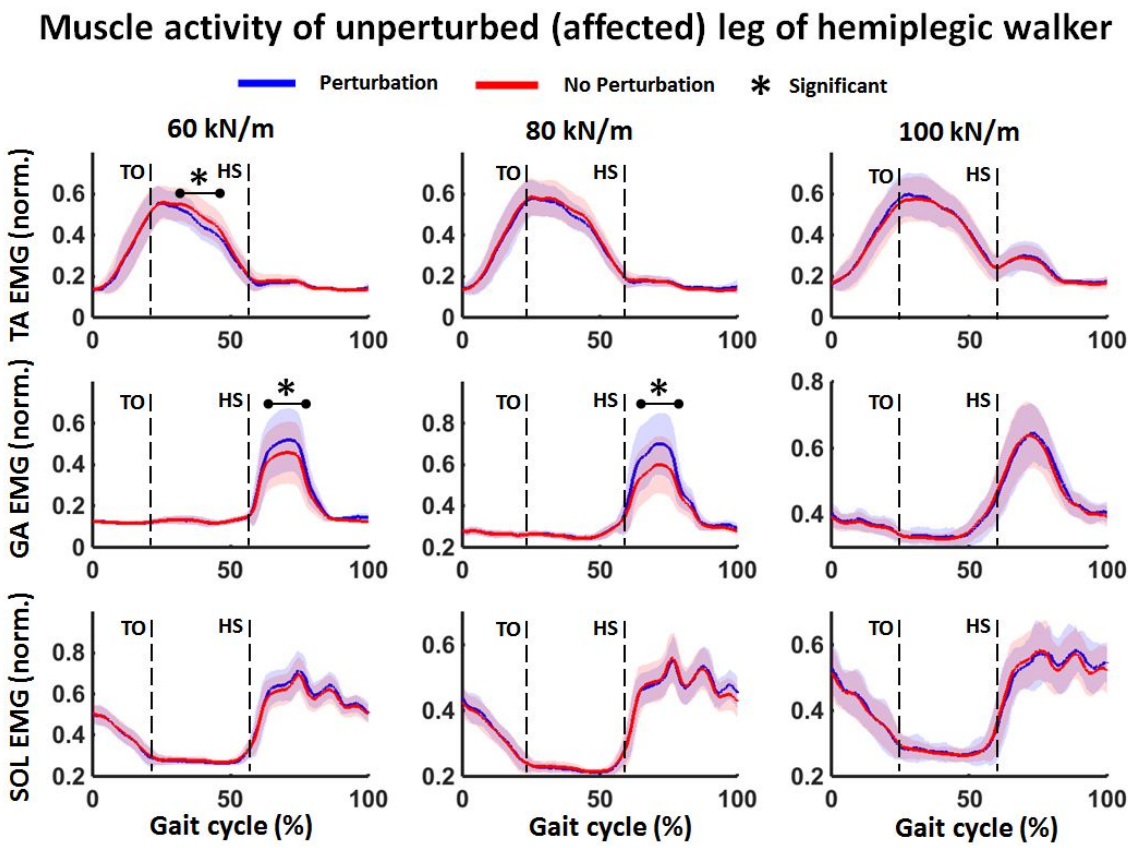

Figure 7.7: Averaged muscle activity of the unperturbed (affected) leg for a the participating subject as function of percent gait cycle, where 0% corresponds to heel-strike of the right (perturbed) leg. Plotted in rows from top to bottom are the normalized TA EMG, normalized GA EMG, and normalized SOL EMG for each level of stiffness perturbation (60, 80, and 100 kN/m, from left to right, respectively). Mean (darker lines) and standard deviations (lightly shaded areas) values are shown. Statistically significant changes are indicated by black bars placed beneath a black asterisk. Heel-strike and toe-off of the left leg are indicated by HS and TO, respectively. The duration of the gait cycle is approximately 1.6 s (Skidmore and Artemiadis (2016b), ©2016 IEEE).

previously with healthy subjects (see Section 5.3.2). Moreover, the significant changes in GA activity are only seen for the 60 and 80 kN/m perturbations, but not for the 100 kN/m perturbation. This agrees with the result from Case Study I in which significant changes in muscle activation were only seen for the lower stiffness perturbations (see Section 7.1.4). This suggests that a certain threshold of perturbation magnitude must be reached before significant evoked response will be seen. With higher stiffness

perturbations there will be less deflection under the load of the subject, leading to smaller changes in sensory feedback and, therefore, a minor contralateral response.

An interesting difference in the results from this case study compared to all previous experiments is the significant decrease in TA EMG at the 60 kN/m level. This mostly likely results from the fact that this subject was walking while facing the opposite direction than all other subjects. In general, the walking direction should not have any influence when walking on a compliant surface; however, the unique characteristics of the VST make the walking direction an important experimental parameter.

First of all, since the treadmill belts of the VST system deflect rotationally instead of vertically, the relative inclination of the treadmill to the subject's leg will impact the ankle angle. Since the foot contacts the walking surface over an area (as opposed to point contact), walking while facing the pivot point of the treadmill belt will create a dorsiflexion perturbation while walking away from the pivot point will create a plantarflexion perturbation, even for the same vertical deflection of the treadmill at the center of pressure of the foot. An illustration of this concept is shown in Figure 7.8.

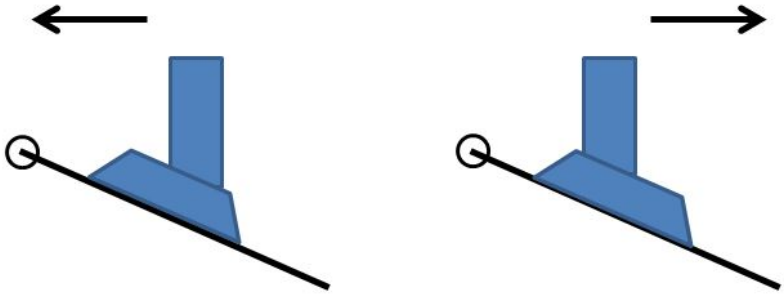

Figure 7.8: Illustration of the impact of the walking direction on the VST. Walking while facing the pivot point of the treadmill belt will create a dorsiflexion perturbation (left) while walking away from the pivot point will create a plantarflexion perturbation (right).

Secondly, the location of the foot on the treadmill will impact the angular deflection of the treadmill. In the VST system, the vertical stiffness, as opposed to rotational stiffness, is controlled. Therefore, for a constant force and a given stiffness level, the vertical deflection at the point of the applied force will be the same. However, the rotational deflection of the treadmill will vary depending on the location of the applied force. Therefore, a stiffness perturbation that is commanded to begin shortly after heel-strike will create different angular deflections of the treadmill if heel-strike occurs close to the pivot point (left facing walking) or far away from the pivot point (right facing walking). An illustration of this concept is shown in Figure 7.9.

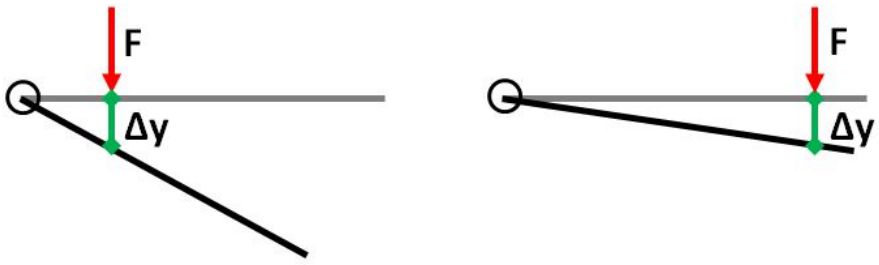

Figure 7.9: Illustration of the impact of location of an applied force on the treadmill. An applied force (F) will create a vertical deflection (Δy) independent on the location of the applied force for a compliant surface. However, the angular deflection of the treadmill will vary depending on the location of the applied force.

7.4 Clinical Implications

The results of these case studies suggest that mechanisms of inter-leg coordination remain intact after neurological injury and can be stimulated through low stiffness perturbations (Skidmore and Artemiadis (2016b), ©2016 IEEE). This result, in combination with the results from experiments with healthy subjects, has strong potential for medical application in a novel approach to robotic gait therapy for hemiplegic walkers in which therapy is provided to an impaired leg through physical interaction

with the healthy leg (Skidmore and Artemiadis (2015b), ©2015 IEEE). Of special interest is the fact that muscular activity was evoked in the paretic TA of two of the hemiplegic walkers during swing phase by altering the surface stiffness below the healthy leg. As mentioned in Section 7.1.1, a main deficiency in stroke survivors and other neurologically impaired walkers is insufficient TA activity during swing phase which leads to decreased dorsiflexion and greater risk for falls. The fact that TA activation was evoked (resulting in increased dorsiflexion) in two subjects who experience drop-foot suggests the feasibility of a solution to drop-foot by altering the stiffness of the walking surface underneath the healthy leg in hemiplegic gait.

Chapter 8

CONCLUSIONS

The objective of this research was to identify and model mechanisms of inter-leg coordination in human gait by applying unilateral perturbations to the walking surface stiffness, with the end goal of improving gait rehabilitation for hemiplegic patients. The identification and modeling of sensorimotor mechanisms of inter-leg coordination, such as was described in this dissertation, can revolutionize current approaches to gait therapy. As opposed to simply automating traditional gait training approaches, such as is implemented by current robotic interventions, providing therapy through sensorimotor mechanisms of inter-leg coordination may be more effective at providing needed improvements in gait rehabilitation.

Indeed, the results of this dissertation can be disruptive from a clinical perspective. Studies with healthy and impaired subjects suggest that unilateral perturbations to the stiffness of the walking surface evoke muscle activation in the contralateral leg that is mediated through the motor cortex. Of special interest are the results of this dissertation that show increased activation of the unperturbed tibialis anterior (TA) during the swing phase of gait in both healthy and hemiplegic walkers. A main deficiency in stroke survivors and other neurologically impaired walkers is insufficient TA activity (which is the primary muscle creating dorsiflexion) in the swing phase which results in decreased dorsiflexion. Insufficient dorsiflexion during walking, referred to as drop-foot, is the leading cause of falls post-stroke (Knutsson and Richards, 1979; Takebe and Basmajian, 1976). The results of this dissertation suggest the feasibility of a solution to drop-foot by altering the stiffness of the walking surface underneath the healthy leg in hemiplegic gait. This overall approach of providing therapy to the impaired leg by only physically interacting with the healthy leg provides the advan-

tage over current rehabilitation protocols of the safety of the patient since there is no direct manipulation of the paretic leg (Skidmore and Artemiadis, 2016a).

Future research will include further development of this novel approach to robot-assisted gait therapy by investigating the effect of repeated perturbations (i.e. a change in walking surface stiffness during every gait cycle) in both healthy and impaired populations. Additionally, research into the effect of long-term therapeutic interventions (i.e. repeated gait training sessions over several weeks with impaired walkers) with the proposed methodology will be pursued.

In summary, gait therapy techniques that are more effective in facilitating neurorehabilitation than current approaches will improve the lives of millions of individuals. The methods and results presented in this dissertation are unique and foundational to the development of robotic interventions in gait therapy that utilize sensorimotor mechanisms of inter-leg coordination. Therefore, this research may facilitate a paradigm shift in robot-assisted gait therapy.

REFERENCES

"Heart disease and stroke statistics 2010 update: A report from the american heart association statistics committee and stroke statistics subcommittee [online]", (2010). 1, 11

Af Klint, R., N. Mazzaro, J. B. Nielsen, S. Thomas and M. J. Grey, "Load rather than length sensitive feedback contributes to soleus muscle activity during human treadmill walking", Journal of neurophysiology **103**, 5, 2747–2756 (2010). 45

Af Klint, R., J. B. Nielsen, T. Sinkjær and M. J. Grey, "Sudden drop in ground support produces force-related unload response in human overground walking", Journal of Neurophysiology **101**, 4, 1705–1712 (2009). 18, 19

Artemiadis, P. K. and H. I. Krebs, "Interlimb coordination evoked by unilateral mechanical perturbation during body-weight supported gait", in "Proc. of IEEE 12th International Conference on Rehabilitation Robotics", (2011a). 3, 18

Artemiadis, P. K. and H. I. Krebs, "On the interlimb coordination and synchronization during gait", in "Proc. of IEEE Engineering in Medicine and Biology Society", pp. 1571–1574 (2011b). 3, 18

Arya, K. and S. Pandian, "Interlimb neural coupling: Implications for poststroke hemiparesis", Annals of physical and rehabilitation medicine **57**, 9, 696–713 (2014). 3, 17, 18

Banala, S. K., S. K. Agrawal and J. P. Scholz, "Active leg exoskeleton (alex) for gait rehabilitation of motor-impaired patients", in "Rehabilitation Robotics, 2007. ICORR 2007. IEEE 10th International Conference on", pp. 401–407 (IEEE, 2007). 2, 11, 13, 15

Barbeau, H. and M. Visintin, "Optimal outcomes obtained with body-weight support combined with treadmill training in stroke subjects", Archives of physical medicine and rehabilitation **84**, 10, 1458–1465 (2003). 17

Barkan, A., J. Skidmore and P. Artemiadis, "Variable Stiffness Treadmill (VST): a Novel Tool for the Investigation of Gait", in "Robotics and Automation (ICRA), 2014 IEEE International Conference on", pp. 2838–2843 (IEEE, 2014). x, 22, 28, 30, 31, 32, 33, 36

Barker-Collo, S., V. Feigin, V. Parag, C. Lawes and H. Senior, "Auckland stroke outcomes study part 2: Cognition and functional outcomes 5 years poststroke", Neurology **75**, 18, 1608–1616 (2010). 1

Bates, B., J. Y. Choi, P. W. Duncan, J. J. Glasberg, G. D. Graham, R. C. Katz, K. Lamberty, D. Reker and R. Zorowitz, "Veterans Affairs/Department of Defense Clinical Practice Guideline for the Management of Adult Stroke Rehabilitation Care Executive Summary", Stroke **36**, 9, 2049–2056 (2005). 17

Behrman, A. L. and S. J. Harkema, "Locomotor training after human spinal cord injury: A series of case studies", Phys. Ther. **80(7)**, 688–700 (2000). 10

Belda-Lois, J.-M., S. M. del Horno, I. Bermejo-Bosch, J. C. Moreno, J. L. Pons, D. Farina, M. Iosa, M. Molinari, F. Tamburella, A. Ramos, A. Caria, T. Solis-Escalante, C. Brunner and M. Rea, "Rehabilitation of gait after stroke: a review towards a top-down approach", Journal of NeuroEngineering and Rehabilitation **8**, 1, 66 (2011). 1, 12, 71

Berger, W., V. Dietz and G. Horstmann, "Interlimb coordination of posture in man", Journal of physiology **390**, 135 (1987). 18

Berger, W., V. Dietz and J. Quintern, "Corrective reactions to stumbling in man: neuronal coordination of bilateral leg muscle activity during gait", Journal of physiology **357**, 109–125 (1984). 18

Beyl, P., M. V. Damme, R. V. Ham, R. Versluys, B. Vanderborght and D. Lefeber, "An exoskeleton for gait rehabilitation: prototype design and control principle", in "Proceedings of the International Conference on Robotics and Automation", pp. 2037–2042 (2008). 13, 16

Blaya, J. A. and H. Herr, "Adaptive control of a variable-impedance ankle-foot orthosis to assist drop-foot gait", Neural Systems and Rehabilitation Engineering, IEEE Transactions on **12**, 1, 24–31 (2004). 3

Bouri, M., B. Le Gall and R. Clavel, "A new concept of parallel robot for rehabilitation and fitness: The lambda", in "Robotics and Biomimetics (ROBIO), 2009 IEEE International Conference on", pp. 2503–2508 (IEEE, 2009). 12

Browning, R. C., E. A. Baker, J. A. Herron and R. Kram, "Effects of obesity and sex on the energetic cost and preferred speed of walking", Journal of Applied Physiology **100**, 2, 390–398 (2006). 25, 26

Capaday, C., B. A. Lavoie, H. Barbeau, C. Schneider and M. Bonnard, "Studies on the corticospinal control of human walking. i. responses to focal transcranial magnetic stimulation of the motor cortex", Journal of neurophysiology **81**, 1, 129–139 (1999). 71

Carr, J. H. S. and B. Roberta, "A motor relearning programme for stroke", (1982). 10

Chan, D. Y., C. C. Chan and D. K. Au, "Motor relearning programme for stroke patients: a randomized controlled trial", Clinical rehabilitation **20**, 3, 191–200 (2006). 10

Chang, M. D., E. Sejdić, V. Wright and T. Chau, "Measures of dynamic stability: detecting differences between walking overground and on a compliant surface", Human movement science **29**, 6, 977–986 (2010). 19, 73

Chang, W. H. and Y.-H. Kim, "Robot-assisted therapy in stroke rehabilitation", Journal of stroke **15**, 3, 174–181 (2013). 2, 17

Choi, J. T. and A. J. Bastian, "Adaptation reveals independent control networks for human walking", Nature neuroscience **10**, 8, 1055–1062 (2007). 6

Christensen, L. O., J. B. Andersen, T. Sinkjær and J. Nielsen, "Transcranial magnetic stimulation and stretch reflexes in the tibialis anterior muscle during human walking", The Journal of physiology **531**, 2, 545–557 (2001). 7

Christensen, L. O., P. Johannsen, T. Sinkjær, N. Petersen, H. Pyndt and J. B. Nielsen, "Cerebral activation during bicycle movements in man", Experimental Brain Research **135**, 1, 66–72 (2000a). 6

Christensen, L. O., N. Petersen, J. B. Andersen, T. Sinkjær and J. B. Nielsen, "Evidence for transcortical reflex pathways in the lower limb of man", Progress in neurobiology **62**, 3, 251–272 (2000b). 71

Colombo, G., M. Joerg, R. Schreier and V. Dietz, "Treadmill training of paraplegic patients using a robotic orthosis", Journal of rehabilitation research and development **37**, 6, 693 (2000). 12, 13

Darton, K., O. C. Lippold, M. Shahani and U. Shahani, "Long-latency spinal reflexes in humans", Journal of Neurophysiology **53**, 6, 1604–1618 (1985). 70, 96

Delorme, A. and S. Makeig, "Eeglab: an open source toolbox for analysis of single-trial eeg dynamics including independent component analysis", Journal of neuroscience methods **134**, 1, 9–21 (2004). 75

Delp, S. L., F. C. Anderson, A. S. Arnold, P. Loan, A. Habib, C. T. John, E. Guendelman and D. G. Thelen, "Opensim: open-source software to create and analyze dynamic simulations of movement", IEEE transactions on biomedical engineering **54**, 11, 1940–1950 (2007). 60, 61

Di Lollo, V., J. T. Enns, S. Yantis and L. G. Dechief, "Response latencies to the onset and offset of visual stimuli", Perception & Psychophysics **62**, 1, 218–225 (2000). 64

Díaz, I., J. J. Gil and E. Sánchez, "Lower-limb robotic rehabilitation: literature review and challenges", Journal of Robotics **2011** (2011). 2, 10, 12, 13, 14

Dietz, V., "Interaction between central programs and afferent input in the control of posture and locomotion", Journal of biomechanics **29**, 7, 841–844 (1996). 6

Dietz, V., "Spinal cord pattern generators for locomotion", Clinical Neurophysiology **114**, 8, 1379–1389 (2003). 6, 8

Dietz, V., G. Horstmann and W. Berger, "Interlimb Coordination of Leg-Muscle Activation During Perturbation of Stance in Humans", Journal of neurophysiology **62**, 3, 680–693 (1989). 3, 18

Dietz, V., W. Zijlstra and J. Duysens, "Human neuronal interlimb coordination during split-belt locomotion", Experimental brain research **101**, 3, 513–520 (1994). 18

Ditunno Jr, J. F., A. S. Burns and R. J. Marino, "Neurological and functional capacity outcome measures: essential to spinal cord injury clinical trials", Journal of rehabilitation research and development **42**, 3, 35 (2005). 1

Dixon, S. J., A. C. Collop and M. E. Batt, "Surface effects on ground reaction forces and lower extremity kinematics in running.", Medicine and science in sports and exercise **32**, 11, 1919–1926 (2000). 3, 19, 20

Dobkin, B. H., A. Firestine, M. West, K. Saremi and R. Woods, "Ankle dorsiflexion as an fmri paradigm to assay motor control for walking during rehabilitation", Neuroimage **23**, 1, 370–381 (2004). 7

Dohring, M. E. and J. J. Daly, "Automatic synchronization of functional electrical stimulation and robotic assisted treadmill training", IEEE Transactions on Neural Systems and Rehabilitation Engineering **16**, 3, 310–313 (2008). 1

Dollar, A. M. and H. Herr, "Lower extremity exoskeletons and active orthoses: Challenges and state-of-the-art", IEEE Transactions on Robotics **24**, 1, 144–158 (2008). 8, 9, 10

Duysens, J. and H. W. Van de Crommert, "Neural control of locomotion; part 1: The central pattern generator from cats to humans", Gait & posture **7**, 2, 131–141 (1998). 8

Farley, C. T., H. H. Houdijk, C. Van Strien and M. Louie, "Mechanism of leg stiffness adjustment for hopping on surfaces of different stiffnesses", Journal of Applied Physiology **85**, 3, 1044–1055 (1998). 38

Ferris, D. P. and C. T. Farley, "Interaction of leg stiffness and surface stiffness during human hopping", Journal of applied physiology **82**, 1, 15–22 (1997). 38

Ferris, D. P., K. Liang and C. T. Farley, "Runners adjust leg stiffness for their first step on a new running surface", Journal of biomechanics **32**, 8, 787–794 (1999). 3, 19, 20, 38

Finch, L., H. Barbeau and B. Arsenault, "Influence of body weight support on normal human gait: development of a gait retraining strategy", Physical Therapy **71**, 11, 842–855 (1991). 45

Fitzsimmons, N. A., M. A. Lebedev, I. D. Peikon and M. A. Nicolelis, "Extracting kinematic parameters for monkey bipedal walking from cortical neuronal ensemble activity", Frontiers in integrative neuroscience **3** (2009). 7

Flansbjer, U.-B., A. M. Holmbäck, D. Downham, C. Patten and J. Lexell, "Reliability of gait performance tests in men and women with hemiparesis after stroke.", Journal of rehabilitation medicine **37**, 2, 75–82 (2005). 1

Forrester, L. W., L. A. Wheaton and A. R. Luft, "Exercise-mediated locomotor recovery and lower-limb neuroplasticity after stroke", Journal of rehabilitation research and development **45**, 2, 205 (2008). 6

Freivogel, S., J. Mehrholz, T. Husak-Sotomayor and D. Schmalohr, "Gait training with the newly developed lokohelp-system is feasible for non-ambulatory patients after stroke, spinal cord and brain injury. a feasibility study", Brain Injury **22**, 7-8, 625–632 (2008). 12, 13

Frost, R., J. Skidmore, M. Santello and P. Artemiadis, "Sensorimotor control of gait: a novel approach for the study of the interplay of visual and proprioceptive feedback", Frontiers in human neuroscience **9**, 14 (2015). 42

Galvez, J. and D. Reinkensmeyer, "Robotics for gait training after spinal cord injury", Topics in Spinal Cord Injury Rehabilitation **11**, 2, 18–33 (2005). 11

Gelderblom, G. J., M. D. Wilt, G. Cremers and A. Rensma, "Rehabilitation robotics in robotics for healthcare; a roadmap study for the european commission", in "2009 IEEE International Conference on Rehabilitation Robotics", pp. 834–838 (2009). 2

Goffer, A., "Gait-locomotor apparatus", US Patent 7,153,242 (2006). 12

Grillner, S., "The motor infrastructure: from ion channels to neuronal networks", Nature Reviews Neuroscience **4**, 7, 573–586 (2003). 6, 8

Grillner, S., P. Wallén, K. Saitoh, A. Kozlov and B. Robertson, "Neural bases of goal-directed locomotion in vertebratesan overview", Brain research reviews **57**, 1, 2–12 (2008). 6

Guertin, P. A., "The mammalian central pattern generator for locomotion", Brain research reviews **62**, 1, 45–56 (2009). 6, 8

Gwin, J. T., K. Gramann, S. Makeig and D. P. Ferris, "Electrocortical activity is coupled to gait cycle phase during treadmill walking", Neuroimage **54**, 2, 1289–1296 (2011). 7

Hardin, E. C., A. J. van den Bogert and J. Hamill, "Kinematic adaptations during running: effects of footwear, surface, and duration", Medicine and science in sports and exercise **36**, 5, 838–844 (2004). 3, 19, 20

Hesse, S., C. Bertelt, M. T. Jahnke, A. Schaffrin, P. Baake, M. Malezic and K. H. Mauritz, "Treadmill training with partial body weight support compared with physiotherapy in nonambulatory hemiparetic patients.", Stroke **26(6)**, 976–981 (1995). 10

Hesse, S., D. Uhlenbrock *et al.*, "A mechanized gait trainer for restoration of gait", Journal of rehabilitation research and development **37**, 6, 701–708 (2000). 2, 11

Hidler, J., D. Nichols, M. Pelliccio, K. Brady, D. D. Campbell, J. H. Kahn and T. G. Hornby, "Multicenter randomized clinical trial evaluating the effectiveness of the lokomat in subacute stroke", Neurorehabilitation and Neural Repair **23**, 1, 5–13 (2009). 2, 17

Homma, K., O. Fukuda, J. Sugawara, Y. Nagata and M. Usuba, "A wire-driven leg rehabilitation system: development of a 4-dof experimental system", in "Advanced Intelligent Mechatronics, 2003. AIM 2003. Proceedings. 2003 IEEE/ASME International Conference on", vol. 2, pp. 908–913 (IEEE, 2003). 12

Hornby, T. G., D. D. Campbell, J. H. Kahn, T. Demott, J. L. Moore and H. R. Roth, "Enhanced gait-related improvements after therapist-versus robotic-assisted locomotor training in subjects with chronic stroke a randomized controlled study", Stroke **39**, 6, 1786–1792 (2008). 2, 17

Jafari, A., N. G. Tsagarakis and D. G. Caldwell, "AwAS-II: A new Actuator with Adjustable Stiffness based on the novel principle of adaptable pivot point and variable lever ratio", in "Robotics and Automation (ICRA), 2011 IEEE International Conference on", pp. 4638–4643 (2011). 24

Jezernik, S., G. Colombo, T. Keller, H. Frueh and M. Morari, "Robotic orthosis lokomat: A rehabilitation and research tool", Neuromodulation: Technology at the neural interface **6**, 2, 108–115 (2003). 2, 11

Johannsen, L., A. M. Wing, T. Pelton, K. Kitaka, D. Zietz, N. Brittle, P. van Vliet, J. Riddoch, C. Sackley and R. McManus, "Seated bilateral leg exercise effects on hemiparetic lower extremity function in chronic stroke", Neurorehabilitation and neural repair **24**, 3, 243–53 (2009). 17

Kautz, S. A. and C. Patten, "Interlimb influences on paretic leg function in poststroke hemiparesis", Journal of neurophysiology **93**, 5, 2460–2473 (2005). 18

Kawamoto, H., T. Hayashi, T. Sakurai, K. Eguchi and Y. Sankai, "Development of single leg version of hal for hemiplegia", in "Engineering in Medicine and Biology Society, 2009. EMBC 2009. Annual International Conference of the IEEE", pp. 5038–5043 (IEEE, 2009). 12

Kerdok, A. E., A. A. Biewener, T. A. McMahon, P. G. Weyand and H. M. Herr, "Energetics and mechanics of human running on surfaces of different stiffnesses", Journal of Applied Physiology **92**, 2, 469–478 (2002). 20

Kleim, J. A., "Neural plasticity and neurorehabilitation: teaching the new brain old tricks", Journal of communication disorders **44**, 5, 521–528 (2011). 1

Kleim, J. A. and T. A. Jones, "Principles of experience-dependent neural plasticity: implications for rehabilitation after brain damage", Journal of speech, language, and hearing research **51**, 1, S225–S239 (2008). 1, 2, 11

Knutsson, E. and C. Richards, "Different types of disturbed motor control in gait of hemiparetic patients.", Brain: a journal of neurology **102**, 2, 405–430 (1979). 98, 115

Kuo, A. D., "The relative roles of feedforward and feedback in the control of rhythmic movements", Motor Control **6**, 2, 129–145 (2002). 6

Lam, T., C. Wolstenholme, M. van der Linden, M. Y. Pang and J. F. Yang, "Stumbling corrective responses during treadmill-elicited stepping in human infants", The Journal of physiology **553**, 1, 319–331 (2003). 18

Langhorne, P., J. Bernhardt and G. Kwakkel, "Stroke rehabilitation", The Lancet **377**, 9778, 1693–1702 (2011). 1

Levine, R. V. and A. Norenzayan, "The pace of life in 31 countries", Journal of cross-cultural psychology **30**, 2, 178–205 (1999). 25, 26

Lopez-Calderon, J. and S. J. Luck, "Erplab: an open-source toolbox for the analysis of event-related potentials", Frontiers in human neuroscience **8** (2014). 75

Luft, A. R., R. F. Macko, L. W. Forrester, F. Villagra, F. Ivey, J. D. Sorkin, J. Whitall, S. McCombe-Waller, L. Katzel, A. P. Goldberg *et al.*, "Treadmill exercise activates subcortical neural networks and improves walking after stroke", Stroke **39**, 12, 3341–3350 (2008). 17

Luft, A. R., G. V. Smith, L. Forrester, J. Whitall, R. F. Macko, T.-K. Hauser, A. P. Goldberg and D. F. Hanley, "Comparing brain activation associated with isolated upper and lower limb movement across corresponding joints", Human brain mapping **17**, 2, 131–140 (2002). 7

MacLellan, M. J. and A. E. Patla, "Adaptations of walking pattern on a compliant surface to regulate dynamic stability", Experimental brain research **173**, 3, 521–530 (2006). 3, 19, 20

Mamoto, Y., K. Yamamoto, T. Imai, M. Tamura and T. Kubo, "Three-dimensional analysis of human locomotion in normal subjects and patients with vestibular deficiency", Acta oto-laryngologica **122**, 5, 495–500 (2002). 68

Marigold, D. S. and A. E. Patla, "Adapting locomotion to different surface compliances: neuromuscular responses and changes in movement dynamics", Journal of neurophysiology **94**, 3, 1733–1750 (2005). 3, 19, 20

Mayr, A., M. Kofler, E. Quirbach, H. Matzak, K. Fröhlich and L. Saltuari, "Prospective, blinded, randomized crossover study of gait rehabilitation in stroke patients using the lokomat gait orthosis", Neurorehabilitation and Neural Repair **21**, 4, 307–314 (2007). 2, 17

McMahon, T. A. and P. R. Greene, "The influence of track compliance on running", Journal of biomechanics **12**, 12, 893–904 (1979). 19

Mehrholz, J., C. Werner, J. Kugler and M. Pohl, "Electromechanical-assisted training for walking after stroke (review)", The Cochrane Collaboration **4** (2007). 3

Molinari, M., "Plasticity properties of cpg circuits in humans: impact on gait recovery", Brain research bulletin **78**, 1, 22–25 (2009). 8

Morbi, A., M. Ahmadi and A. Nativ, "GaitEnable: An omnidirectional robotic system for gait rehabilitation", in "Mechatronics and Automation (ICMA), 2012 International Conference on", pp. 936–941 (IEEE, 2012). 2, 11

Moritz, C. T., S. M. Greene and C. T. Farley, "Neuromuscular changes for hopping on a range of damped surfaces", Journal of Applied Physiology **96**, 5, 1996–2004 (2004). 3, 19, 20

Nakazawa, K., N. Kawashima, M. Akai and H. Yano, "On the reflex coactivation of ankle flexor and extensor muscles induced by a sudden drop of support surface during walking in humans", Journal of Applied Physiology **96**, 2, 604–611 (2004). 3, 18

Nielsen, J. B., "How we walk: central control of muscle activity during human walking", The Neuroscientist **9**, 3, 195–204 (2003). 6

Norton, J., "Changing our thinking about walking", The Journal of physiology **588**, 22, 4341–4341 (2010). 6

Pekna, M., M. Pekny and M. Nilsson, "Modulation of neural plasticity as a basis for stroke rehabilitation", Stroke **43**, 10, 2819–2828 (2012). 1, 12

Perry, J., *Gait Analysis: Normal and Pathological Function* (Slack Incorporated, 1992). 50, 69, 71, 110

Perry, J. and J. M. Burnfield, "Gait analysis: normal and pathological function", Journal of Pediatric Orthopaedics **12**, 6, 815 (1992). 25

Peshkin, M., D. A. Brown, J. J. Santos-Munné, A. Makhlin, E. Lewis, J. E. Colgate, J. Patton and D. Schwandt, "Kineassist: A robotic overground gait and balance training device", in "Rehabilitation Robotics, 2005. ICORR 2005. 9th International Conference on", pp. 241–246 (IEEE, 2005). 2, 11, 12

Petersen, N., L. O. Christensen and J. Nielsen, "The effect of transcranial magnetic stimulation on the soleus h reflex during human walking", The journal of physiology **513**, 2, 599–610 (1998). 7

Petersen, N. T., J. E. Butler, V. Marchand-Pauvert, R. Fisher, A. Ledebt, H. S. Pyndt, N. L. Hansen and J. B. Nielsen, "Suppression of emg activity by transcranial magnetic stimulation in human subjects during walking", The Journal of Physiology **537**, 2, 651–656 (2001). 7

Petersen, T. H., M. Willerslev-Olsen, B. A. Conway and J. B. Nielsen, "The motor cortex drives the muscles during walking in human subjects", The Journal of physiology **590**, 10, 2443–2452 (2012). 7

Pietrusinski, M., I. Cajigas, Y. Mizikacioglu, M. Goldsmith, P. Bonato and C. Mavroidis, "Gait rehabilitation therapy using robot generated force fields applied at the pelvis", in "Haptics Symposium, 2010 IEEE", pp. 401–407 (IEEE, 2010). 13, 16

Pohl, M., C. Werner, M. Holzgraefe, G. Kroczek, I. Wingendorf, G. Hoölig, R. Koch and S. Hesse, "Repetitive locomotor training and physiotherapy improve walking and basic activities of daily living after stroke: a single-blind, randomized multicentre trial (deutsche gangtrainerstudie, degas)", Clinical Rehabilitation **21**, 1, 17–27 (2007). 2, 17

Poskanzer, E. H., "Movement therapy in hemiplegia: a neurophysiologic approach", Journal of Gerontology **27**, 2, 290–290 (1972). 18

Presacco, A., L. W. Forrester and J. L. Contreras-Vidal, "Decoding intra-limb and inter-limb kinematics during treadmill walking from scalp electroencephalographic (EEG) signals", Neural Systems and Rehabilitation Engineering, IEEE Transactions on **20**, 2, 212–219 (2012). 7

Reinkensmeyer, D., J. Wynne and S. Harkema, "A robotic tool for studying locomotor adaptation and rehabilitation", in "Engineering in Medicine and Biology, 2002. 24th Annual Conference and the Annual Fall Meeting of the Biomedical Engineering Society EMBS/BMES Conference, 2002. Proceedings of the Second Joint", vol. 3, pp. 2353–2354 (IEEE, 2002). 13, 14

Reinkensmeyer, D. J., D. Aoyagi, J. L. Emken, J. A. Galvez *et al.*, "Tools for understanding and optimizing robotic gait training", Journal of rehabilitation research and development **43**, 5, 657 (2006). 13, 15

Riener, R., L. Lunenburger, S. Jezernik, M. Anderschitz, G. Colombo and V. Dietz, "Patient-cooperative strategies for robot-aided treadmill training: first experimental results", Neural Systems and Rehabilitation Engineering, IEEE Transactions on **13**, 3, 380–394 (2005). 17

Roerdink, M., P. J. Bank, C. L. E. Peper and P. J. Beek, "Walking to the beat of different drums: Practical implications for the use of acoustic rhythms in gait rehabilitation", Gait & posture **33**, 4, 690–694 (2011). 65

Rose, D. K. and C. J. Winstein, "Temporal coupling is more robust than spatial coupling: an investigation of interlimb coordination after stroke", Journal of motor behavior **45**, 4, 313–324 (2013). 18

Rossignol, S., R. Debuck and J.-P. Gossard, "Dynamic sensorimotor interactions in locomotion", Physiological reviews **10**, 1152, 86–89 (2006). 6, 7, 59, 64, 66, 68, 71

Roy, A., H. I. Krebs, D. Williams, C. T. Bever, L. W. Forrester, R. M. Macko and N. Hogan, "Robot-aided neurorehabilitation: A robot for ankle rehabilitation", IEEE Transaction on Robotics **25:3**, 569–582 (2009). 3

Sahyoun, C., A. Floyer-Lea, H. Johansen-Berg and P. Matthews, "Towards an understanding of gait control: brain activation during the anticipation, preparation and execution of foot movements", Neuroimage **21**, 2, 568–575 (2004). 7

Sanders, O. P., D. N. Savin, R. A. Creath and M. W. Rogers, "Protective balance and startle responses to sudden freefall in standing humans", Neuroscience letters **586**, 8–12 (2015). 66, 67

Schmidt, H., C. Werner, R. Bernhardt, S. Hesse and J. Krüger, "Gait rehabilitation machines based on programmable footplates", Journal of neuroengineering and rehabilitation **4**, 1, 2 (2007). 10

Schmitt, C. and P. Métrailler, "The motion maker: a rehabilitation system combining an orthosis with closed-loop electrical muscle stimulation", in "8th Vienna International Workshop on Functional Electrical Stimulation", No. LSRO2-CONF-2006-011, pp. 117–120 (2004). 12

Schubert, M., A. Curt, L. Jensen and V. Dietz, "Corticospinal input in human gait: modulation of magnetically evoked motor responses", Experimental brain research **115**, 2, 234–246 (1997). 71

Shemmell, J., J. H. An and E. J. Perreault, "The differential role of motor cortex in stretch reflex modulation induced by changes in environmental mechanics and verbal instruction", Journal of Neuroscience **29**, 42, 13255–13263 (2009). 71, 80, 96

Skidmore, J. and P. Artemiadis, "Leg muscle activation evoked by floor stiffness perturbations: A novel approach to robot-assisted gait rehabilitation", in "Robotics and Automation (ICRA), 2015 IEEE International Conference on", pp. 6463–6468 (IEEE, 2015a). 4

Skidmore, J. and P. Artemiadis, "Unilateral floor stiffness perturbations systematically evoke contralateral leg muscle responses: a new approach to robot-assisted gait therapy", IEEE Transactions on Neural Systems and Rehabilitation Engineering (2015b). xi, 50, 51, 72, 114

Skidmore, J. and P. Artemiadis, "On the effect of walking surface stiffness on interlimb coordination in human walking: toward bilaterally informed robotic gait rehabilitation", Journal of NeuroEngineering and Rehabilitation **13**, 1, 1 (2016a). xi, 2, 3, 4, 17, 18, 19, 20, 21, 22, 26, 44, 46, 53, 55, 57, 58, 70, 71, 116

Skidmore, J. and P. Artemiadis, "Sudden changes in walking surface compliance evoke contralateral emg in a hemiparetic walker: A case study of inter-leg coordination after neurological injury", in "Engineering in Medicine and Biology Society (EMBC), 2016 IEEE 38th Annual International Conference of the", pp. 4682–4685 (IEEE, 2016b). xi, 107, 109, 111, 113

Skidmore, J. and P. Artemiadis, "Unilateral walking surface stiffness perturbations evoke brain responses: Toward bilaterally informed robot-assisted gait rehabilitation", in "Robotics and Automation (ICRA), 2016 IEEE International Conference on", pp. 3698–3703 (IEEE, 2016c). xi, 4, 11, 73, 74, 77, 78

Skidmore, J., A. Barkan and P. Artemiadis, "Investigation of contralateral leg response to unilateral stiffness perturbations using a novel device", in "Intelligent Robots and Systems (IROS 2014), 2014 IEEE/RSJ International Conference on", pp. 2081–2086 (IEEE, 2014). x, 28

Skidmore, J., A. Barkan and P. Artemiadis, "Variable Stiffness Treadmill (VST): System Development, Characterization and Preliminary Experiments", IEEE/ASME Transactions on Mechatronics **20**, 4, 1717–1724 (2015). x, 23, 24, 25, 26, 27, 28, 29, 38, 39, 40, 41, 42, 43

Surdilovic, D. and R. Bernhardt, "String-man: a new wire robot for gait rehabilitation", in "Robotics and Automation, 2004. Proceedings. ICRA'04. 2004 IEEE International Conference on", vol. 2, pp. 2031–2036 (IEEE, 2004). 13, 16

Takebe, K. and J. Basmajian, "Gait analysis in stroke patients to assess treatments of foot-drop.", Archives of physical medicine and rehabilitation **57**, 1, 305–310 (1976). 98, 115

Thaut, M., G. McIntosh and R. Rice, "Rhythmic facilitation of gait training in hemiparetic stroke rehabilitation", Journal of the Neurological Sciences **151**, 2, 207 – 212 (1997). 65

van der Linden, M. H., D. S. Marigold, F. J. Gabreëls and J. Duysens, "Muscle reflexes and synergies triggered by an unexpected support surface height during walking", Journal of neurophysiology **97**, 5, 3639–3650 (2007). 3, 18

Veneman, J. F., R. Kruidhof, E. E. Hekman, R. Ekkelenkamp, E. H. Van Asseldonk and H. Van Der Kooij, "Design and evaluation of the lopes exoskeleton robot for interactive gait rehabilitation", Neural Systems and Rehabilitation Engineering, IEEE Transactions on **15**, 3, 379–386 (2007). 2, 11, 13, 16

Wernig, A., S. Müller, A. Nanassy and E. Cagol, "Laufband therapy based on rules of spinal locomotion is effective in spinal cord injured persons", European Journal of Neuroscience **7**, 4, 823–829 (1995). 10

West, R. G., "Powered gait orthosis and method of utilizing same", US Patent 6,689,075 (2004). 13, 14

Whitney, S. L., G. F. Marchetti, M. Pritcher and J. M. Furman, "Gaze stabilization and gait performance in vestibular dysfunction", Gait & posture **29**, 2, 194–198 (2009). 68

Wieser, M., J. Haefeli, L. Bütler, L. Jäncke, R. Riener and S. Koeneke, "Temporal and spatial patterns of cortical activation during assisted lower limb movement", Experimental brain research **203**, 1, 181–191 (2010). 7

Yang, J. F. and M. Gorassini, "Spinal and brain control of human walking: implications for retraining of walking", The Neuroscientist **12**, 5, 379–389 (2006). 6, 8

Yang, J. F., T. Lam, M. Y. Pang, E. Lamont, K. Musselman and E. Seinen, "Infant stepping: a window to the behaviour of the human pattern generator for walking", Canadian journal of physiology and pharmacology **82**, 8-9, 662–674 (2004). 8

Yavuz, Ş. U., N. Mrachacz-Kersting, O. Sebik, M. B. Ünver, D. Farina and K. S. Türker, "Human stretch reflex pathways reexamined", Journal of neurophysiology **111**, 3, 602–612 (2014). 70, 96

Yeomans, J. S., L. Li, B. W. Scott and P. W. Frankland, "Tactile, acoustic and vestibular systems sum to elicit the startle reflex", Neuroscience & Biobehavioral Reviews **26**, 1, 1–11 (2002). 69

Zehr, E., T. Komiyama and R. Stein, "Cutaneous reflexes during human gait: electromyographic and kinematic responses to electrical stimulation", Journal of neurophysiology **77**, 6, 3311–3325 (1997). 62

Zuur, A. T., M. S. Christensen, T. Sinkjær, M. J. Grey and J. B. Nielsen, "Tibialis anterior stretch reflex in early stance is suppressed by repetitive transcranial magnetic stimulation", The Journal of physiology **587**, 8, 1669–1676 (2009). 71, 80, 96

APPENDIX A

LIST OF PUBLICATIONS

The following publications have resulted from research related to this dissertation. Portions of several of these papers have been used in the dissertation and are correspondingly cited within the text.

Peer-Reviewed Journal Articles

1. Jeffrey Skidmore and Panagiotis Artemiadis, "On the effect of walking surface stiffness on inter-limb coordination in human walking: toward bilaterally informed robotic gait rehabilitation." Journal of NeuroEngineering and Rehabilitation, 13.23, pp. 1-15, 2016.

2. Jeffrey Skidmore and Panagiotis Artemiadis, "Unilateral Floor Stiffness Perturbations Systematically Evoke Contralateral Leg Muscle Responses: a New Approach to Robot-assisted Gait Therapy," IEEE Transactions on Neural Systems and Rehabilitation Engineering, vol. 24(4), pp. 467-474, 2016.

3. Ryan Frost, Jeffrey Skidmore, Marco Santello, and Panagiotis Artemiadis, "Sensorimotor control of gait: A novel approach for the study of the interplay of visual and proprioceptive feedback," Frontiers in Human Neuroscience 9 (2015): 14.

4. Jeffrey Skidmore, Andrew Barkan, and Panagiotis Artemiadis, "Variable Stiffness Treadmill (VST): System Development, Characterization and Preliminary Experiments," IEEE/ASME Transactions on Mechatronics, vol. 20, issue 4, pp. 1717-1724, 2015.

Peer-Reviewed Conference Proceeding Articles

1. Jeffrey Skidmore and Panagiotis Artemiadis, "Sudden changes in walking surface compliance evoke contralateral EMG in a hemiparetic walker: a case study

of inter-leg coordination after neurological injury," 38th Annual International Conference of the IEEE Engineering in Medicine and Biology Society (EMBC'16), 2016.

2. Jeffrey Skidmore and Panagiotis Artemiadis, "Unilateral Walking Surface Stiffness Perturbations Evoke Brain Responses: Toward Bilaterally Informed Robot-assisted Gait Rehabilitation," IEEE International Conference on Robotics and Automation (ICRA), 2016.

3. Jeffrey Skidmore and Panagiotis Artemiadis, "Leg Muscle Activation Evoked by Floor Stiffness Perturbations: A Novel Approach to Robot-assisted Gait Rehabilitation," IEEE International Conference on Robotics and Automation (ICRA). May 29, 2015.

4. Jeffrey Skidmore, Andrew Barkan, and Panagiotis Artemiadis, "Investigation of Contralateral Leg Response to Unilateral Stiffness Perturbations using a Novel Device," IEEE/RSJ International Conference on Intelligent Robots and Systems (IROS). September 15, 2014.

5. Andrew Barkan, Jeffrey Skidmore, and Panagiotis Artemiadis, "Variable Stiffness Treadmill (VST): a Novel Tool for the Investigation of Gait," IEEE International Conference on Robotics and Automation (ICRA). June 2, 2014.

APPENDIX B

COPYRIGHTED MATERIAL

In reference to IEEE copyrighted material which is used with permission in this dissertation, the IEEE does not endorse any of Arizona State University's products or services. Internal or personal use of this material is permitted. If interested in reprinting/republishing IEEE copyrighted material for advertising or promotional purposes or for creating new collective works for resale or redistribution, please go to `http://www.ieee.org/publications_standards/publications/rights/rights_link.html` to learn how to obtain a License from RightsLink.

APPENDIX C

CO-AUTHOR PERMISSION

All co-authors have given permission for inclusion of material from published co-authored papers in this dissertation.